2012

Wireless Power Transfer For Space Applications: System Design And Electromagnetic Compatibility Compliance Of Radiated Emissions

Ramos Gabriel Vazquez
University of Central Florida

WIRELESS POWER TRANSFER FOR SPACE APPLICATIONS: SYSTEM DESIGN AND ELECTROMAGNETIC COMPATIBILITY COMPLIANCE OF RADIATED EMISSIONS

by

GABRIEL VAZQUEZ RAMOS

B.S. University of Puerto Rico, 2005
M.S. Florida Institute of Technology, 2008

A dissertation submitted in partial fulfillment of the requirements
for the degree of Doctor of Philosophy
in the Department of Electrical Engineering and Computer Science
in the College of Engineering and Computer Science
at the University of Central Florida
Orlando, Florida

Summer Term
2012

Major Professor: Jiann S. Yuan

ABSTRACT

This dissertation evaluates the possibility of wireless power transfer (WPT) systems for space applications, with an emphasis in launch vehicles (rockets). After performing literature review for WPT systems, it was identified that magnetic resonance provides the more suited set of characteristics for this application. Advanced analysis, simulation and testing were performed to magnetic resonance WPT systems to acquire system performance insight. This was accomplished by evaluating/varying coupling configuration, load effects and magnetic element physical characteristics (i.e. wire material, loop radius, etc.). It was identified by analysis, circuit simulation and testing that the best coupling configuration for this application was series-series and series-shunt with Litz wire loop inductors.

The main concern identified for the implementation of these systems for space applications was radiated emissions that could potentially generate electromagnetic interference (EMI). To address this EMI concern, we developed the Electromagnetic Compatibility Radiated Emissions Compliance Design Evaluation Approach for WPT Space Systems. This approach systematically allocates key analyses, simulations and tests procedures to predict WPT EMC compliance to NASA's EMC standard Mil-Std-461E/F. Three prototype/magnetic elements were successfully assessed by implementing the WPT EMC design approach. The electric fields intensity generated by the WPT prototypes/magnetic elements tested were: 30.02 dBµV/m, 28.90 dBµV/m and 82.13 dBµV/m (requirement limit: 140 dBµV/m). All three prototypes successfully transferred power wirelessly and successfully met the NASA EMC requirements.

This work is dedicated to my wife and son: Jacelis and Sebastián…
Thanks for showing me what life is about...

…to my parents: Dr. Pedro Vázquez Báez and Prof. Myriam R. Ramos Serrano…
Sir Isaac Newton once said: "If I have seen further, it is by standing on the shoulders of giants". Thanks for being those giants in my life…

…and to my sibling, niece and goddaughter: Pedro, María, Myriam, Alanis and Adriana.
Throughout the years, we faced challenges together, we triumphed together, and we grew up together… Thanks for being there…

ACKNOWLEDGMENTS

I would like to thank my professor advisor, Dr. Jiann S. Yuan, for accepting me as one of his PhD students. He allowed me the freedom to pursue and conduct my research to not only answer the university's Electrical Engineering PhD Program requirements, but also to comply with my sponsor's research requirement (NASA-Kennedy Space Center). The laboratory equipment and lab software available in Dr. Yuan's laboratory (UCF Nano-electronics Reliability Laboratory) was a great environment to conduct my research. Thank you for supporting me in pursuing PhD studies in the UCF Electrical Engineering and Computer Science department.

I also would like to thank Dr. Félix A. Soto-Toro for been part of my PhD board and mentoring me though the process of being a full time NASA-KSC engineer and, at the same time, pursue my dreams of completing a doctoral program in electrical engineering. It wasn't easy, but his experience and dedication helped me identify the opportunities and tools available to successfully complete the E.E. PhD program.

I would like to thank the PhD committee members Dr. Kalpathy B. Sundaram and Dr. Thomas X. Wu for their feedback provided throughout the PhD process. Especially for their interest in the publication of my work in the 2012 IEEE SouthEast Conference, in which Dr. Sundaram was the Technical Chair of the proceedings.

My thanks also to my sponsor the National Aeronautics and Space Administration located at Kennedy Space Center. Their involvement constituted a vital support for the completion of this PhD program by accepting me into their KSC Graduate Fellowship Program (KGFP) and

sponsoring my tuition and allowing me times to conduct my research. I would like to also thank Kenneth A. Hale (NASA-KSC's Mission Assurance Branch Chief, my former supervisor) who was my sponsoring supervisor and advocate for my KGFP nomination. Thanks for mentoring me throughout the early years of my career.

My sincere gratitude to NASA's Launch Service Program (LSP) for funding the Wireless Power Transfer for Space Applications experiments and for providing me with the state-of-the-art tools to complete my research. Especially I would like to thank Dr. Paul A. Schallhorn (NASA-LSP's Environments and Launch Approval Branch Chief, my current supervisor), Dr. Dawn H. Trout (NASA-LSP's RF/EMC Team Lead), Paul R. Edwards (NASA-LSP's RF/EMC teammate) and the rest of the NASA-LSP's RF/EMC team. Thanks you very much for been extremely supportive with my academic endeavors and for providing me your LSP launch vehicle flight environments experience. Your support and technical feedback were fundamental for the completion of the PhD program requirements; for that I am deeply grateful.

On a personal note, I would like to thank my parents-in-law Juan García Carambot and Waleska Casillas Santos for providing family support during the completion of this dissertation. Especially before, during and after the birth of my son Sebastián, that overlapped the final year of this study. ¡Muchas gracias!

TABLE OF CONTENTS

LIST OF FIGURES

LIST OF TABLES

LIST OF ACRONYMS AND SYMBOLS

∇	Vector Differential Operator
3D	Three Dimensional
a	Loop Inductor Conductor Radius
AC	Alternate Current
ADS	Advanced Design Systems
AF	Antenna Factor
B	Magnetic Flux Density
c	Speed of Light Constant
C_1	Source (Primary) Coupling Capacitor
C2	Load (Secondary) Coupling Capacitor
D	Separation Distance Between Source and Load
D_e	Electric Flux Density
$D_{RE\text{-}101}$	RE-101 sensor separation distance (= 7cm)
$D_{RE\text{-}102}$	RE-102 sensor separation distance (= 1m)

DC	Direct Current
DoD	US Department of Defense
E	Electric Field Intensity
EMI	Electromagnetic Interference
EMC	Electromagnetic Compatibility
EMPro	Electromagnetic Professional
f_0	Frequency of operation
FDTD	Finite Difference Time Domain
FEM	Finite Elements Methods
G	Antenna Gain
H	Magnetic Field Intensity
IEEE	Institute of Electrical and Electronics Engineers
J	Current Density
k	Mutual Coupling Coefficient
KSC	Kennedy Space Center
L_1	Source (Primary) Inductor Inductance

L_2	Load (secondary) Inductor Inductance
LCR Meter	Inductance, Capacitance, and Resistance Meter
$L_{leakage1}$	Non-Ideal Transformer Model Primary Leakage Inductance
$L_{leakage2}$	Non-Ideal Transformer Model Secondary Leakage Inductance
L_M	Mutual Inductance
LSP	Launch Services Program
Mil-Std	Military Standard
N_1	Number of Turns in the Source (Primary) Inductor
N_2	Number of Turns in the Load (Secondary) Inductor
NASA	National Aeronautics and Space Administration
PA	Power Amplifier
ρ_V	Volume Charge Density
P_W	Power (Watts)
Q-factor	Quality Factor
r	Loop Inductor Radius

R_1	Source (Primary) Inductor Resistance
R_2	Load (Secondary) Inductor Resistance
RE	Radiated Emissions
RF	Radio Frequency
R_{load}	Electrical Load
R_o	Ohmic Resistance
R_r	Radiation Resistance
RS	Radiated Susceptibility
σ	Conductivity
SA	Spectrum Analyzer
S-parameters	Scattering parameters (S_{11}, S_{12}, S_{21} and S_{22})
SPICE	Simulation Program with Integrated Circuit Emphasis
μ_0	Vacuum Permeability
μ_r	Relative Permeability
USAF	United States Air Force
V	Voltage

V_{in}	Input Voltage
VNA	Vector Network Analyzer
ω	Frequency (rad/s)
WPT	Wireless Power Transfer
WPT 4-2	Four Stages-Two Single Loops WPT magnetic element
WPT 4-4	Four Stages-Four Single Loops WPT magnetic element
WPT J1	Two Stages-Two Single Loops WPT magnetic element
Z	Antenna Impedance

CHAPTER ONE: INTRODUCTION

1.1 Motivation

Since the 1950's space exploration has captivated our imagination with extraordinary endeavors such as: first artificial satellite (1957), first animal in orbit (1957), first human in space (1961), first manned moon landing (1969), first Space Shuttle launch (1981), first spacecraft impact with a comet (2005), and so on [1] [2]. All the major space exploration accomplishments to date have something in common: the same power distribution approach from load to source (using cables and physical connections). This dissertation research evaluated the emerging Wireless Electric Power Transfer (WPT) technology and its possible implementation as a power distribution alternative for space systems. A new approach to distribute electrical power can unfold new technologies and missions to expand our capabilities for space exploration [3] [4].

Due to the nature of the WPT technology operation (magnetic resonance), the greatest concern for its implementation into space systems is the electric and magnetic field intensities radiated emissions. The radiated emissions can provide a detrimental effect in the operation of the near-by sub-systems. For that reason, it was developed the Electromagnetic Compatibility (EMC) Radiated Emissions Compliance Design Evaluation Approach for Wireless Power Transfer Space Systems. This design evaluation approach consists of 5 steps that provides WPT system operation insight and EMC requirement compliance predictions taking into account:

(1) WPT parameter computation, (2) circuit simulation to evaluate the electrical models using the Simulation Program with Integrated Circuit Emphasis (SPICE) and Advanced Systems Design (ADS), (3) WPT electromagnetic computational analyses based on the Finite-Difference Time-Domain (FDTD) and Finite Elements Methods (FEM) numerical techniques, (4) electric and magnetic field intensity testing in accordance with the US military standard: Mil-Std-461E/F and (5) simulation and testing compliance evaluation for NASA and military standards for the use in NASA's expendable launch vehicles (rockets).

1.2 Research Goals

The work will focus on solving the following issues:

1. Develop an approach for transmitting electrical power wirelessly within space systems.
2. Evaluate the architectural configuration of wireless power transfer (WPT) systems.
3. Analyze and test the various coupling configurations associated with WPT systems.
4. Analyze and test various magnetic loop materials for wireless power transmission
5. Develop a design research approach to determine WPT systems EMC compliance for space standards currently used by NASA.
6. Computational electromagnetic simulation implementation for radiated emissions characterization.
7. Perform magnetic and electric fields radiated emissions testing to the developed WPT prototypes and magnetic elements.

1.3 Outline

Chapter Two will focus on the wireless power transfer (WPT) techniques known to date, including a thorough comparison and selection of the best technology for space systems. WPT magnetic resonance characterization and modeling will be discussed in Chapter Three. Various WPT experiments analyses and implementations will be provided in Chapter Four. In order to verify compliance with NASA's EMC standards, Chapter Five will describe the developed "EMC Radiated Emissions Compliance Design Evaluation Approach for Space Systems". Three WPT magnetic elements will be used to demonstrate the EMC WPT design approach in Chapter Six and the conclusions will be provided in Chapter Seven.

CHAPTER TWO: LITERATURE REVIEW

There are multiple ways in which a contactless (wireless) power connection can be implemented. Short, medium and long range power transmissions has been studied and implemented throughout the years. The main scope of this research is possible contactless power applications that could be feasible for space systems and, therefore, space exploration. Out of the multiple techniques studied to date, three techniques were identified to be feasible for the application intended: Magnetic resonance, inductive coupling and capacitive coupling. Below is a brief description of these technologies.

2.1 Magnetic Resonance

In classical physics the mechanics of resonance has been widely demonstrated in mechanical applications. Figure 1 illustrates the concept of acoustic resonance: when one of two identical tuning forks is impacted, the other tuning fork will vibrate based on the excitation (resonance) provided by the vibration energy at natural frequency generated by the source tuning fork. A team from the Massachusetts Institute of Technology (MIT) demonstrated this same principle on electric circuits by the implementation of magnetic resonance [3] [5]. It was demonstrated by having a source circuit inducing a resonance (magnetic) signal at a specific frequency through a coil and a secondary circuit, tuned to the same frequency as the primary, was excited by magnetic resonance. This process will transfer energy from the source circuit to the load circuit. The energy received as a magnetic signal is transformed to an electrical signal (output) [3] [5].

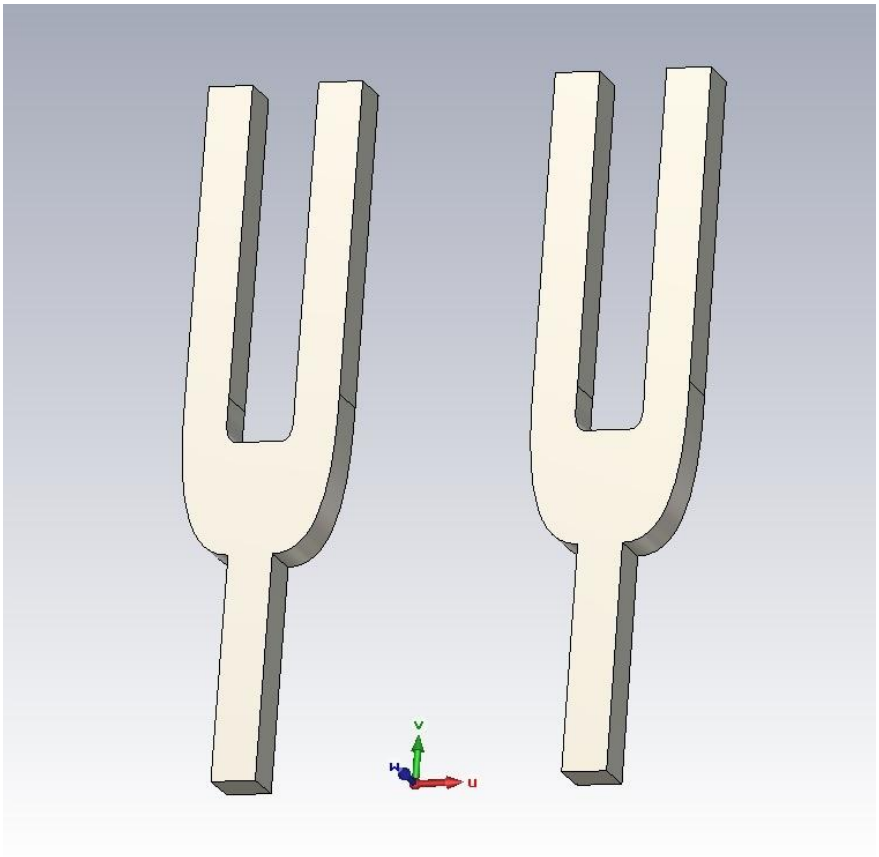

Figure 1: Mechanical example of the resonance concept using tuning folks

2.1.1 Magnetic Resonance Advantages

The major advantage of magnetic resonance is that this system will only transfer power to the loads that are tuned to the same frequency as the source circuit [5]. Since the demonstration of this technology has only been developed for low to medium power (tens of W), under controlled conditions, this implementation can represent no concern to humans working around it [5]. This is due to the fact that the system only produces a magnetic field and, in moderate levels,

magnetic fields are not detrimental to human tissue [5]. The power transmission can extend within a few meters and the efficiency varies with the variation of the distance [5].

2.1.2 Magnetic Resonance Disadvantages

Magnetic resonance is a promising technology but unfortunately it has not been tested for high power applications. It has not been characterized what magnetic fields will be required to transfer power in the order of kilo-watts. Other concern that this technology generates is the study required of the surrounding systems [6] [7] [8] [9]. The system frequency of operation selected to transfer power via magnetic resonance, should be a frequency that cannot excite other communication system, spacecraft circuitry or material. If the frequency selected is the same as any other subsystem or material around, the energy propagated will be dissipated in an unintended material or subsystem.

2.2 Magnetic Induction

Magnetic induction technique can be characterized by a magnetic field generated by an inductor on the primary (source) side and a receiving inductor on the secondary (load) side [10]. The electrical energy is transformed to magnetic signal on the primary side of the system, and the secondary side receives this magnetic signal and transformed into an electrical signal (output) [11]. Figure 2 illustrate a generic block diagram of an inductive coupling contactless power connector.

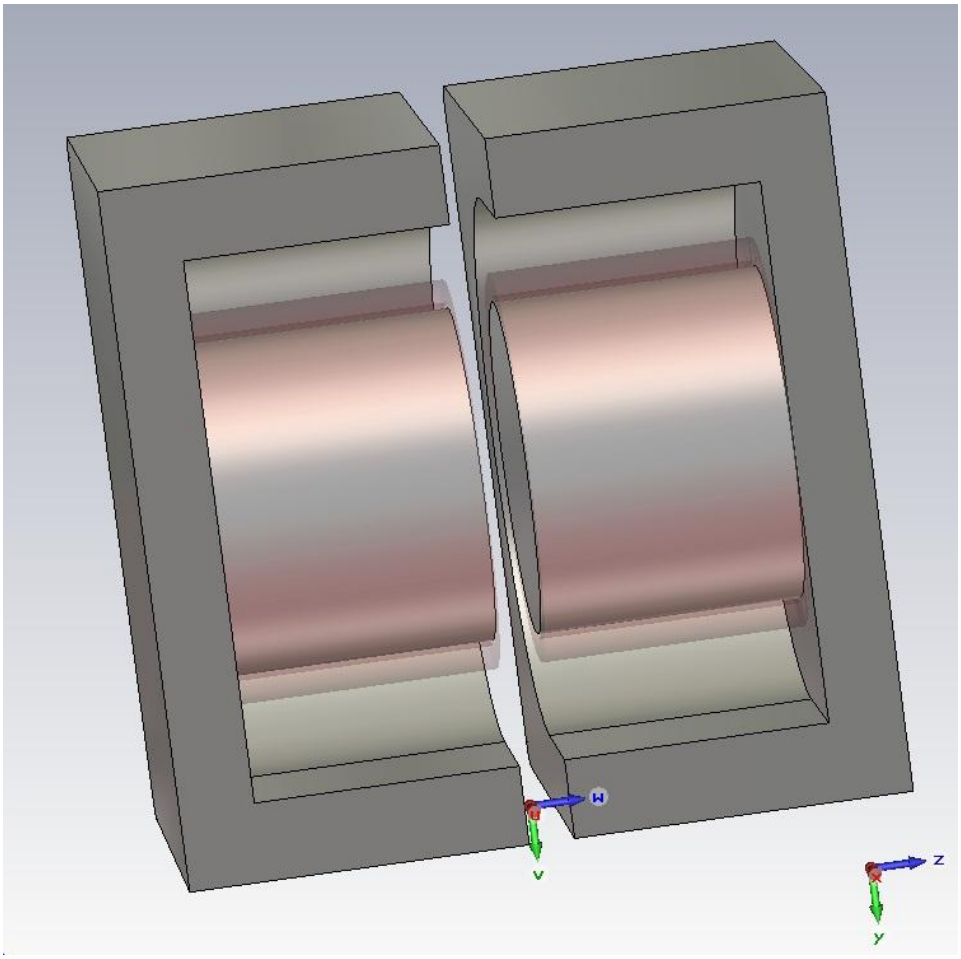

Figure 2: Example of magnetic induction contactless power transfer

2.2.1 Magnetic Induction Advantages

The inductive coupling configuration can achieve one of the highest efficiencies for the contactless technologies (> 90%) [12]. Another advantage of this approach is that the area of magnetic influence is small. This can be a major advantage if the application is highly sensitive to magnetic environments, since the magnetic induction field is localized within centimeters. This has been the reason for its implementation on underwater mining applications (lamp

recharging). The magnetic induction technology has been also implemented for wireless power applications (in the order of kilo-Watts) [12].

2.2.2 Magnetic Induction Disadvantages

One of the major disadvantages is the separation distance between the source and the load; needs to be within a centimeter (cm) [11]. As mentioned previously, the area of influence is considered to be an advantage from the point of view that it has the potential of not affecting electronics that are outside the small magnetic area of influence. However, the two modules of the contactless connector need to be within the area of influence [10] [11].

2.3 Capacitive Coupling

Capacitive coupling consists of a similar approach than the magnetic induction; however, the main difference between the two is the coupling approach. In the capacitive coupling, the capacitance effect is used to transmit the power from the primary to the secondary [13]. This means that the primary (source) will have one set of electrodes that will match with the set of electrodes located at the secondary (load). Figure 3 illustrates a block diagram capacitance coupling contactless power transfer [14] [15].

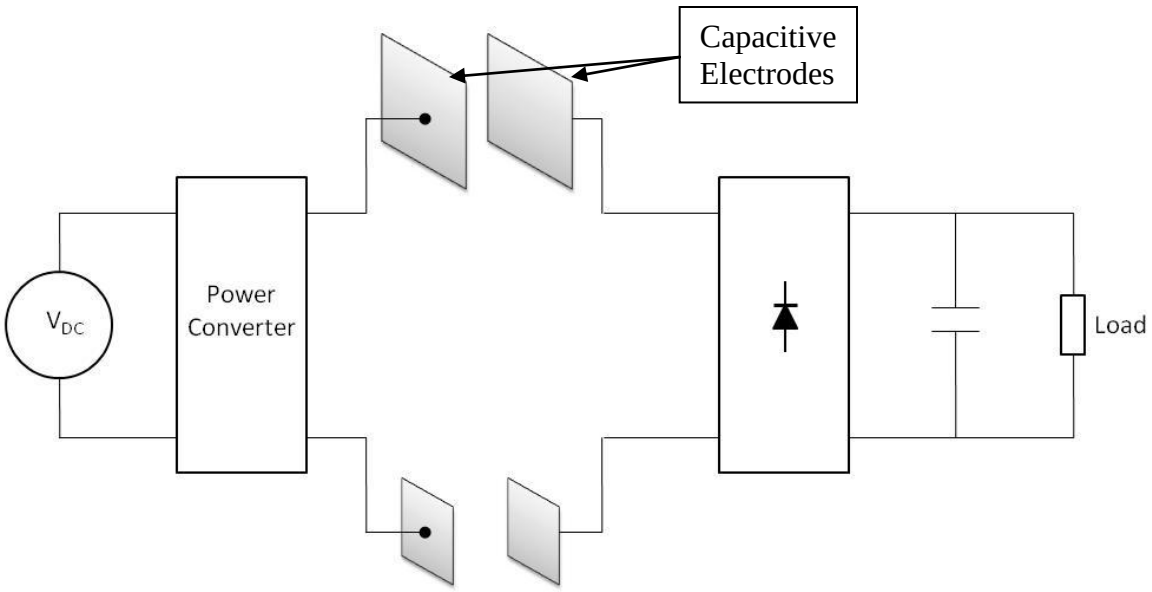

Figure 3: Capacitance Coupling Contactless Power Transfer [14] [15]

2.3.1 Capacitive Coupling Advantages

Compared with the previous two Contactless Power Connector methods, the capacitive coupling provides a contactless solution without the need of using heavy magnetic cores (like in the Inductive Coupling configuration) to transfer the power between the primary and the secondary [13]. This will significantly reduce the total system weight due to the fact that magnetic cores are usually the heaviest component in the Inductive Coupling configuration. Another benefit is the fact that multiple loads can receive power from a single source. An example of multiple loads with a single source is the Duracell charging pad "myGrid" [16].

2.3.2 Capacitive Coupling Disadvantages

The capacitance coupling configuration is commonly used for low power applications (a few W). Similar to a conventional capacitor, by working with large amounts of power, the level of complexity increases. These concerns can become safety issues by dealing with a large electric field in the configuration implemented for the capacitive coupling; capacitive electrodes on the source side generating electric fields with the electrodes on the load side. The separation distance is also relatively small, less than one cm [14] [15].

2.4 Basics of EMC Parameters and Conversions

This section will discuss Decibel conversions for the unit used in later chapters. This section will also discuss the approach to determine the antenna factor for the radiated emissions magnetic and electric field intensities (RE-101 and RE-102) testing.

2.4.1 EMC Decibel Conversions

The following Decibel conversions are commonly used for EMC applications. These equations will be used throughout this study.

Table 1: Decibel conversions are commonly used for EMC applications [17] [18] [19]

From	To	Equation	Equation # in this Document
V	$dB\mu V$	$dB\mu V = 20\ log_{10}(V) + 120$	(1)
$dB\mu V$	V	$V = 10^{[(dB\mu V - 120)/20]}$	(2)
P_W	dBm	$dBm = 10\ log_{10}(P_W) + 30$	(3)
dBm	P_W	$P_W = 10^{[(dBm - 30)/10]}$	(4)
dBm	$dB\mu V/m$	$\frac{dB\mu V}{m} = dBm + 10\log(Z) + 90$	(5)
$dB\mu V/m$	$dB\mu A/m$	$\frac{dB\mu A}{m} = \frac{dB\mu V}{m} - 20\log(Z)$	(6)
$dB\mu A/m$	$\mu A/m$	$\frac{\mu A}{m} = 10^{[(dB\mu A)/20]}$	(7)
$dB\mu A/m$	$dBpT$	$dBpT = \frac{dB\mu A}{m} + 2$	(8)

Where V is voltage, $dB\mu V$ is the voltage in Decibel micro-volts, P_w is power in Watts, dBm is power in Decibel milli-Watts, $dB\mu V/m$ is electric field intensity in Decibel micro-Volts over meters, $dB\mu A/m$ is magnetic field intensity in Decibel micro-Ampere over meters and $dBpT$ is the magnetic field intensity in Decibel pico-Teslas.

2.4.2 Antenna Factor Implementation for Radiated Emissions Testing

One of the greatest challenges of measuring electric and magnetic field intensities is to identify the "real" value once you factor in your equipment performance. A special focus of the radiated emissions testing performed according to Mil-Std-461E/F is the antenna factor. In this subsection we will be evaluating the antenna factor consideration for magnetic field radiated emission and electric field radiated emission.

To determine the effective magnetic field intensity of the experiments including the antenna factor, the following unit conversion strategy is recommended to the spectrum analyzer reading the values recommended in [20]:

$$dBm \rightarrow \frac{dB\mu V}{m} \rightarrow \frac{dB\mu A}{m} \rightarrow dBpT \tag{9}$$

To determine the effective electric field intensity including the antenna factor to the spectrum analyzer reading, the following antenna factor equation need to be implemented [20]:

$$AF = \frac{f_0}{c\sqrt{G}} * \sqrt{\frac{480\pi^2}{Z}} \tag{10}$$

where AF is the antenna factor, f_0 is the frequency of operation, c is the speed of light, G is the antenna gain provided in [21] and Z is the load impedance.

2.4.3 Definition of Radiated Emissions and Radiated Susceptibility

Radiated Emissions (RE) are considered to be the electric (E-Fields) and magnetic (H-Fields) fields generated by an electric device (unintentional radiation) or by Radio Frequency (RF)

system (intentional radiation). Most, if not all, the avionics and electronics systems used for space exploration are EMC tested in accordance of Mil-Std-461E/F to avoid electromagnetic interference (EMI) generated by RE [22]. Radiated Susceptibility (RS) is the immunity of a system to withstand electric and magnetic fields environments [23]. Figure 4 illustrates the definition of radiated emissions and radiated susceptibility.

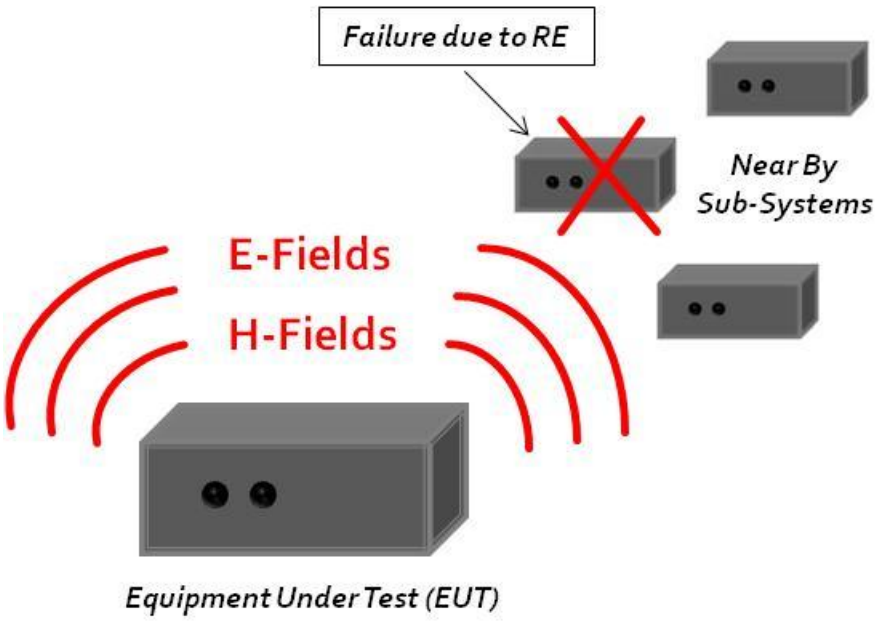

Figure 4: Radiated emissions (RE) and radiated susceptibility (RS) definition

2.5 Computational Electromagnetic Numerical Techniques

Computational electromagnetic numerical techniques will be required to identify the performance and radiated emission characteristics of the wireless power transfer (WPT) prototypes and magnetic elements. Two numerical techniques will be used for performance and radiated emissions characterization: Finite-Difference Time Domain (FDTD) and Finite

Elements Methods (FEM). Both of these computation tools operate using the Maxwell equations in its differential form:

$$\nabla \cdot D_e = \rho_V \tag{11}$$

$$\nabla \cdot B = 0 \tag{12}$$

$$\nabla x E = -\frac{\partial B}{\partial t} \tag{13}$$

$$\nabla x H = J - \frac{\partial D}{\partial t} \tag{14}$$

where ∇ is the vector differential operator, D is the electric flux density, B is the magnetic flux density, E is the electric field intensity, H is the magnetic field intensity, ρ_V is the volume charge density and J is the current density.

2.5.1 Finite-Difference Time Domain (FDTD)

The Finite-Difference Time-Domain (FDTD) computational method operates by simulating the structure or system as a whole by discretizing the structure into cubes (also known as VOXEL) [24]. The E and H components are defined on each cell without the need of matrix solutions as with other computational techniques (i.e. FEM) [25]. FDTD was developed based on the Yee cell, with the special feature that the E and H fields are one half space cell apart. Figure 5 illustrates the electric and magnetic field intensities definitions in accordance to the Yee Cell.

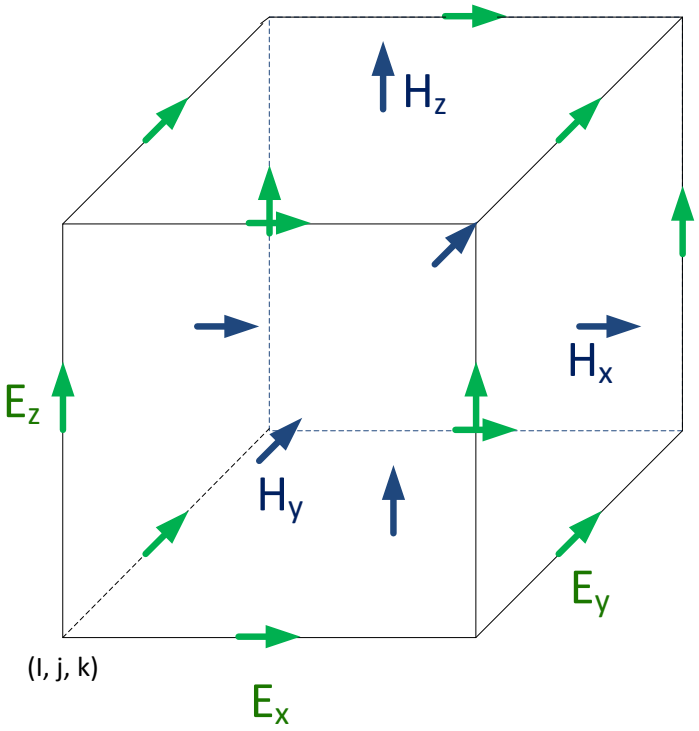

Figure 5: FDTD Yee Cell [24] [25]

Another aspect that makes the FDTD tool a good choice for EM simulation is its capability for simulating in "life-like" events [26]. By simulating in the time domain, the transient events are captured during the simulation. These characteristics will make this computational electromagnetic technique ideal for the characterization of the electric and magnetic field radiated emissions of the wireless power transfer elements (WPT).

2.5.2 Finite Elements Method (FEM)

The Finite Element Method is a computational technique used to solve partial deferential equations by transforming them into a matrix equation [25]. In other words, the problem gets

divided into smaller sections in which are represented as local functions [27]. The fact that the computational tool uses tetrahedral elements provides greatest precision for shapes that are rounded; this is considering the fact that the potential on the corners is calculated [27] [28]. Figure 6 illustrates and example of a FEM tetrahedral element. The FEM computational electromagnetic tool operates in the frequency domain, making this tool ideal to determine scattering parameters (S-Parameters). Another good characteristic about this computational technique is that the results are calculated in steady state.

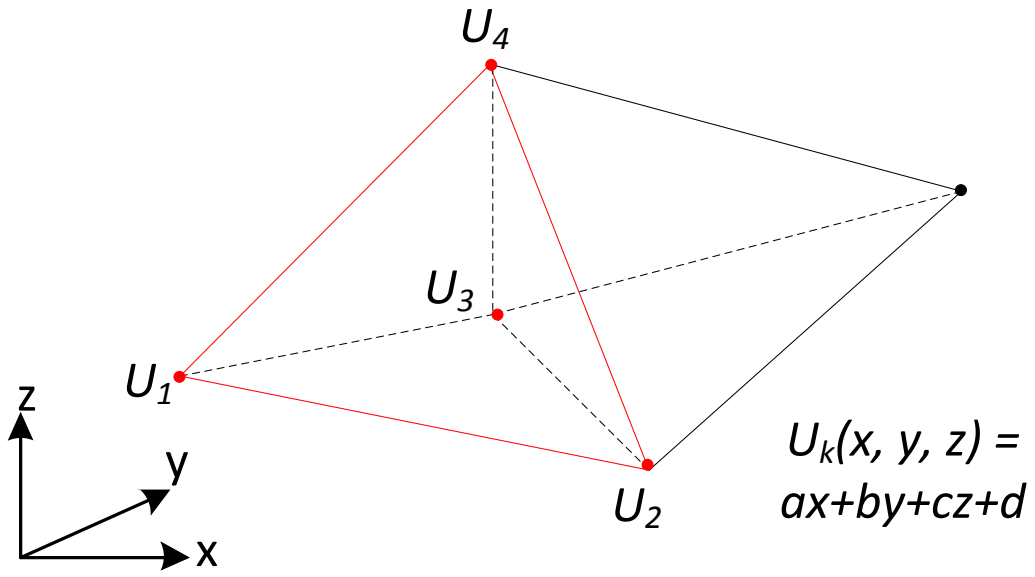

Figure 6: FEM tetrahedral element example [29]

CHAPTER THREE: WPT MAGNETIC RESONANCE MODELING

3.1 Magnetic Resonance Circuit Design

In the late 1800's and early 1900's, Nikola Tesla generated remarkable and unprecedented research regarding alternating current and wireless power transfer. He extensively worked the magnetic principles resulting in a number of US patents for developing apparatus and prototypes that can provide power transmission without cables [30] [31] [32] [33]. Based on the current increase in the use of handheld devices, an increased interest has emerged in the need of wireless power transmission to be use as a recharging minimum. A research team from the Massachusetts Institute of Technology (MIT) has usefully adapted Nikola Tesla's work into a modern solution for wireless power transmission application [5]. This has opened the door for new and innovative applications of this technology, including its use in space systems. [3] [4] [34] [35].

Based on literature review, the wireless power transfer architecture primarily suited for use in space systems will have the components illustrated in Figure 7. The power source (V_{in}) is composed of a DC voltage source supplying electrical power to a Power Amplifier (PA). A function generator will establish the frequency of operation in which the DC power from the source will be amplified by the PA. The amplified power is fed into the source resonator circuit composed of a coupling capacitor (C_1) the source inductor (L_1). The source resonator will be tuned to the same frequency as the function generator and its inductor will generate a magnetic field that will be magnetically coupled with the load resonator inductor (L_2). The load resonator will also have a coupling capacitor (C_2) to maintain a frequency of oscillation similar to the

function generator. The received signal from the load resonator will be rectified by a diode bridge and later filtered by either a capacitor or a DC-DC converter. The load will receive DC power to emulate the power provided by the source without the need to a physical connection with it.

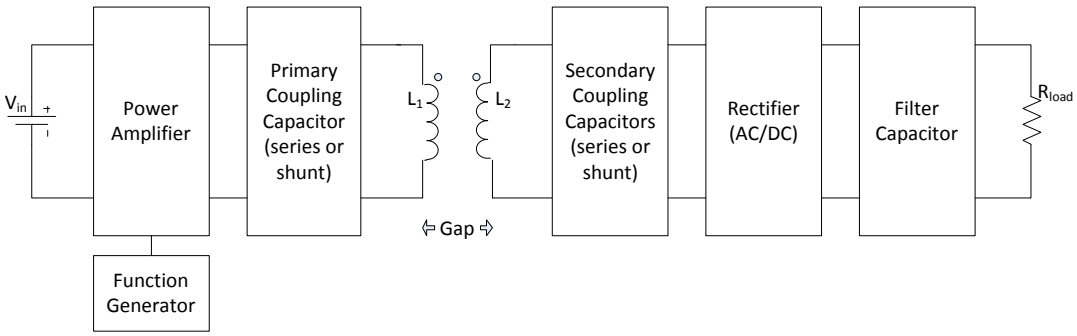

Figure 7: WPT system generic block diagram [3]

The block diagram provided in Figure 7 will be used to describe the general performance of WPT. Since we are considering using a loop inductor with no magnetic core, the inductance is given by [36].

$$L = N^2 r \mu_0 \left[\ln\left(\frac{8r}{a}\right) - 1.75 \right] \tag{15}$$

where N is the number of turns in the loop, r is the radius of the loop, μ_0 is the permeability of vacuum, and a is the loop conductor resistance.

For the source and load resonant circuits, it is important to determine the coupling capacitance required to resonate at the desired frequency. This can be given by: $C = 1/(\omega_0 * L)$; where C is the coupling capacitance required, ω_0 is the frequency of oscillation [rad/sec], and L is the inductance of the coil [18]. By having the source resonant circuit and the load resonant circuit

oscillating at the same frequency, wireless power will be transferred from the source to the load [3] [4]. It is important to mention that these equations are approximations made for solid wire conductors wrapped together; for helix inductors the "1.75" term can be replaced with a "2" [37]. For an accurate representation of the resonant frequency of the system, it is recommended to use an LCR Meter or a spectrum analyzer [3].

Another important parameter for the model characterization of the WPT system is the mutual inductance. This value will be used to during the circuit simulation in order to calculate the overall system performance using the Simulation Program with Integrated Circuit Emphasis (SPICE) and Agilent's Advanced Systems Design (ADS) tool. The mutual inductance can be estimated with [38]:

$$k = \frac{1}{\left[1 + 2^{2/3} \frac{D^2}{r_1 r_2}\right]^{3/2}} \tag{16}$$

where k is the mutual coupling coefficient, D is the physical distance between the first and second inductors (gap), r_1 is the radius of the loop 1, and r_2 is the radius of the loop 2. This mutual coupling coefficient equation can be used to evaluate the wireless power transfer performance based on the separation distance for low to medium power systems [38].

As Figure 1 illustrates, the source (primary) and the load (secondary) circuitry have coupling capacitors right beside the inductor loops. This is to create the resonant circuits in the source and load circuits in order to transfer power wirelessly between them. The coupling capacitors could be located in two configurations per resonator: series or shunt. Four possible cases can be

identified from the WPT under study for the source resonator and load resonator: series-series, series-shunt, shunt-series and shunt-shunt [39].

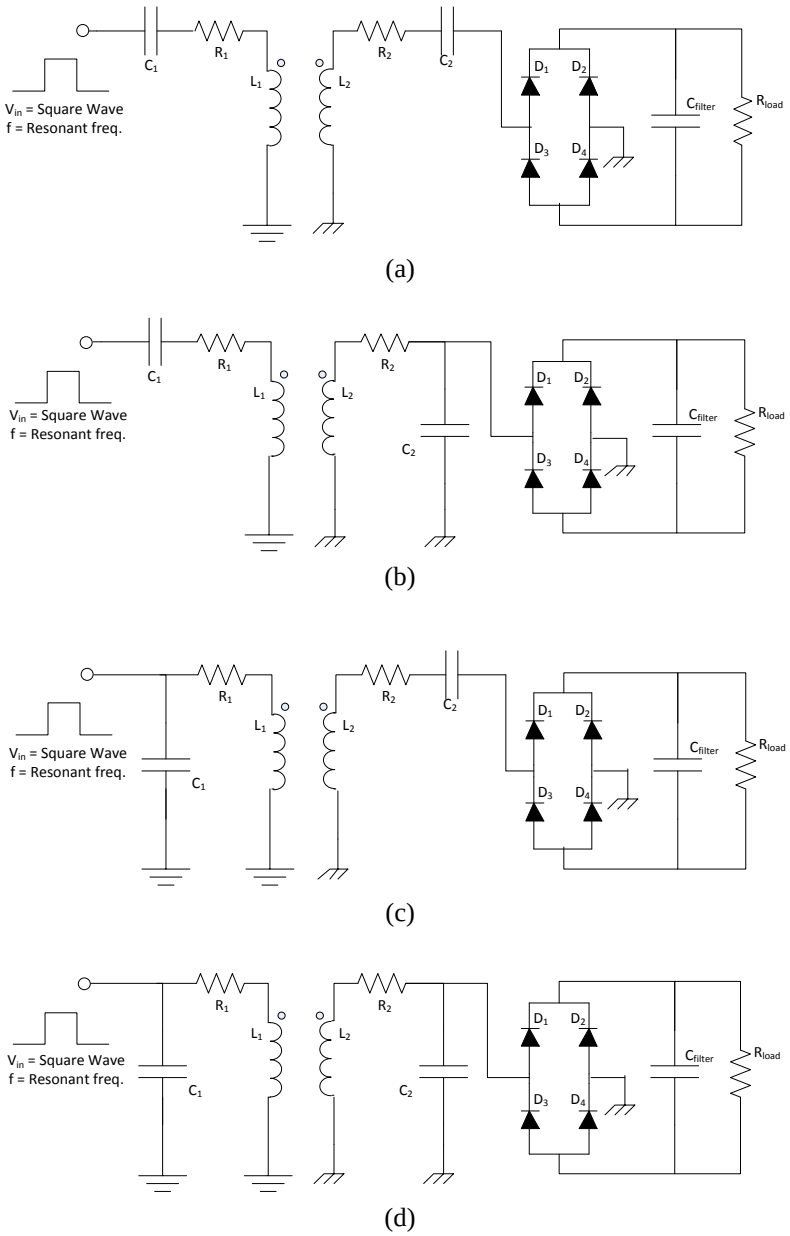

Figure 8: Wireless power transfer models coupling configuration to be evaluated: (a) series-series coupling, (b) series-shunt coupling, (c) shunt-series coupling, and (d) shunt-shunt coupling [4].

With the mutual coupling coefficient provided in Equation 16, the mutual inductance (L_M) can be calculated with: $L_M = k\sqrt{L_1 L_2}$; where L_1 is the inductance of the loop 1 and L_2 is the inductance of the loop 2 [40].

Another important parameter for the implementation of circuit equivalent models is the loop series resistance R. This loop series resistance is composed by adding the ohmic resistance (R_o) and the radiation resistance (R_r) [37]:

$$R_o = \sqrt{\frac{\omega * \mu_0 * \mu_r}{2\sigma}} * \frac{r}{a} \tag{17}$$

$$R_r = 20\left[\left(\frac{2\pi f_0}{c}\right)^2 * \pi r^2\right]^2 \tag{18}$$

Figure 9 illustrates the circuit equivalent circuit used for the simulation of the hollow (non-core) loops in WPT systems taking the coupling coefficient factor model approach and transforming it into the non-ideal model.

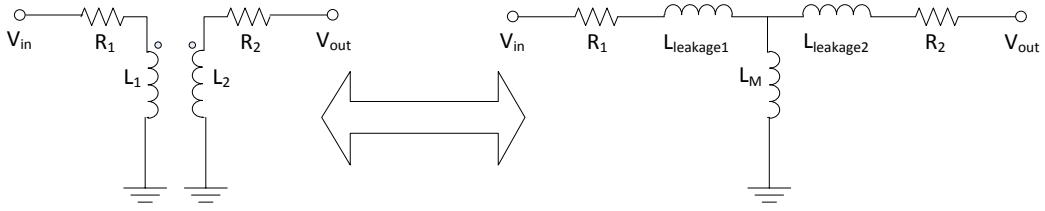

Figure 9: Equivalent circuit of the hollow inductors (N_1=N_2): on the left is the coupling coefficient (k) factor model approach and on the right is the non-ideal transformer model [41]

3.2 WPT System Circuit Simulation

Various experiments will be later discussed in Chapter Four. However, to demonstrate the WPT system circuit simulation approach, the parameters of the WPT system advanced characterization will be used in this section. Table 2 list the parameters required for the development of the WPT system proof-of-concept prototype [4]. The values were selected in order to create a system that can transfer ~ 5W of power for a separation distance of 3 to 5cm. This subsection will demonstrate how to use the parameters derived to execute the SPICE simulation.

Table 2: WPT system advanced characterization prototype characteristics

Parameter	**Symbol**	**Value**	**Units**
Number of turns	N_1 & N_2	8	turns
Radius of the Loops	R_1 & R_2	0.12	m
Loop conductor radius	r_1 & r_2	~ 0.001	m
Loop conductor resistance (for 20 kHz)	a	~ 0.4	Ohm
Frequency of operation	f_0	~15	kHz
	ω_0	94.24	kRad/s
Vacuum Permeability	μ_0	$4*\pi*10^{-7}$	H/m
Separation distance	D	0.03	m
Load	R_{load}	4	Ohms

With the characteristics for the two hollow loops proof-of-concept prototype we can calculate the required additional parameters for the circuit model, as described earlier in the section 3.1.

These parameters include: loops self inductance, mutual inductance, coupling capacitance and leakage inductances. Table 3 illustrates the calculated prototype circuit parameters required for the circuit simulation.

Table 3: Calculated prototype circuit parameters from specifications provided in Table 2

Parameter	**Symbol**	**Value**	**Units**
Self Inductance	L_1 & L_2	49.38	µH
Mutual Inductance	L_m	42.85	µH
Coupling Capacitor	C_1 & C_2	2.2	µF
Leakage Inductances	$L_{leakage1}$ & $L_{leakage2}$	6.533	µH

Using the parameters provided by Table 2 and the parameters calculated in Table 3, a series of SPICE and ADS simulations were performed. Since we are also interested in the performance variations provided by coupling configurations in Figure 8, individual simulations will be performed for each case. Figure 10 illustrates the output power of the four WPT prototype simulations (one for each coupling configuration). The SPICE netlists of these simulations are documented in Appendix B.

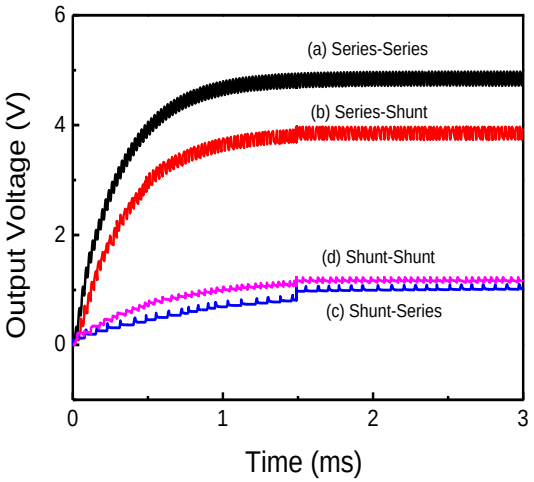

Figure 10: WPT system prototype SPICE simulations varying the capacitor coupling configurations: (a) series-series, (b) series-shunt, (c) shunt-series, and (d) shunt-shunt

It can be seen in Figure 10 that the coupling configurations of interest for this application are series-series and series-shunt. This is due to the fact that SPICE simulation shows a significant advantage of having a series coupling configuration in the source circuitry (Figure 8a and Figure 8b) by having greater output voltage. The shunt coupling configuration in the source circuit (Figure 8c and Figure 8d) provides a significant less desirable performance providing less output power. Therefore some of the analyses will be focusing only on the coupling configurations that contains series coupling configurations (Figure 8a and Figure 8b).

3.3 WPT Equivalent Impedance Characterization

An additional parameter to determine the performance of the WPT system is its equivalent input impedance. This can be a useful parameter for the design of the PA output impedance and establish an impedance matching strategy with the WPT system. The WPT system equivalent

impedance is defined in Figure 11 for the two coupling configurations with better performance (series-series and series shunt), as identified in the previous subsection (3.2).

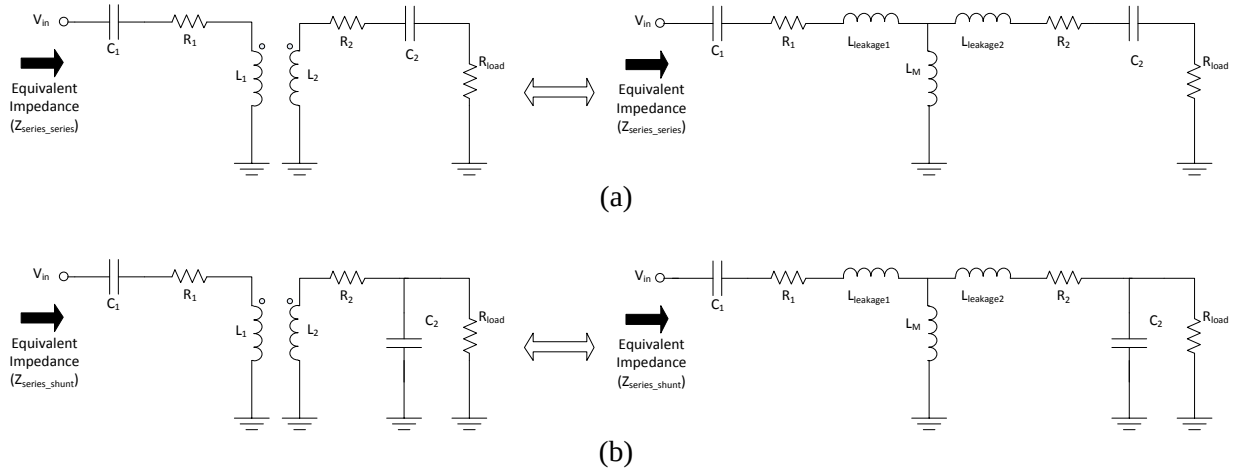

Figure 11: Circuits used to determine equivalent impedance: (a) series-series coupling configuration and (b) series-shunt coupling configuration

The equivalent impedance of the WPT system with the series-series coupling configuration (Figure 11a) was derived and illustrated in Equation 19. The equivalent impedance of the WPT system with the series-shunt coupling configuration (Figure 11b) was derived and illustrated in Equation 20. These derivations were performed using Matlab's Symbolic Math Toolbox. The Matlab code generated to solve these equivalencies is provided in Appendix C.

$$Z_{series-series} = R_1 + sL_{leakage1} + \frac{1}{sC_1} + \frac{1}{\frac{1}{R_2 + R_{load} + sL_{leakage2} + \frac{1}{sC_2}} + \frac{1}{sL_M}} \tag{19}$$

$$Z_{series-shunt} = R_1 + sL_{leakage1} + \frac{1}{sC_1} + \frac{1}{\frac{1}{R_2 + sL_{leakage2} + \frac{1}{sC_2 + (1/R_{load})}} + \frac{1}{sL_M}} \tag{20}$$

A Matlab program was generated to automatically calculate the numerical equivalent impedance for the WPT series-series and series-shunt system configurations given the parameters provided in Table 2. The output of this program is illustrated in Figure 12, and the Matlab code created for this program is provided in Appendix D.

```
########################################################################
########################################################################
###                                                                  ###
###           WPT Equivalent Impedance Calculation                   ###
###    Series-Series and Series-Shunt Coupling Configuration         ###
###            Prepared by: Gabriel Vázquez Ramos                    ###
###                                                                  ###
########################################################################
########################################################################


**********************************************************************
***                          OUTPUT                                ***
**********************************************************************


Equivalent WPT Impedance with Series-Series Coupling:

Zeq_series_series =

   9.0938 - 0.2115i


Equivalent WPT Impedance with Series-Shunt Coupling:

Zeq_series_shunt =

   3.5981 - 4.8686i
```

Figure 12: Matlab program generated to automatically calculate the equivalent input impedance for series-series and series-shunt WPT system coupling configurations

CHAPTER FOUR: WPT SYSTEMS ADVANCED CHARACTERIZATION ANALYSIS AND PROTOTYPE IMPLEMENTATION

4.1 WPT Technology Pathfinder Demonstration

Chapter 3 provides a generic approach to design WPT systems. However, before developing advanced WPT prototypes, a WPT technology pathfinder demonstration was performed. The purpose of this experiment is to provide a midpoint between WPT system design and system prototype by focusing in the most challenging aspect of the WPT systems: the magnetic element.

4.1.1 Pathfinder Demonstration Analysis

The technical approach for the demonstration of wireless power transmission with this experiment was to develop two hollow loop inductors and test them for various frequencies. The scope of this prototype demonstration is to measure voltage induction in the load loop due to magnetic resonance. Table 4 lists the characteristics of the inductor pairs. The three frequencies of operation selected for the demonstration were: 84 kHz, 839 kHz and 1.757 MHz.

Table 4: WPT technology pathfinder demonstration loop design characteristics

Characteristic	**Magnetic Loop 1**	**Magnetic Loop 2**
Radius [cm]	*7.5*	*7.5*
Number of Turns	*7*	*7*

Based on the design approach proposed in Chapter 3, the coupling capacitances for the WPT magnetic element were identified for all three frequencies of operation. Appendix E shows the MathCAD calculation file used for the determination of the prototype coupling capacitances.

4.1.2 Pathfinder Demonstration Experiment

Using the test configuration illustrated in Figure 13, the WPT technology pathfinder demonstration prototype experiment configuration was tested for: 84 kHz, 839 kHz and 1.757 MHz. The function generator was adjusted to the frequency of operation while the coupling capacitors (C_1 and C_2) were used in accordance with the calculation showed in Appendix E for its correspondent frequency. It used the same function generator voltage setting for all the cases: 20 $V_{Pk\text{-}Pk}$. The loops separation distances selected for this pathfinder demonstration are: 0 cm, 4 cm and 14 cm. Figure 14 illustrates the output power provided by the three frequencies tested (84 kHz, 839 kHz and 1.757 MHz) at the three separation distances evaluated (0 cm, 4 cm and 14 cm). It was demonstrated that wireless power was transferred for all the cases tested and agreement was demonstrated between the design approach and prototype experimentation.

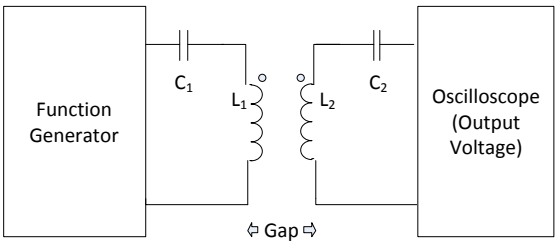

Figure 13: WPT technology pathfinder demonstration prototype testing configuration

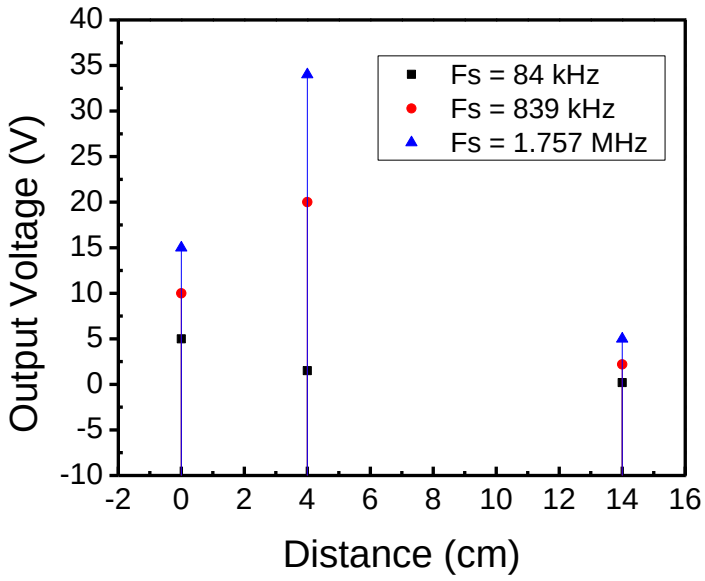

Figure 14: WPT technology pathfinder demonstration output voltages for the frequencies evaluated (84 kHz, 839 kHz and 1.757 MHz) and the separation distances evaluated (0 cm, 4 cm and 14 cm)

4.2 Proof-of-Concept Prototype

After demonstrating wireless power transmission in the previous sub-section *(WPT Technology Pathfinder Demonstration)* with the recommended approach in Chapter Three, a proof-of-concept prototype was designed to operate as a standalone device. The main objective of this experiment was to demonstrate wireless power transfer capability from a standalone device.

4.2.1 Proof-of-Concept Prototype Analysis

The first step taken was to look for the required components illustrated in Figure 7. Table 5 provides a description of the components selected for the small scale proof-of-concept prototype and its description.

Table 5: Small scale proof-of-concept prototype components

Component	**Description**	**Comments**
Input Voltage	DC power source that provides 30V to the multiple electronics components.	Lexmark z23 printer power adapter (30 Vdc and up to 0.5 Amp) [42].
Power distribution elements (V_{IN})	The voltage was stepped down with voltage regulators to support the multiple electronics components and input voltage requirement needs.	LM7809, LM7812 and LM7815 were used [43].
Function Generator	Two function generation approaches where taken: IC oscillator and audio track programmed with a sinusoidal at the desired frequency	(1) XR2206 function generator integrated circuit [44] and (2) Matlab "*wavwrite()*" command for audio track [45] .
Power Amplifier (PA)	An audio power amplifier was used since the frequency of operation was within audible frequencies (15.56 kHz).	Velleman-Kit 4001 7W Audio Power Amplifier [46].
Coupling Capacitors (C_1 & C_2)	Using the design approach proposed in Chapter three, coupling capacitors were calculated	$C_1 = C_2 = 2.2$ µF ± 10% (The frequency of operation of this prototype is 15.56 kHz)
Loop inductors	The loop inductors were manually manufactured according to the requirements previously established	The loops were made out of Litz wire, 8 turns, radius of 12 cm, and a conductor radius of 1 mm
AC/DC Rectifier	A Schottky barrier rectifier diode bridge was used	Part number 1N5817 [47]
Filter Capacitor	To reduce the ripple voltage of the diode bridge, a electrolytic capacitor will be used.	100 µF
Load	Light bulb	4 Ω

The WPT circuit selected to be used is based on the series-shunt capacitor coupling configuration due to the fact that this was one of the best performing coupling configurations as discussed in Chapter Three. Using the WPT schematic provided in Figure 8b and the approach delineated in Chapter Three to acquire the system parameters, a SPICE simulation was

performed to characterize the output voltage of the system (Figure 15). The SPICE netlist used for the SPICE simulation output in Figure 15 is provided in Appendix F.

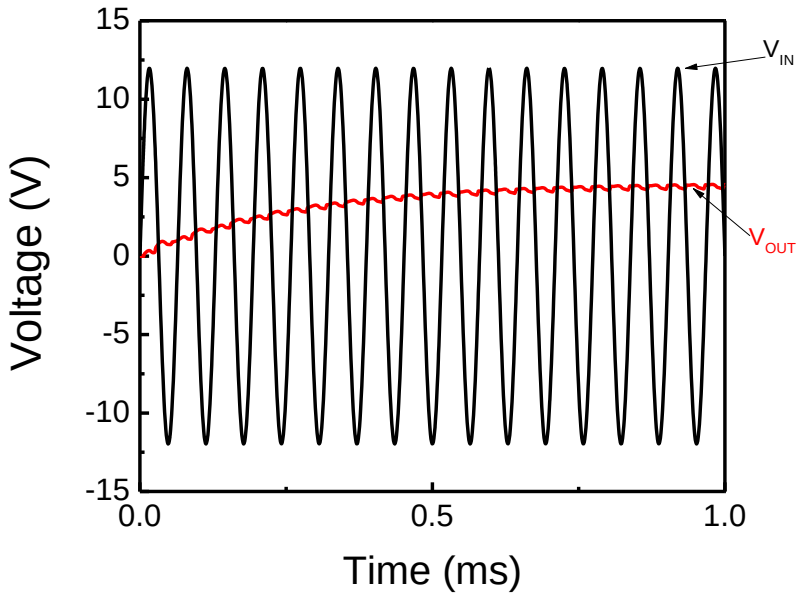

Figure 15: Small scale proof-of-concept prototype SPICE simulation to characterized the WPT system output voltage based on the characteristics provided in Table 5

4.2.2 Proof-of-Concept Prototype Testing

The proof-of-concept prototype successfully transfers power wirelessly as a standalone unit. Figure 16 illustrates the operational small scale proof-of-concept prototype. The load (light bulb) turned on at a distance of about 15 cm from the source, with the highest intensity at about 3 cm. To evaluate the performance of the WPT system, a series of measurements were taken in various points in order to characterize the circuit behavior.

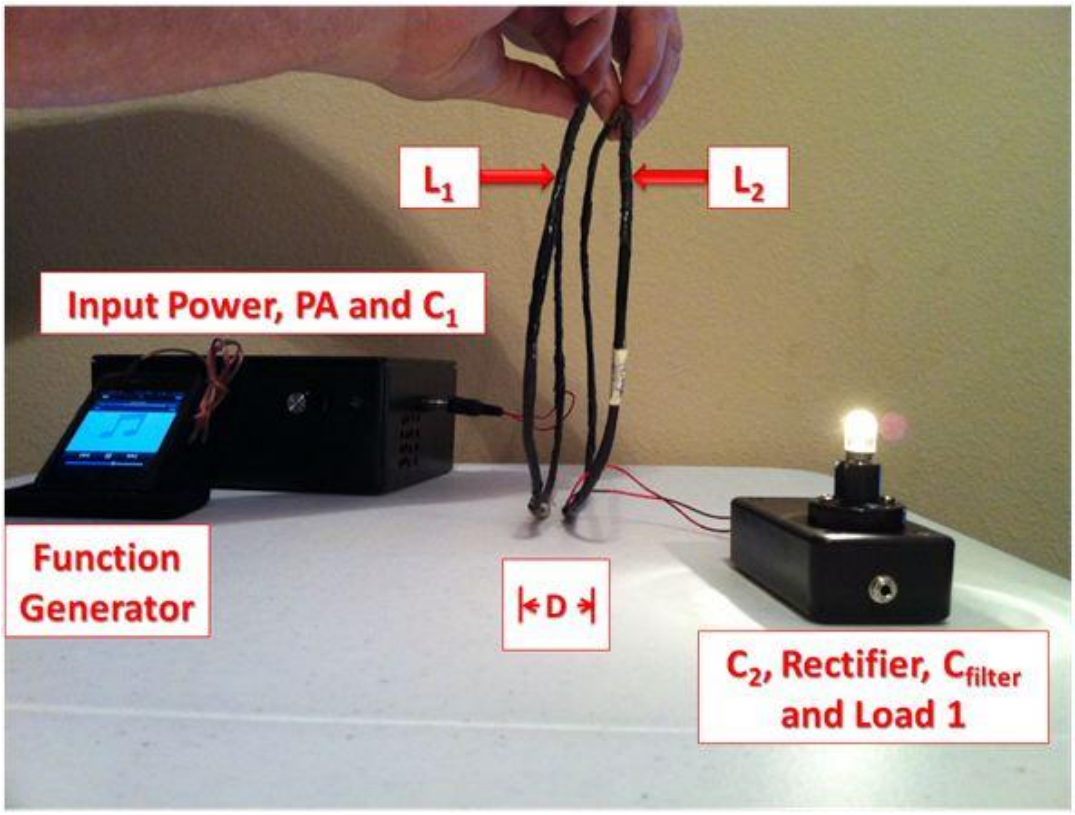

Figure 16: Operational small scale WPT proof-of-concept prototype

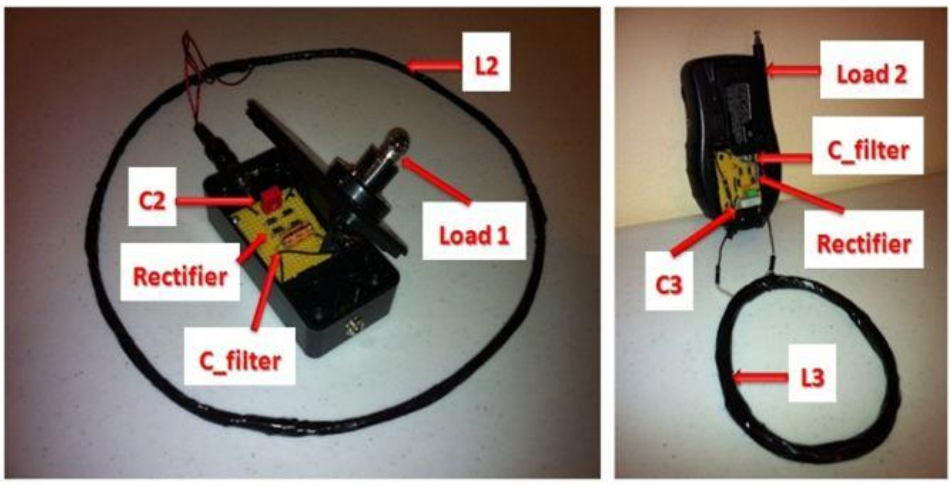

(a) (b)

Figure 17: Small scale WPT proof-of-concept prototype loads: (a) light bulb receiver circuit and (b) handheld radio with a WPT receiver to be operational without batteries

The WPT system showed in Figure 16 performed as expected. The excitation signal was initiated by the function generator (Figure 18) with a frequency of approximately ~15 kHz. This signal was later amplified by the PA and the source resonant circuit (C_1 and L_1) oscillated at the same frequency as the function generator allowing a magnetic field to be propagated. The load resonant circuit, composed of L2 and C2, received the magnetic signal and transformed into an AC electric signal (Figure 19). The signal at the load resonator circuit was rectified by a diode H-bridge and a filter capacitor, providing a DC signal to the load (Figure 20). It is important to note that there was agreement between the WPT system simulation (Figure 15) and the prototype output (Figure 20) validating the functionality and applicability of the WPT design approach proposed in Chapter Three.

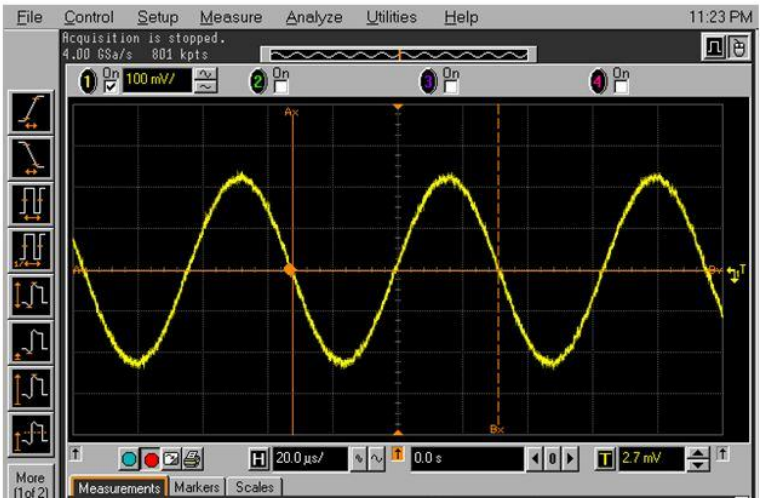

Figure 18: WPT proof-of-concept prototype function generator voltage signal

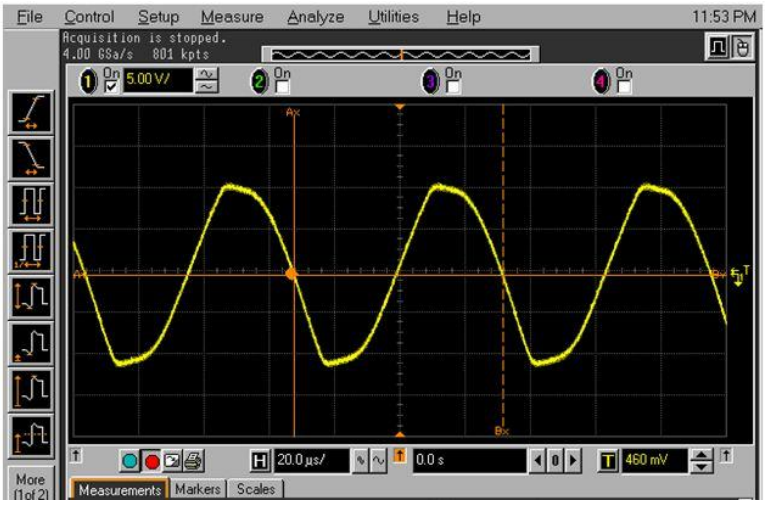

Figure 19: WPT proof-of-concept prototype load loop (L_2) AC voltage signal

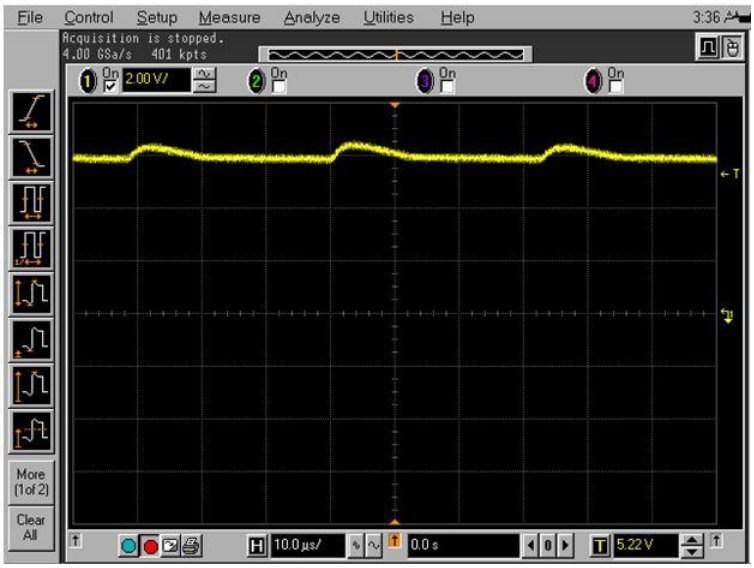

Figure 20: WPT proof-of-concept prototype light bulb (load) DC voltage signal

4.3 WPT Systems Advanced Characterization

After successfully demonstrating the standalone capabilities of WPT systems, and advanced characterization approach was executed to acquire additional insight in these systems. In this sub-section (WPT systems advanced characterization) we will be evaluating a series of prototypes with variations in some of the key WPT system components in order to determine the most effective design.

4.3.1 WPT Systems Advanced Characterization Analysis

The loop inductors are considered one of the most critical items in the WPT system. Therefore a great emphasis will be placed on these components. Three types of wire materials will be used for the loop inductors to determine the impact on overall system performance: solid wire (single conductor), speaker wire (multiple conductor) and Litz wire (insulated multiple conductors). A specific characterization of the loop inductance and loop Q-factor will be performed to determine the best material. The WPT prototypes were designed in a way that the parameters under comparison could be easily varied and data could be captured for the various test cases. Figure 21 illustrates the WPT system advanced characterization test setup. Other than the loop material characterization, the coupling configuration and the load will be varied in order to identify the overall WPT system performance effect. Since the WPT systems advanced characterization prototypes of this subsection will have the same system characteristics of Table 2 and Table 3, the SPICE simulation results previously showed in Figure 10 will be applicable for this analysis.

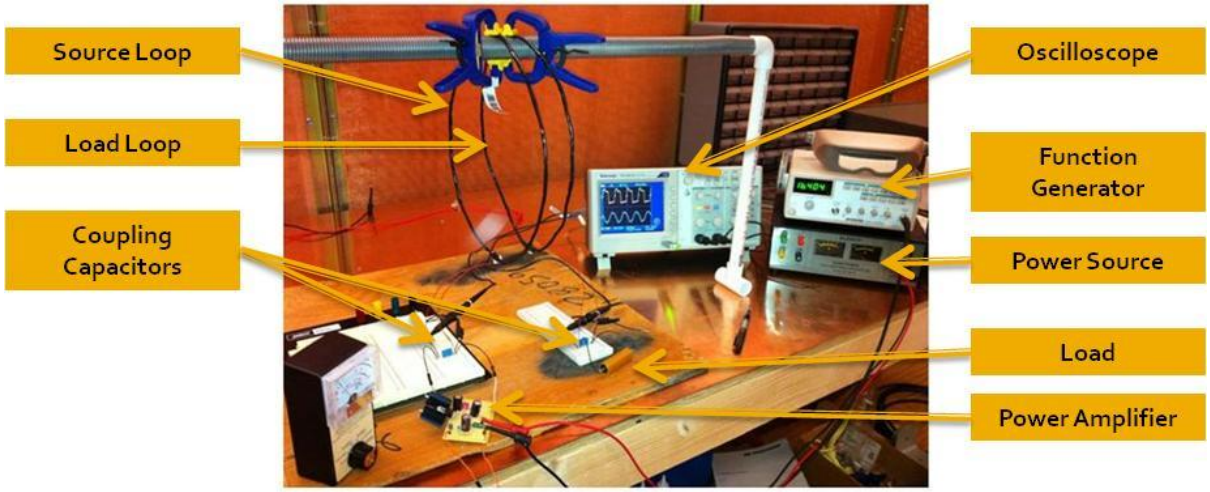

Figure 21: WPT systems advanced characterization test setup

This WPT advanced characterization analysis will involve the use of inductor loops with four different loop radius (1.5 cm, 3.5 cm, 5 cm and 12 cm) and three different loop materials (solid, speaker and Litz wire). Since there is a pair of inductor loops for each of these cases (radius vs. conductor material), a total of 24 loops were tested for inductance and Q-factor properties. Figure 22 illustrates the twelve loop pair cases used in the WPT advanced analysis.

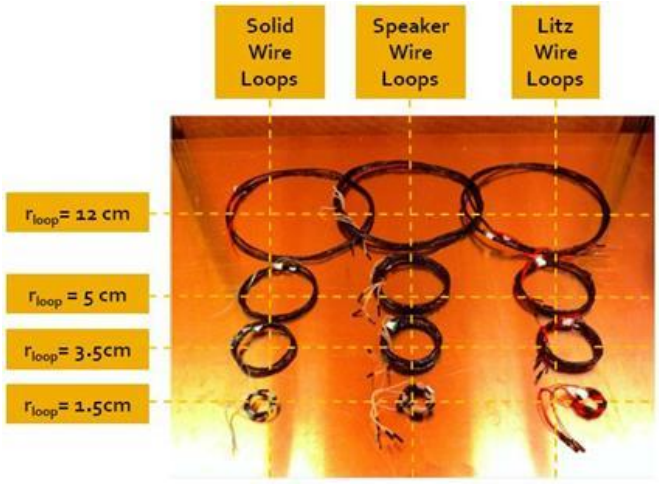

Figure 22: Twelve loop pairs cases used of the WPT advanced analysis characterization

The inductances were measured for all the 12 cases (24 loops) to identify the accuracy of the calculated inductance versus the conductor material and size performance. Figure 23 illustrates the measured inductances the 12 cases divided by inductor loop size: (a) 1.5 cm of radius, (b) 3.5 cm of radius, (c) 5 cm of radius, and (d) 12 cm of radius. Except for the Litz wire and the speaker wire inductor loops with 12 cm radius (Figure 23d), it can be noticed that for all the rest of the cases the inductance remained relatively steady. This could be due to the proximity effect.

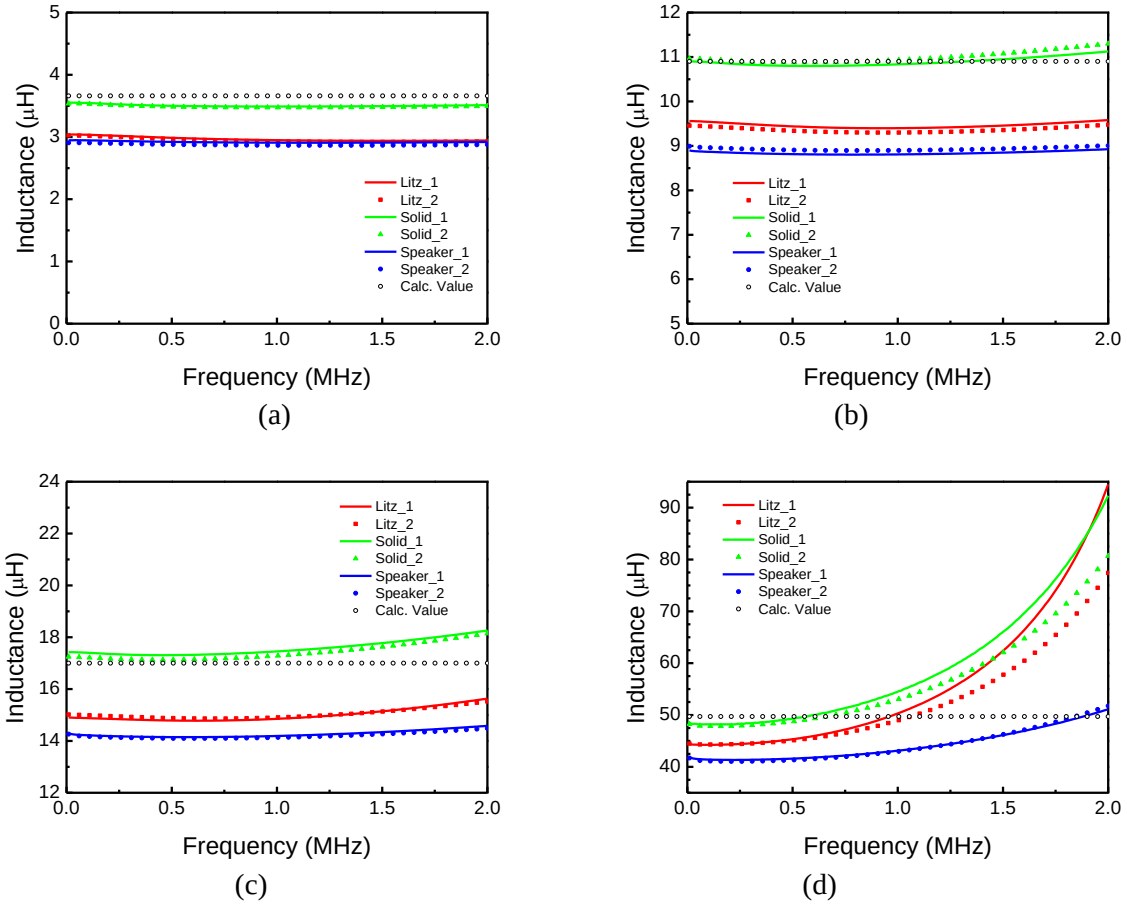

Figure 23: Measured inductances for the designed hollow loops inductors: (a) 1.5 cm of radius, (b) 3.5 cm of radius, (c) 5 cm of radius, and (d) 12 cm of radius.

An additional loop characteristic that is considered a key parameter for wireless power transmission is its Q-factor. Having a greater Q-factor is desirable since the number of oscillations that are possible within the inductor increases without fast dissipation of energy with parasitic resistances [18]. Figure 24 illustrates the measured Q-factors for the designed hollow loops inductors for the four radius cases previously mention. For the low frequencies that we are intending to operate (~20 kHz), the best performing loop from the Q-factor stand point is the Litz wire with a radius of 12 cm.

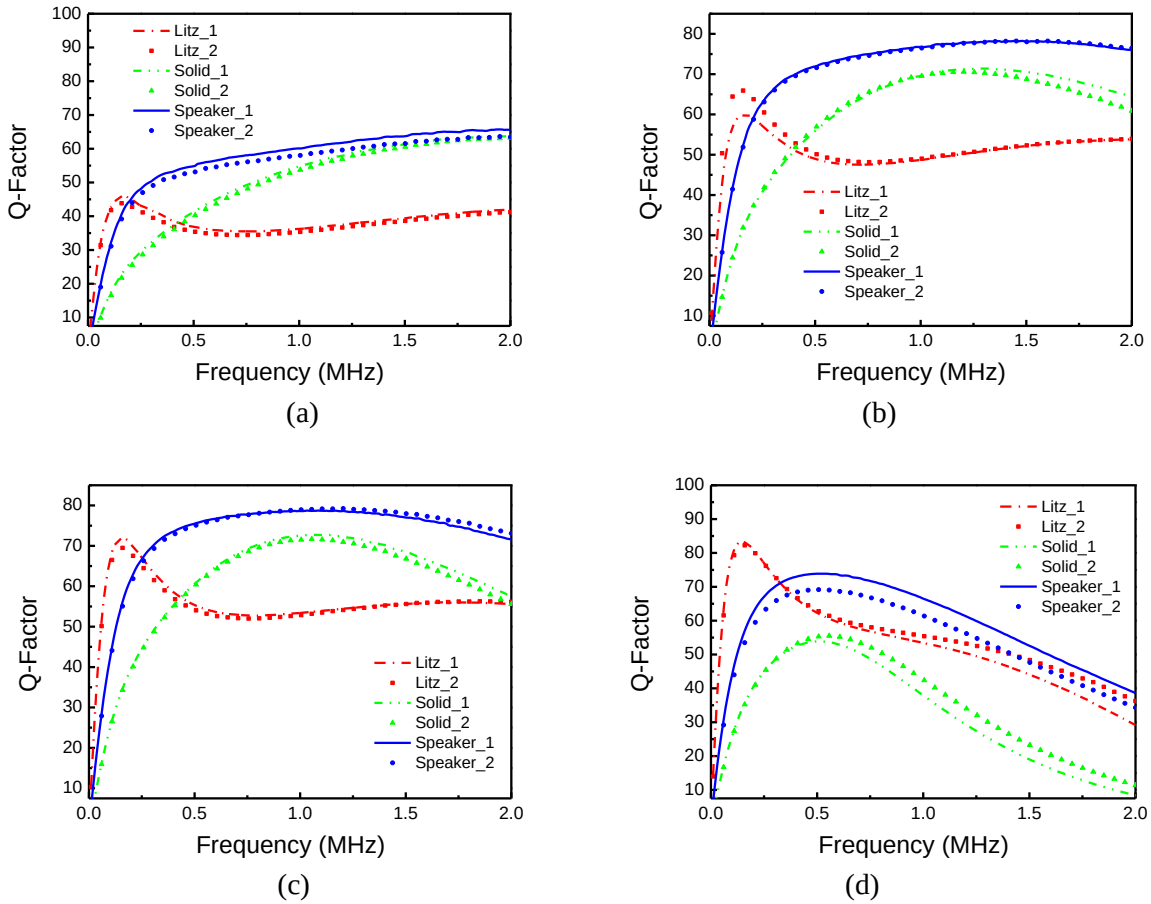

Figure 24: Measured Q-factors for the designed hollow loops inductors: (a) 1.5 cm of radius, (b) 3.5 cm of radius, (c) 5 cm of radius, and (d) 12 cm of radius.

4.3.2 WPT System Advanced Characterization Testing

After the loop inductor characterization was completed in the previous section and the rest of the WPT systems have been evaluated, a series of advanced characterization testing was performed to various prototypes. To narrow down the best capacitive coupling configuration for this WPT application, an advanced characterization testing was developed to validate the results shown in Figure 10, favoring by SPICE simulation the series-series and series-shunt configurations. It can be noticed comparing Figure 10 and Figure 25 that there is agreement between the SPICE simulation and the prototype testing, validating that the two best performing coupling configurations are series-series and series-shunt.

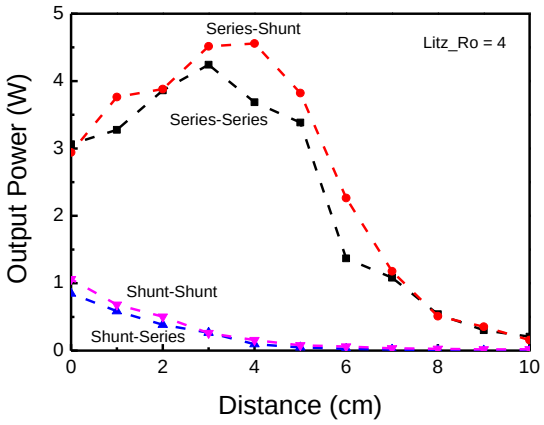

Figure 25: Measured output power vs. separation distance for WPT prototypes with Litz wire inductor loops (12 cm of radius) and 4Ω load with varying their coupling configurations as shown in Figure 8

Some of the WPT system analysis variation experimented were the two best performing coupling configurations illustrated in Figure 25 (series-series and series-shunt), the three inductor conductor materials (solid, speaker and Litz wire) and varying the output resistance (2.5Ω and

4Ω). This gives a total of 12 WPT prototypes tested during this advanced analysis characterization. Figure 26 illustrates the measured output powers versus separation distances (1 to 10 cm) of the WPT prototypes by varying the loop material, coupling configuration and load: (a) Litz wire inductors, (b) Solid wire inductors, and (c) speaker wire inductors.

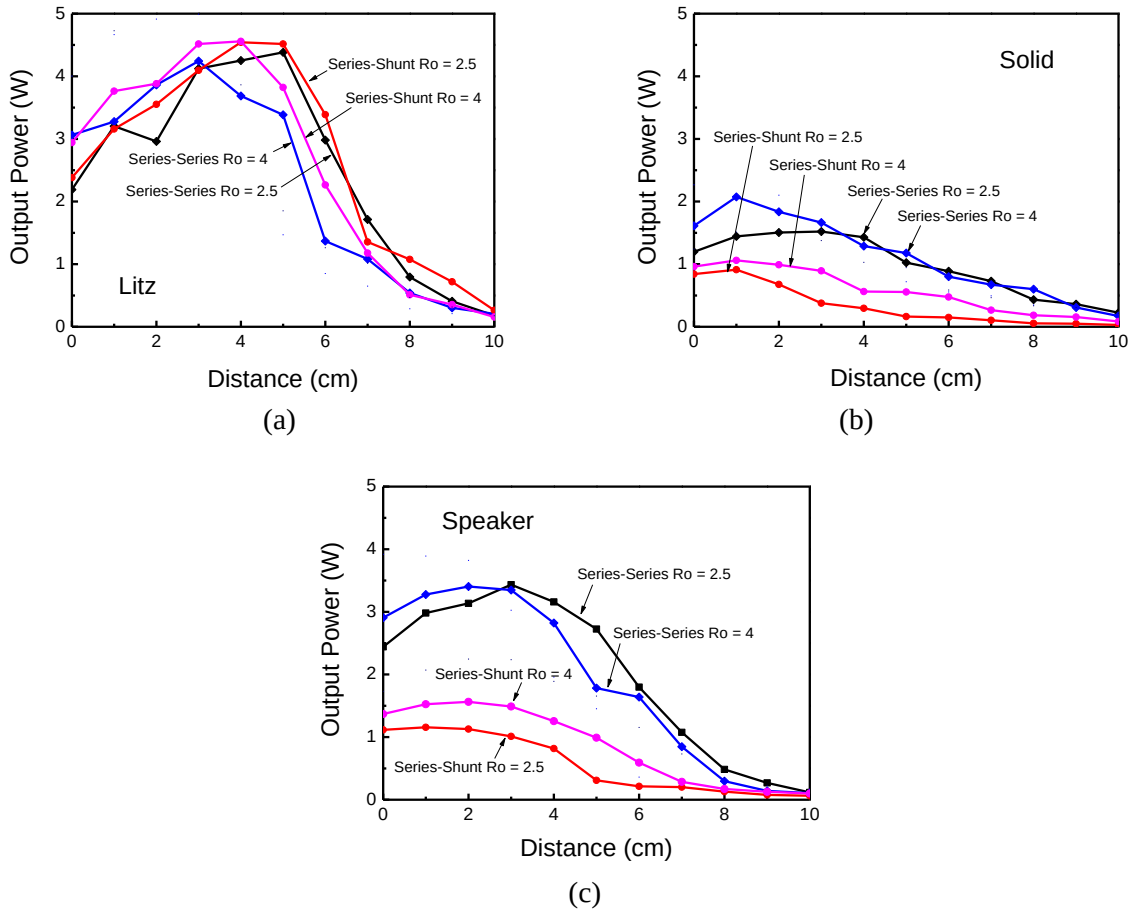

Figure 26: Measured output powers varying the loop material, coupling configuration and load: (a) Litz wire inductors, (b) Solid wire inductors, and (c) speaker wire inductors

Output voltage measurements at a separation distance (D) of 3 cm were taken for all the WPT prototype systems evaluated. By varying the load (2.5 Ω and 4 Ω), the coupling configurations

(series-series, series-shunt, shunt-series, and shunt-shunt) and the inductor loop material, a total of 24 WPT prototype variations were tested. Figure 27 and Figure 28 illustrates output voltage of these prototypes in radar plots. The testing results agree with simulation and analysis by identifying the 4 Ω load, Litz wire inductor material, and the series-series/series-shunt coupling configurations as the best performing characteristics from the ones analyzed and tested.

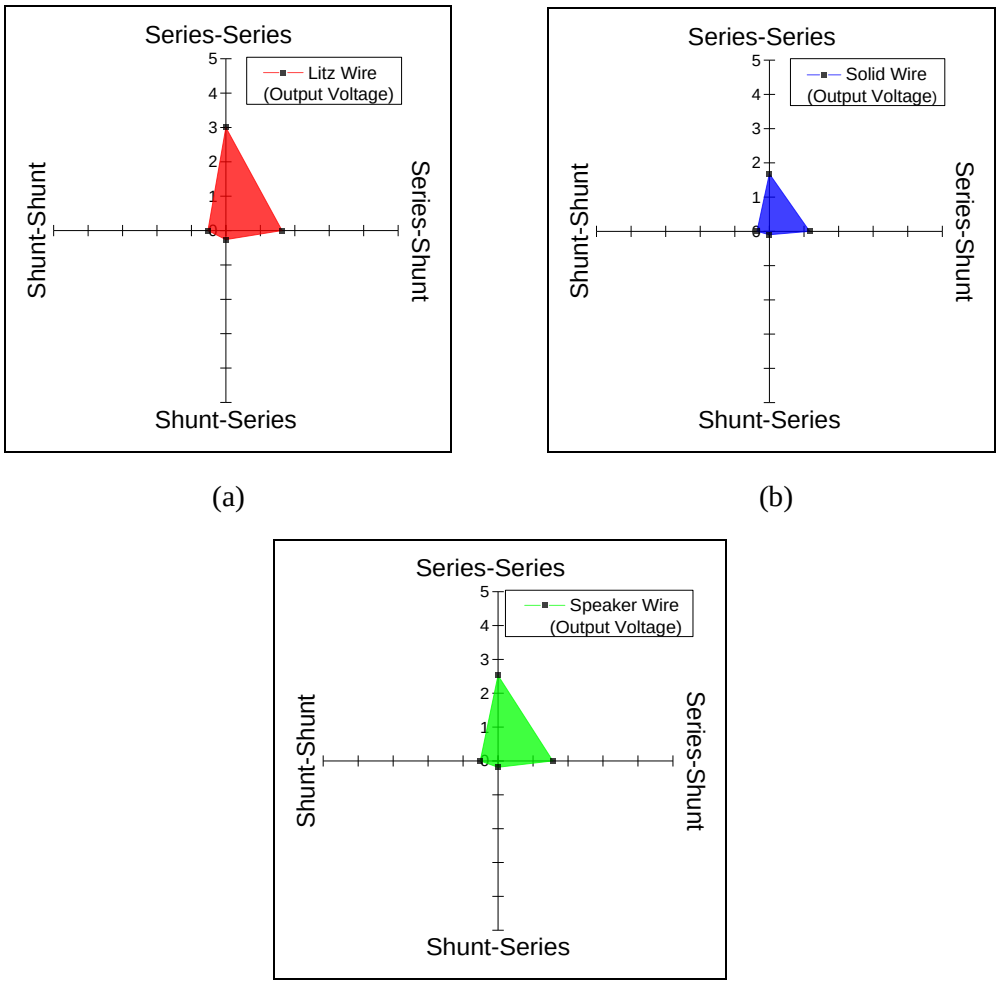

Figure 27: Measured output voltage of WPT prototypes with 2.5 Ω loads for the four coupling configurations evaluated (series-series, series-shunt, shunt-series and shunt-shunt) at D = 3cm. The results are displayed by inductor loop material: (a) Litz wire, (b) solid wire, and (c) speaker wire.

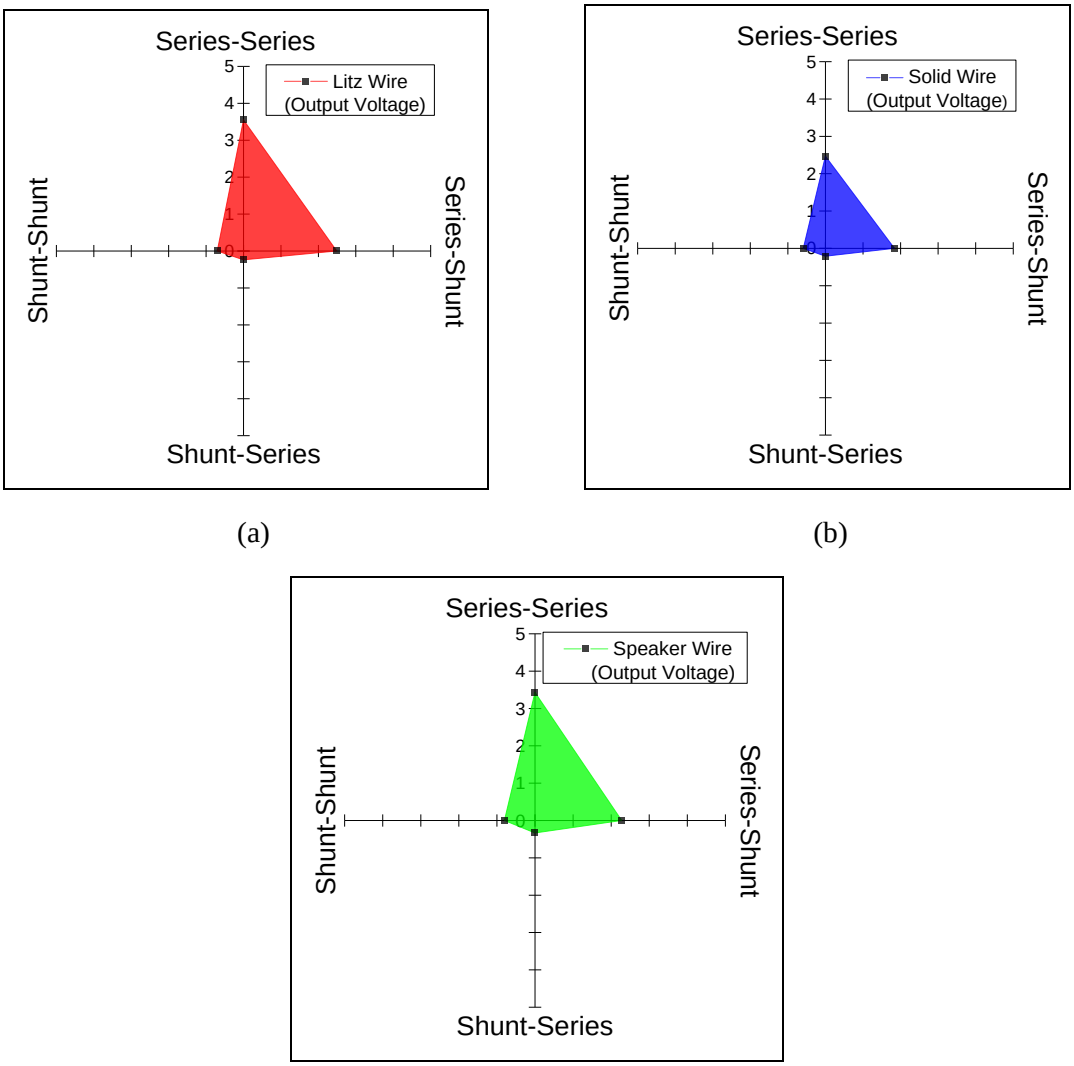

Figure 28: Measured output voltage of WPT prototypes with 4 Ω loads for the four coupling configurations evaluated (series-series, series-shunt, shunt-series and shunt-shunt) at D = 3cm. The results are displayed by inductor loop material: (a) Litz wire, (b) solid wire, and (c) speaker wire.

CHAPTER FIVE: EMC RADIATED EMISSIONS COMPLIANCE DESIGN EVALUATION APPROACH FOR WPT SPACE SYSTEMS

After evaluating the magnetic resonance element design in Chapter Three and the WPT system advanced characterization analysis in Chapter Four, this chapter will evaluate the possibly of implementing WPT technology in space applications. A systematic approach was developed for the conceptualization and implementation of WPT systems (Figure 29).

The primary space application emphasis will be NASA expendable launch vehicles (Atlas V, Delta II, Delta IV, Pegasus, Taurus and Falcon 9) electromagnetic compatibility (EMC) considerations. A design approach considering EMC will be proposed and demonstrated by the implementation of various WPT cases.

The proposed approach takes into consideration the parameter computation, circuit simulation for transient response, circuit simulation for frequency response, circuit simulation for S-Parameters extraction, computational electromagnetic modeling for accurate WPT element characterization and testing. Each of the main processes illustrated in Figure 29 and will be briefly described in upcoming subsections.

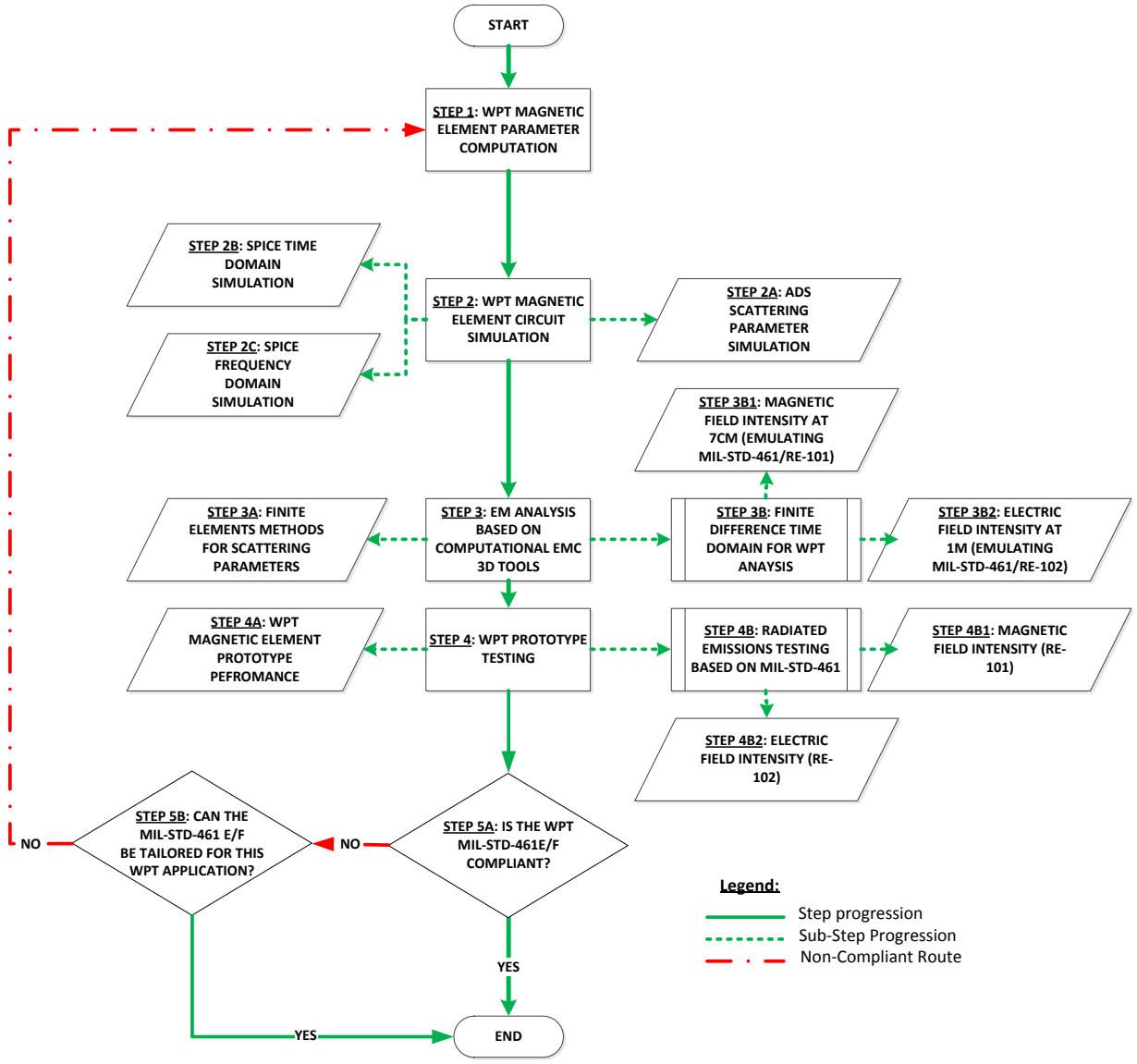

Figure 29: EMC radiated emissions compliance design evaluation approach for WPT space systems

5.1 Step 1: WPT Magnetic Element Parameters Computation

The parameters computation of the WPT magnetic element process is performed to acquire the basic systems characteristics based on the initial requirements. The information required to

perform this process step is to define the basic characteristics of the desired WPT system: loop dimensions and characteristics and frequency of operation. The parameters to be calculated in this step are inductance of the loops, the resonance capacitance for the resonator systems, coupling coefficient, mutual inductance and leakage inductances. These parameters will be computed by using the described equations earlier and will be later used by the next process step as the initial point. Figure 30 illustrates the inputs required by this process step and the expected output parameters.

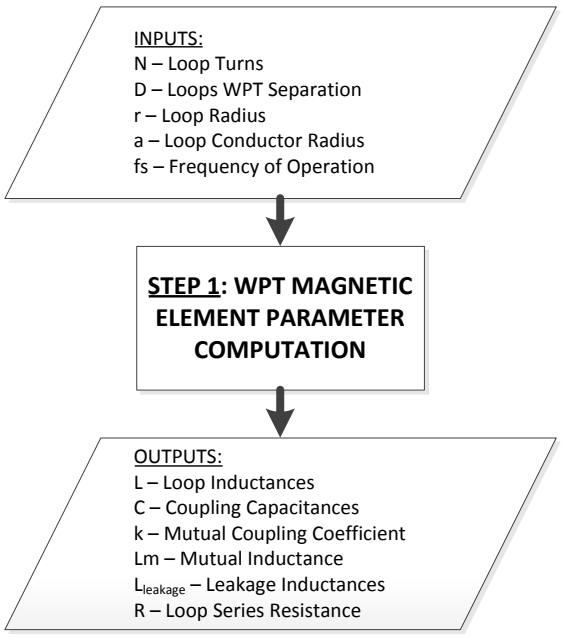

Figure 30: WPT Magnetic element parameters computation process inputs and outputs (Step 1)

5.2 Step 2: WPT Magnetic Element Circuit Simulation

Using the non-ideal transformer WPT modeling technique presented in Chapter Three, and mutual coupling constant, various circuit simulations can be performed in order to acquire

additional insight on the behavior of the WPT magnetic element. Three different simulation approaches have been identified with the use of the Simulation Program with Integrated Circuit Emphasis (SPICE) variations: frequency domain, time domain and scattering parameters extraction. The frequency domain SPICE simulation is performed to determine the attenuation factor of the WPT magnetic element based on the magnitude value (in dBV) of the WPT's frequency response. The time domain SPICE simulation is performed to determine the overall WPT element performance, as well as determine specific circuit analysis parameters. By using the Advanced System Design (ADS) RF SPICE software package, scattering parameters can be calculated from the WPT circuit model. A special emphasis is taken on S_{21} since this parameter will provide the efficiency prediction of the ideal WPT case.

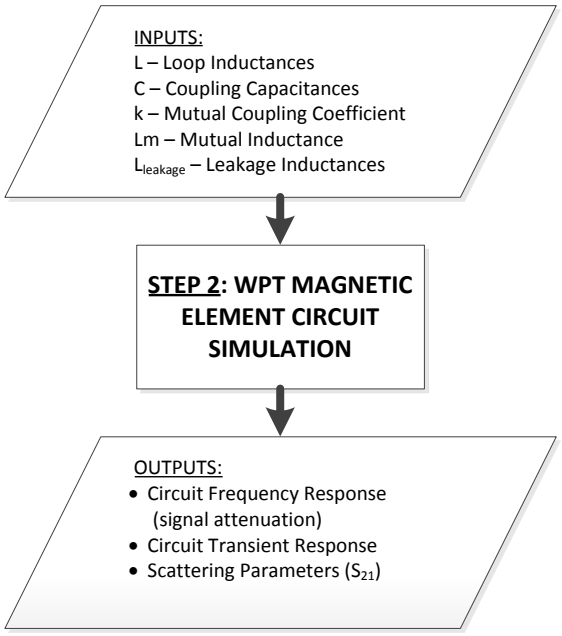

Figure 31: WPT magnetic element circuit simulation inputs and outputs (Step 2)

5.3 Step 3: EM Analysis Based on Computational EMC Tools

There are two computational methods that had been identified to be favorable for the characterization of WPT systems, Finite Elements Methods (FEM) and Finite-Difference Time-Domain (FDTD). These methods help to provide a deeper understanding of the WPT magnetic element since they will be able to characterize parasitic effects based on geometry that the circuit simulation cannot capture.

The FEM 3-dimentional (3D) computational tool (EMPro made by Agilent) will provide the scattering parameters simulation of the WPT magnetic element. An interesting outcome of this simulation is that, without the frequency of operation input, the software will determine the resonant frequency by modeling the WPT magnetic element structure. FEM simulation also provides scattering parameters. The parameter S_{21} provides the attenuation of the WPT magnetic element as well as the theoretical efficiency at the resonant frequency. The FDTD simulation will be performed with Agilent's EMPro software. It will provide a 3D characterization of the EM power transmission based on the system physical characteristics (including parasitic effects), specially simulated estimations of electric and magnetic field intensities.

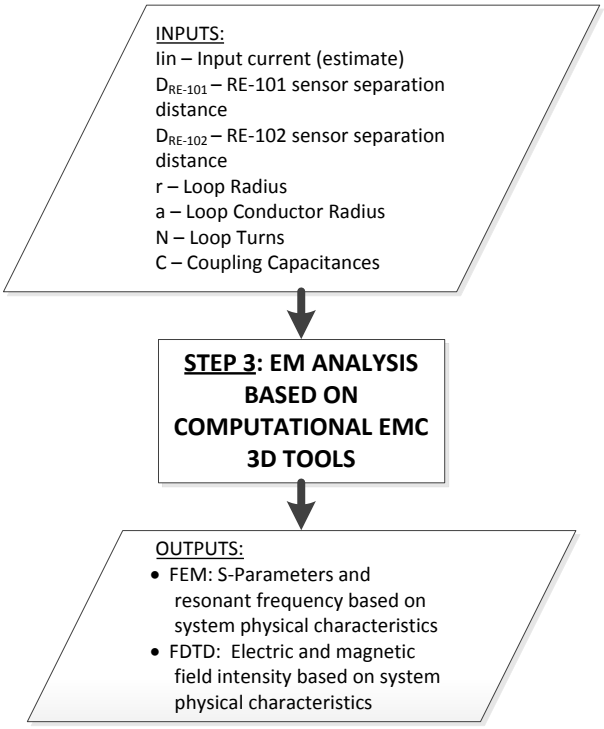

Figure 32: EM analysis based on computational EMC tools inputs and outputs (Step 3)

5.4 Step 4: WPT Magnetic Element Prototype Testing

To validate the calculated parameters and the circuits and structures simulations of the WPT magnetic element design, two sets of tests will be performed for each case: WPT magnetic element performance and radiated emissions testing according to Mil-Std-461E/F.

The WPT magnetic element test consist of determine the output voltage based on the provided input voltage. Since the systems are terminated to 50Ω, efficiency interpolation can be determined by the voltage relation. Figure 33 illustrates the block diagram of the prototype performance test set-up.

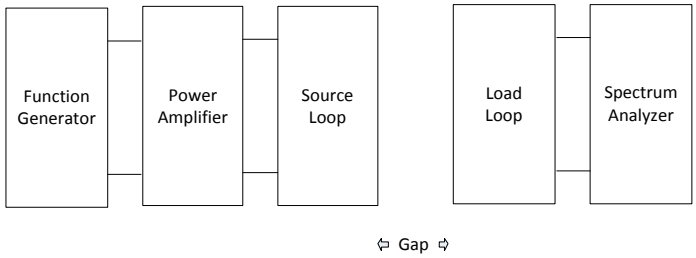

Figure 33: Block diagram of the WPT magnetic element performance test set-up

With this test configuration, we provide the amplified power to the WPT magnetic element to establish wireless power transmission source loop. The load loop will be connected to a spectrum analyzer to measure the voltage generated. The power amplifier is connected to the spectrum analyzer to determine what is the voltage without the WPT elements (input voltage). By using the SPICE frequency response simulation and the FEM EMPro simulation, one can expect a frequency of operation around the one provided by these analyses. It is important to mention that a slight variation from the analytical/simulated frequency of operation is expected depending on the fidelity of the manufactured loops. Table 6 provides the lab equipment available for the performance of these tests.

Table 6: WPT magnetic element performance testing equipment

Device	**Model**	**Characteristics**
Function Generator	Instek Model: SFG-2004	Frequency Range: 0 Hz – 4 MHz
	Agilent Technologies Model: E8257D	Frequency Range: 250 MHz – 20 GHz
Power Amplifier	Amplifier Research: Model: 25A250A	Frequency Range: 10 kHz – 250 MHz
	Amplifier Research: Model: 10S1G4A	Frequency Range: 500 kHz – 4.2 GHz
Spectrum Analyzer	Rohde and Schwarz Model: FSP38	Frequency Range: 9 kHz – 40 GHz

The radiated emission testing is performed by powering the source loop with the power amplifier (at the operating frequency) and measuring the electric field intensity and the magnetic field intensity in accordance of Mil-Std-461E/F. For the electric field intensity measurement, a rod antenna is placed at 1 m of separation [6] [7]. For the magnetic field intensity measurement, a loop antenna is placed 7 cm from the source of the device [6] [7].

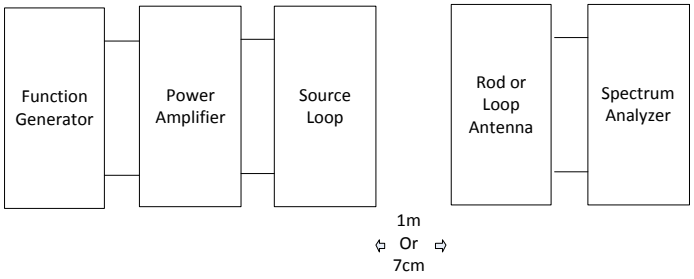

Figure 34: Electric and magnetic field intensity test set-up [6] [7]

For the radiated emissions testing, two different antennas are required to measure field intensities: a rod antenna for the electric field and a loop antenna for the magnetic field. Table 7 provides the model and characteristic of the antenna used for the radiated emissions testing. Table 6 list the test equipment used for the tests.

Table 7: Antennas used for the radiated emissions testing

Antenna	**Model**	**Characteristics**
Loop	Solar Electronics: Model 7334 [20]	Frequency Range: 30 Hz – 100 kHz
Rod	ETS Lindgren Model: 3301B [21]	Frequency Range: 10 kHz – 50 MHz

5.5 Step 5: Mil-Std-461E/F Compliance Verification

Wireless power transmission within a launch vehicle (rockets) is something that has not been attempted in the past. These systems operations are based on the magnetic resonance principle. Therefore, one of the greatest constraints that can be immediately identified is the possible interference of the magnetic field with to the other rocket (or space application) sub-system. To determine whether or not a system is identified to be a non-harmful system from the electromagnetic point of view, EMC radiated emission (RE) considerations needs to be evaluated. The primary standard used by the National Aeronautics and Space Administration (NASA) for the EMC RE compliance is the Military Standard 461E/F (Mil-Std-461E/F). A few cases were selected to evaluate the EMC radiated emissions approach and demonstrate the possibility of wireless power transmission for space applications from the EMC point of view. This standard requires the evaluation of two environments: the magnetic field intensity and the electric field intensity. These field intensity requirements will be evaluated in the following sub-sections. Figure 35 illustrates the Flight Analysis Division model validation facility at NASA-KSC.

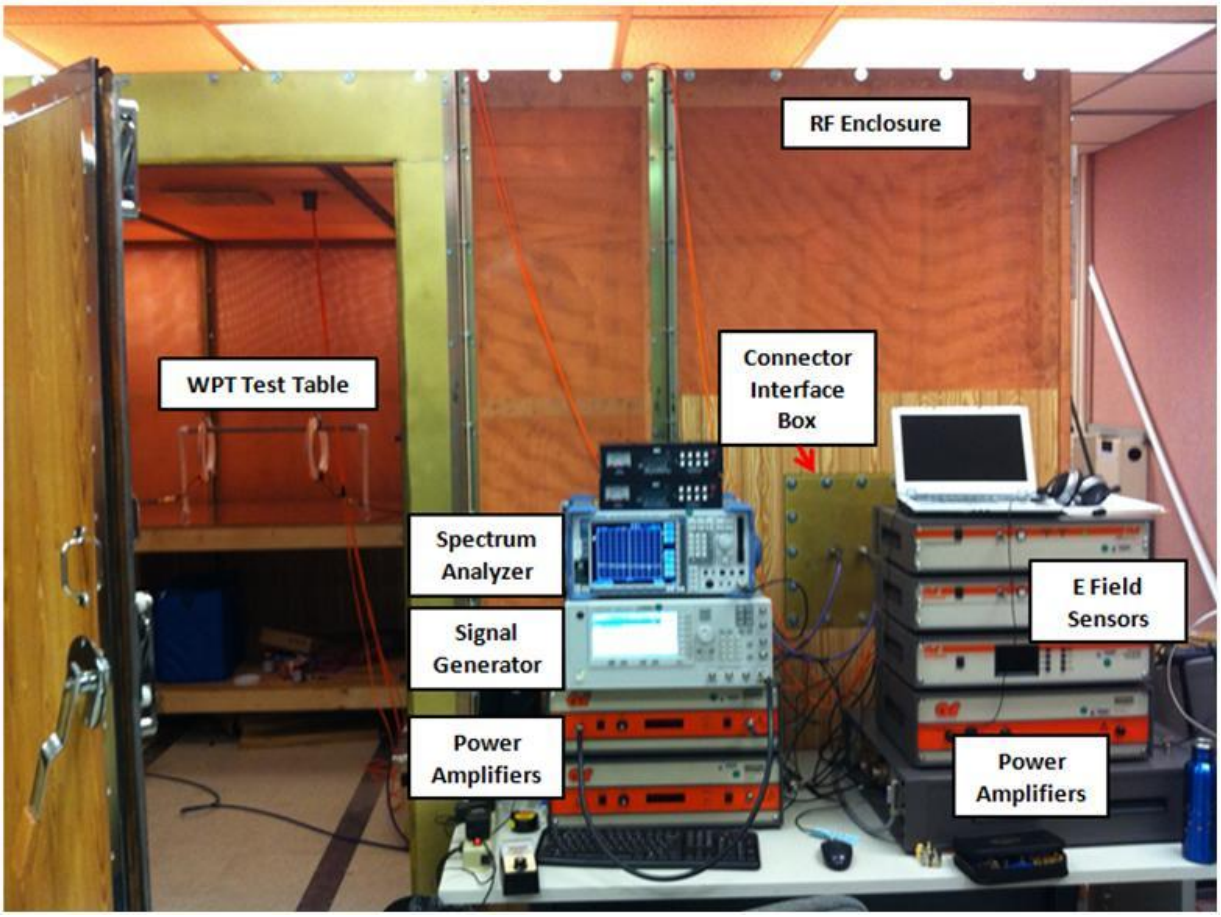

Figure 35: Flight Analysis Division model validation facility at NASA-KSC

5.5.1 Magnetic Field Intensity Radiated Emissions

For systems that operate below 100 kHz, the NASA standard used to determine compatibility compliance for the magnetic field (Mil-Std-461E/F) uses what is known as the magnetic fields radiated emission requirement RE-101 [6]. Figure 36 illustrates the level of magnetic field intensity that is allowed by the standard. It is important to mention that exceptions could be allowed depending on specific system circumstances. During WPT cases implementation, we will be discussing requirements exceptions as they occur.

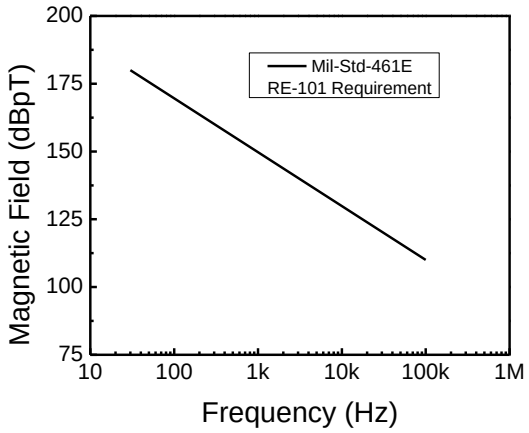

Figure 36: Mil-Std-461E/F magnetic field intensity radiated emissions requirement (RE-101) [6] [7]

5.5.2 Electric Field Intensity Radiated Emissions

The electric field radiated emissions allowed by Mil-Std-461E/F are illustrated in Figure 37 [6] [7]. It can be seen that depending on which frequency is evaluated, the electric field allowed varies. For electric field radiated emissions, the electric field intensity is measured in the low levels of dBµV/m due to the fact that what is been trying to be accomplished by this test is to not interfere with sensitive onboard receivers. For space exploration, especially for expendable launch vehicles, various exceptions exist and possible known mitigations can be implemented. We will be discussing exceptions as they occur during the WPT cases implemented.

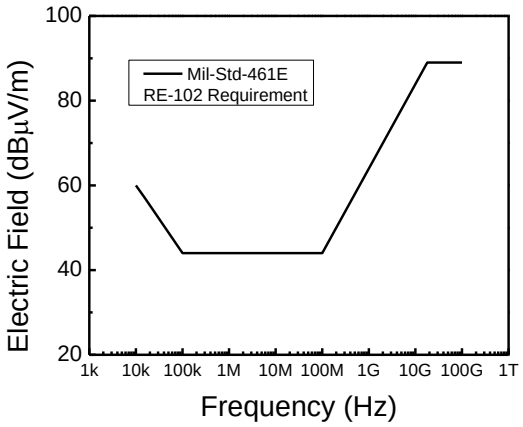

Figure 37: Mil-Std-461E/F electric field intensity radiated emissions requirement (RE-102) [6] [7]

5.5.3 Mil-Std-461E/F Launch Vehicles Exceptions

The military standards were developed by the Department of Defense to have standardized processes across the various US defense agencies [6] [7] [8] [9]. However, modifications of these standards are allowed as long as adequate system compliance rationale is presented for the specific application. For Launch Services Program (LSP), all avionics components need to comply with a radiated susceptibility test (RS) making sure that systems can withstand electric and magnetic field environments. Due to qualification rational for other environments in the launch vehicle industry, systems are test to 6dB above the flight environment and are consider qualified for flight [9]. Therefore, in some launch vehicle cases regarding radiated environments, if the system is beyond the Mil-Std-461 RE requirements, due to RS testing one can make the case that the systems has been tested at least 6dB or more from the flight environments for the new device. To put this in perspective, the version of Mil-Std-461 (ver. E)

states that all avionics components must be tested to 20 V/m [6]. This means that systems that emit lower electric field intensities than 10 V/m or 140 dBµV/m (6 dB less than 20 V/m), have the potential to create an exception if a sound technical argument is presented. Same will happened with the current Mil-Std-461F, since it requires the avionics systems to be tested to 200 V/m, systems that emit lower electric field intensities than 100 V/m or 160 dBµV/m (6 dB less than 200 V/m), have the potential to create an exception if a sound technical argument is presented. We will be evaluating a little further potential exceptions of the Mil-Std-461 requirement during our cases implementation.

CHAPTER SIX: DEMONSTRATION AND IMPLEMENTATION OF THE EMC COMPLIANCE DESIGN EVALUATION APPORACH FOR WPT RADIATED EMISSIONS

In this Chapter we are going to be evaluating various WPT magnetic elements for the purpose of validating the EMC compliance design evaluation approach for WPT radiated emission described in the previous Chapter. The WPT cases were selected based on their possible implementation in launch vehicles by being lightweight and having low-medium power range capabilities. Three cases will be evaluated: the two loops prototype (WPT J1), the four stages-four single loop WPT magnetic element (WPT 4-4) and the four stages-two loops WPT magnetic element (4-2). The main objective of this Chapter is to go step by step in the EMC radiated emissions compliance design evaluation approach for WPT space systems illustrated in Figure 29.

6.1 Two Loops WPT prototype (WPT-J1)

The two loops WPT prototype is a compilation of the design, simulations and experimentation performed in the first four Chapters, but applying the design approach presented in Chapter 5. Then, later in this chapter, two new cases will be designed using this design approach. The WPT J1 consists of two resonant stages each containing an inductor and a coupling capacitor. The block diagram for this configuration is illustrated in Figure 7 and the operational prototype is illustrated in Figure 16. A detailed diagram of the WPT J1 prototype magnetic elements is illustrated in Figure 38. The parameters used to develop this EMPro 3D Model are provided in Table 5.

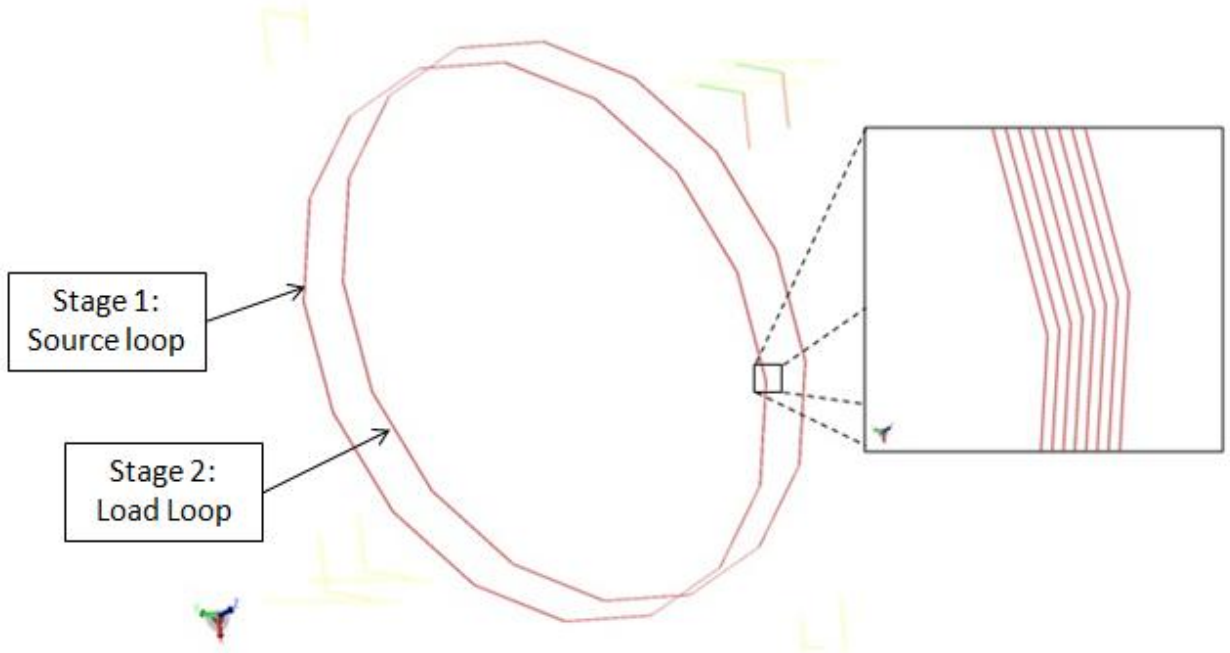

Figure 38: WPT J1 prototype EMPro 3D model

6.1.1 Step 1: WPT J1 Prototype Parameter Computation

Since the design aspects of this prototype and multiple variations of this configuration were evaluated in earlier chapters, the information for this design step has already been presented in this document and will not be repeated here. Table 3 lists the calculated parameters required for the EM design approach of the WPT J1 prototype. For the MathCAD worksheet of the parameter computation, please refer to the Appendix G.

6.1.2 Step 2: WPT J1 Circuit Simulation

Using the parameters listed in Table 2 and Table 3, a circuit simulation approach was executed in accordance with the EMC radiated emissions compliance design evaluation approach described in Chapter 5. A frequency domain Simulation Program with Integrated Circuit Emphasis (SPICE) simulation was executed to determine the WPT frequency of operation, a time domain SPICE simulation to determine the voltage induced in the secondary and Advanced Design Systems (ADS) simulation to determine system performance based on the scattering parameter S_{21}.

Using the non-ideal transformer equivalent circuit approach explained in Chapter 3, a simulation in the SPICE was executed for the frequency response. Figure 39 shows the resonant characteristic expected. The SPICE model estimates that the circuit is resonating at about 12 kHz (been closed to the design frequency, 15 kHz).

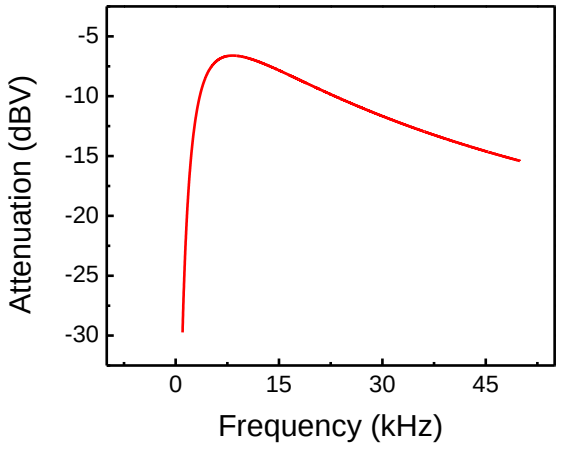

Figure 39: WPT J1 frequency response SPICE simulation for a separation distance of 3cm (optimal)

Using the same SPICE non-ideal transformer WPT electrical model, a transient response simulation is performed. Figure 40 illustrates the transient simulation during the steady state.

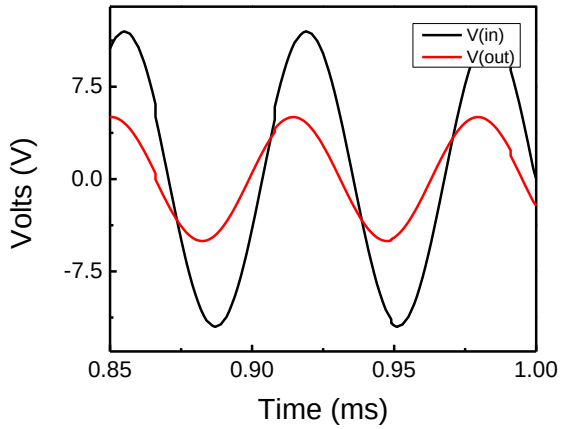

Figure 40: WPT J1 transient SPICE simulation (steady state) for a separation distance of 3cm

Using Agilent's ADS tool, the S-parameters where determine for the WPT J1 prototype. Figure 41 illustrates that the WPT J1 prototype can provide efficiency of up to 71 % (S_{21} = -1.5 dB) at ~ 15 kHz. Please refer to Appendix H for additional circuit simulation insight.

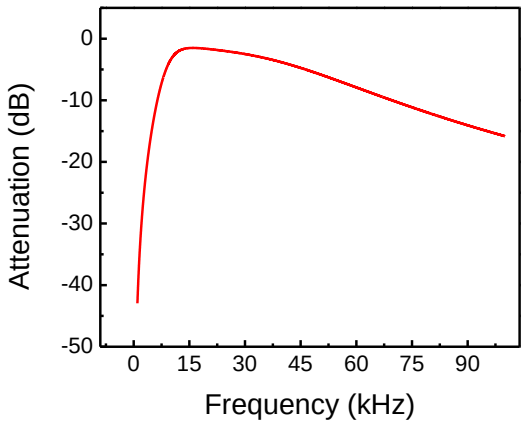

Figure 41: WPT J1 S_{21} Parameter (Attenuation) ADS simulation for a separation distance of 3cm

6.1.3 Step 3: WPT J1 RF Characterization Using Computational EMC Tools

In this subsection we are going to evaluate the Electromagnetic Professional (EMPro) 3D model of the WPT J1 shown in Figure 38. Two computational electromagnetic techniques will be performed to the model: Finite Elements Methods (FEM) and Finite-Difference Time-Domain (FDTD). The FEM will be performed to determine the scattering parameters of the WPT J1 according to the 3D model physical characteristics. Figure 42 illustrates FEM perspective and top mesh views details for the WPT J1 simulation. It can be noticed that adequate mesh density was identified in the areas of interest (between the cables).

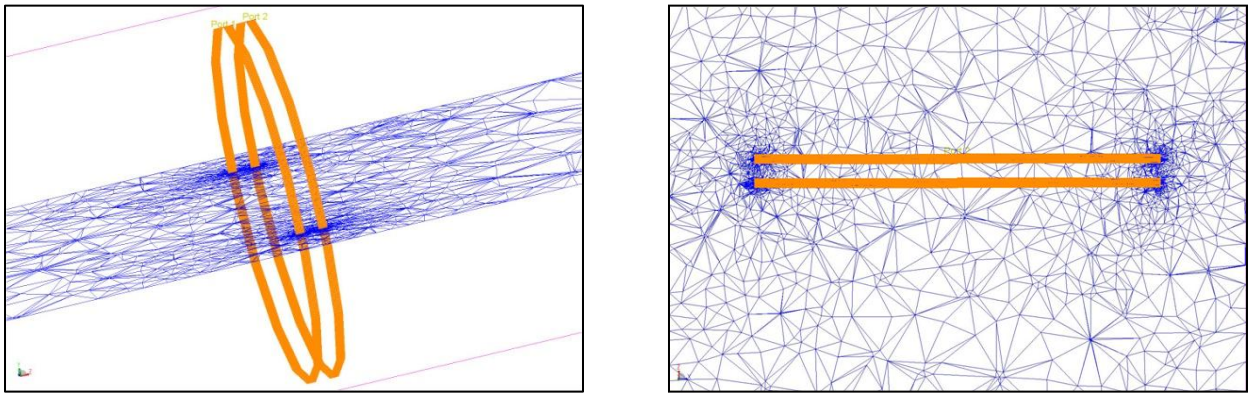

(a) (b)

Figure 42: WPT J1 EMPro FEM mesh simulation details views: (a) perspective, and (b) top

The EMPro 3D model was FEM simulated according to the mesh described in Figure 42 to acquire the WPT J1 S-parameters (specially the S_{21}). It shows a resonant frequency of about 10 kHz. It is important to mention that even if this system provides an approximate representation of the magnetic loops presented for the WPT J1 prototype, the turn's configuration are slightly different: the 3D model has the loop turns perfectly alighted, while the prototype loops has it turns all wrapped up one on top of the other.

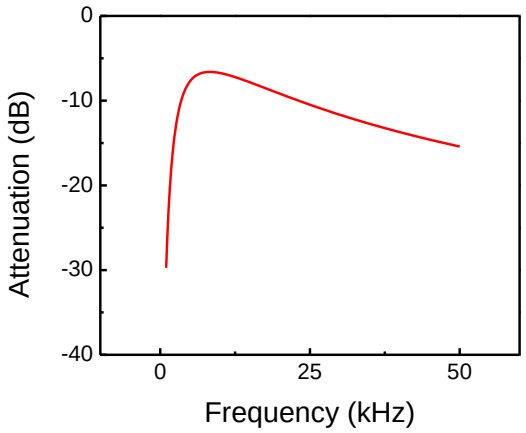

Figure 43: WPT J1 S_{21} parameters (attenuation) based on the EMPro FEM simulation

To determine the electric and magnetic field intensity radiated emissions generated by the WPT J1 prototype, FDTD simulation was performed. Figure 44 illustrates the FDTD simulated WPT J1 magnetic field intensity reflected at a 7cm distance separation. The FDTD simulated magnetic field intensity illustrated in Figure 44 shows a magnetic field of approximately 4 mA/m. Figure 45 illustrates the WPT J1 FDTD simulation for the magnetic field intensity.

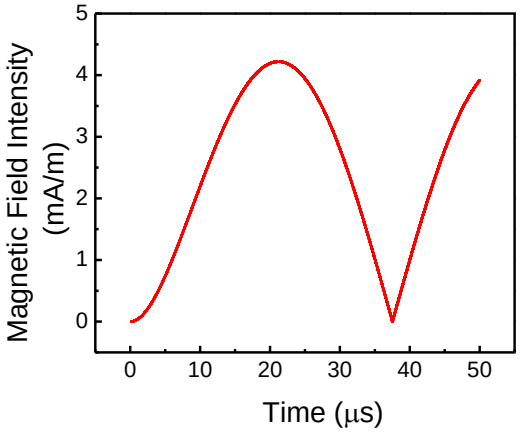

Figure 44: WPT J1 magnetic field intensity FDTD simulation according to Mil-Std-461E/F (7cm of separation between the source loop and the magnetic field intensity meter)

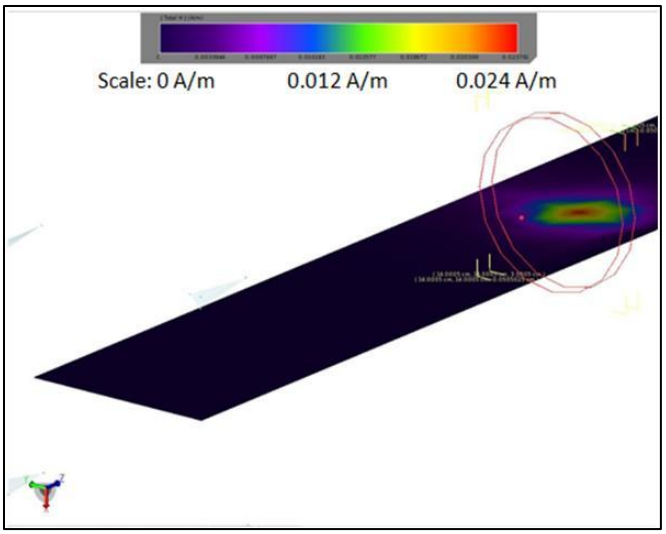

Figure 45: WPT J1 FDTD simulation for the magnetic field intensity (color scale from 0 to 0.024 A/m)

In addition to the magnetic field intensity FDTD simulation, an electric field intensity FDTD simulation (Figure 47) was performed to emulate/predict the outcome of the Mil-Std-461E/F by measuring the E-Field at 1 meter of separation [6] [7]. Figure 46 illustrated the measured FDTD simulated electric field intensity at 1m of separation (maximum been about ~ 50 dBµV/m).

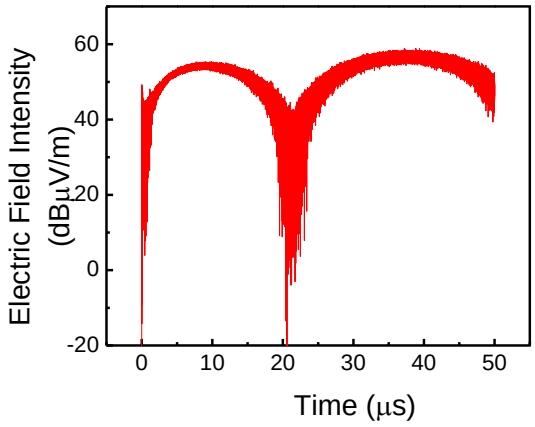

Figure 46: WPT J1 electric field intensity FDTD simulation according to Mil-Std-461E/F (1m of separation between the source loop and the electric field intensity meter)

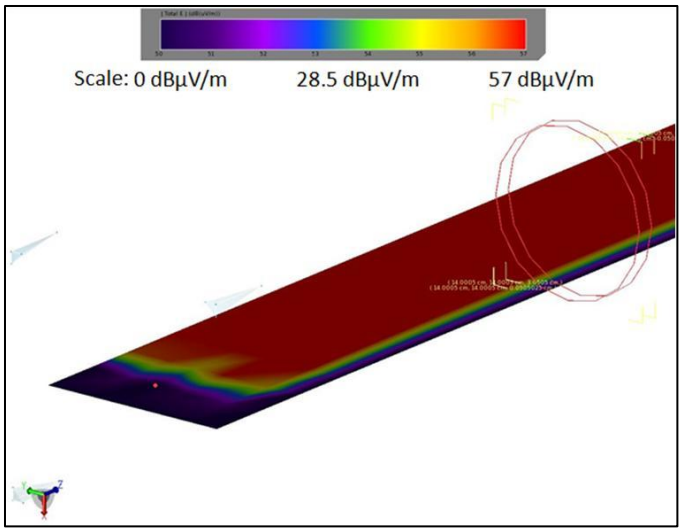

Figure 47: WPT J1 FDTD simulation for the magnetic field intensity (color scale from 0 to 57 dBµV/m)

6.1.4 Step 4: WPT J1 Prototype Testing

The WPT J1 prototype was tested to determine its performance and acquire insight into its EMC radiated emissions. Since the performance of this prototype was previously discussed in earlier chapters, this subsection will only provide the key prototype performance aspects. The operating WPT J1 prototype is illustrated in Figure 16. The WPT J1 prototype provides approximately 5 V as output voltage (Figure 20), and by having an output resistance of 4 Ω, the output power is estimated to be around 6.2W. The Velleman-Kit 4001 power amplifier used in the prototype is based on the TDA-2003 integrated circuit rated for 10W [48]. This provides an efficiency of 68%. The efficiency is measured from the power amplifier to the load at the design separation distance of 3 cm (for additional insight in the block diagram, please refer to Figure 7). The prototype output power (68%) has great agreement with the maximum power expected by this WPT system according with the S-Parameter circuit simulation in Figure 41 (71%).

In addition to the performance of the WPT J1 prototype, radiated emissions (RE) testing were performed. The focus was magnetic field intensity and electric field intensity as suggested by the Mil-Std-461E/F [6] [7]. Figure 48 illustrates the WPT J1 prototype RE-101 (magnetic field intensity) test setup using the process previously described in Figure 34 and in Table 7. Figure 49 shows the spectrum analyzer results from the RE-101 testing at the frequency of operation. Using the EMC testing unit conversion as described in Chapter 2, it was identified that the 4.96 dBm spectrum analyzer reading, showed in Figure 49, correspond to 82.93 dBpT. By changing the units to dBpT, we will be able to compare this measurement with the actual Mil-Std-461E/F RE-101 requirement (uses the same units).

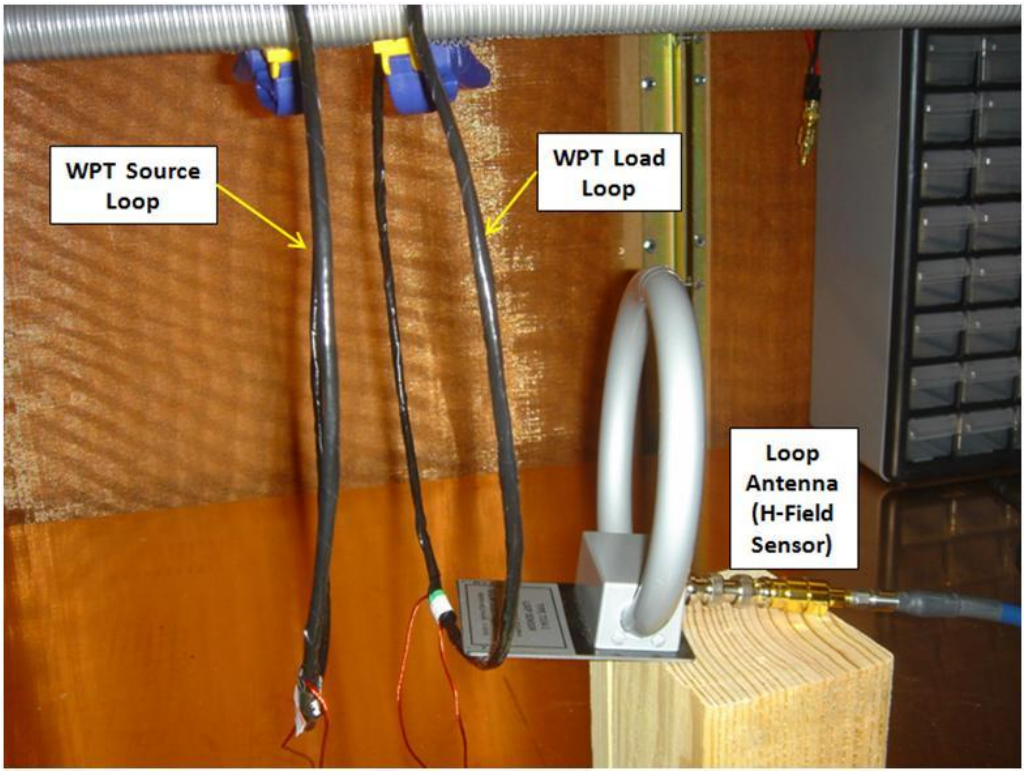

Figure 48: WPT J1 prototype RE-101 (magnetic field intensity) test setup

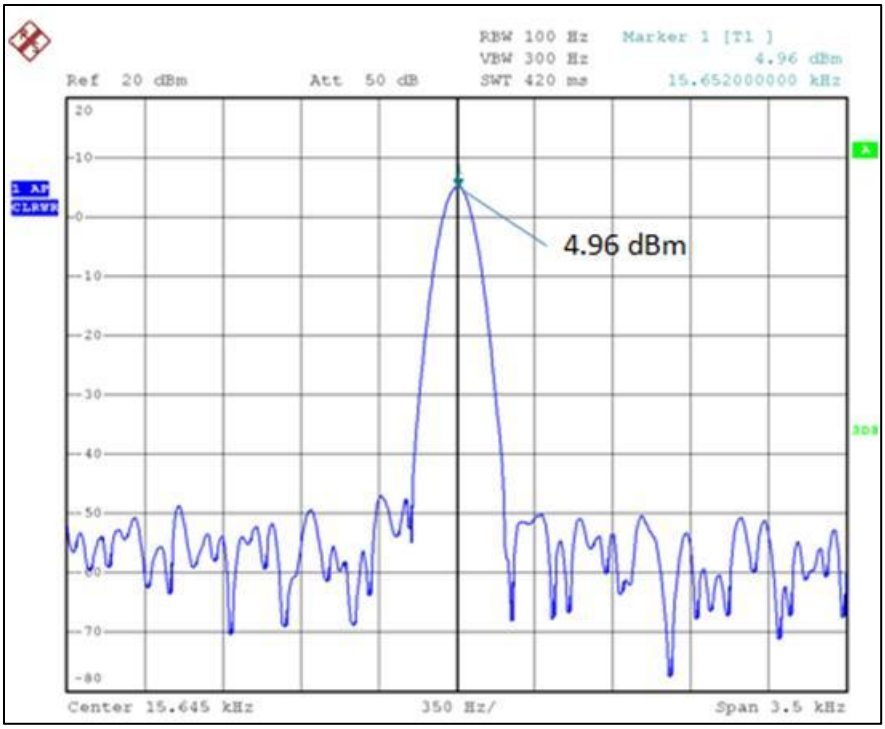

Figure 49: WPT J1 prototype RE-101 testing results at the frequency of operation

In addition to the magnetic field intensity test (RE-101), the WPT J1 prototype was tested for electric field radiated emissions (RE-102). Figure 50 illustrates the WPT J1 prototype RE-102 (electric field intensity) test setup using the process previously described in Figure 34 and in Table 7. Figure 51 shows the spectrum analyzer results from the RE-102 testing at the frequency of operation. Using the EMC testing unit conversion as described in Chapter 2, it was identified that the 85.27 dBµV/m spectrum analyzer reading, showed in Figure 51, correspond to 30.02 dBµV/m. For this particular measurement, we will have to factor in the antenna factor (AF), for that reason the measurement reflected by the testing setup is about 50 dBµV/m less that the spectrum analyzer reading.

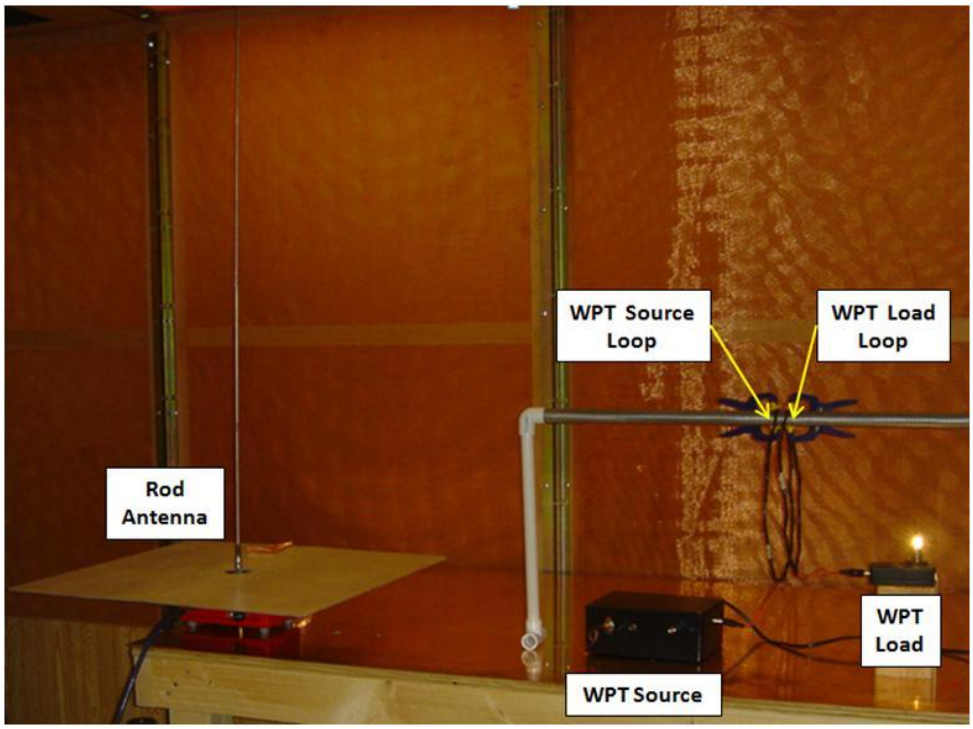

Figure 50: WPT J1 prototype RE-102 (electric field intensity) test setup

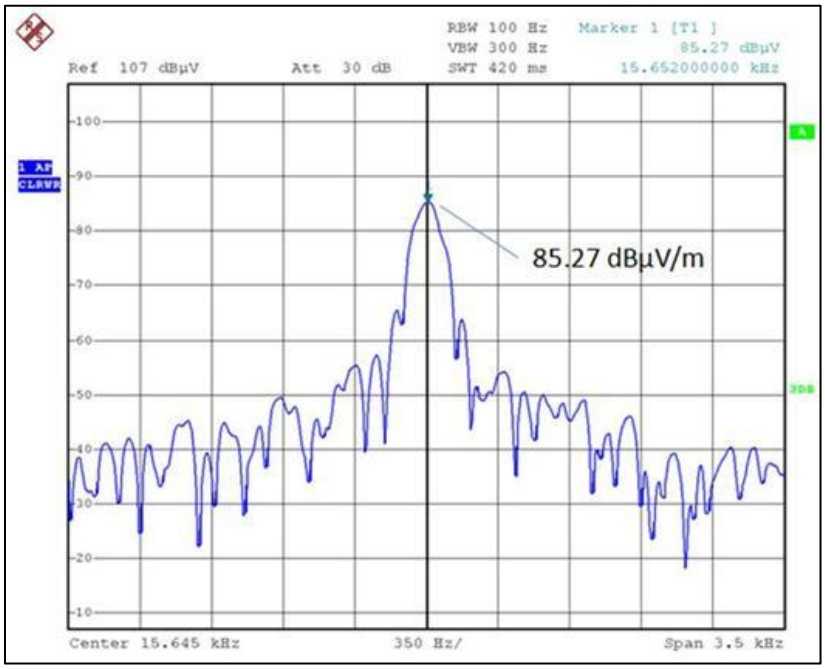

Figure 51: WPT J1 prototype RE-102 testing results at the frequency of operation

6.1.5 Step 5: WPT J1 Prototype Compliance with Mil-Std-461E/F for Radiated Emissions

For this EMC radiated emissions compliance design evaluation approach step we will be evaluating and comparing the results obtained in the WPT J1 RF characterization using computational EMC tools section and the WPT J1 prototype testing section. The primary focus is to identify if these systems comply with the Mil-Std-461E/F with or without requirements tailoring. Figure 52 illustrates the magnetic field intensity requirement (RE-101) compared with the EMC computational tool result and prototype testing. It can be noticed that the WPT J1 prototype was compliant with the military standard by significant margin (about 44 dB of margin for the EMPro simulation and about 51 dB of margin for the RE-101 testing results).

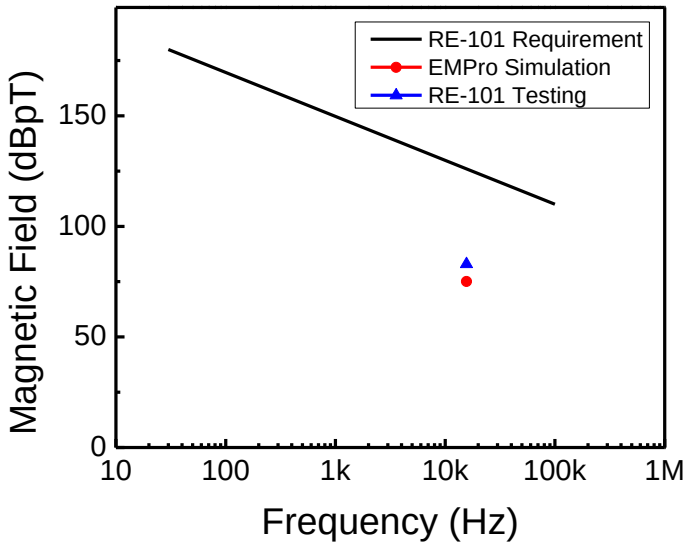

Figure 52: WPT J1 RE-101 (magnetic field intensity) results comparison between Mil-Std-461E requirements, simulations and prototype testing

The other radiated emissions requirement that is relevant for this application is the radiated electric field intensity. Figure 53 illustrates the electric field intensity requirement (RE-102) compared with the EMC computational tool result and prototype testing. It can be noticed that the WPT J1 prototype was compliant with the military standard (about 7 dB of margin for the EMPro simulation and about 27 dB of margin for the RE-101 testing results). It is important to mention that a slight difference between the simulated and tested electric field intensities was expected due to the geometry modeling limitations of the EMPro software package. The EMPro simulation was performed by aligning each turn as a helix (Figure 38). By having a helix shaped inductor with wires in close proximity, parasitic capacitance is expected. Even though that the actual inductor irregular wraps of the turns (as shown in prototype Figure 48) also provides parasitic capacitances, there is an expected slight difference between irregular wrapped turns inductors and the helix inductors.

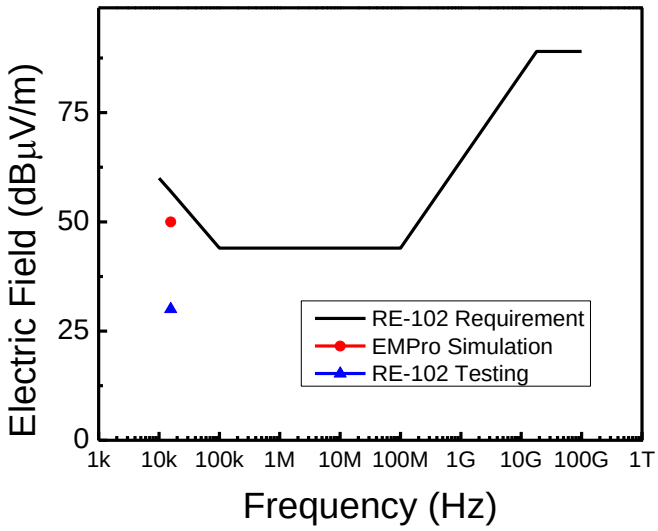

Figure 53: WPT J1 RE-102 (electric field intensity) results comparison between Mil-Std-461E requirements, simulations and prototype testing

6.2 Four Stages -Four Single Loops WPT Magnetic Element (WPT 4-4)

The four stages-four single loops WPT magnetic element (will be called WPT 4-4 for simplicity) was design taking in consideration the conductor size and the separation distance for wireless power transmission. This configuration has been identified as one of the main ideas for wireless power transmission by magnetic resonance without the use of magnetic cores [37] [49]. A WPT magnetic example was designed to demonstrate this configuration. However, the values of this example can be changed to fit the particular need of a different application. Figure 54 provides an initial overview of the four stage-four loops wireless power transfer magnetic element.

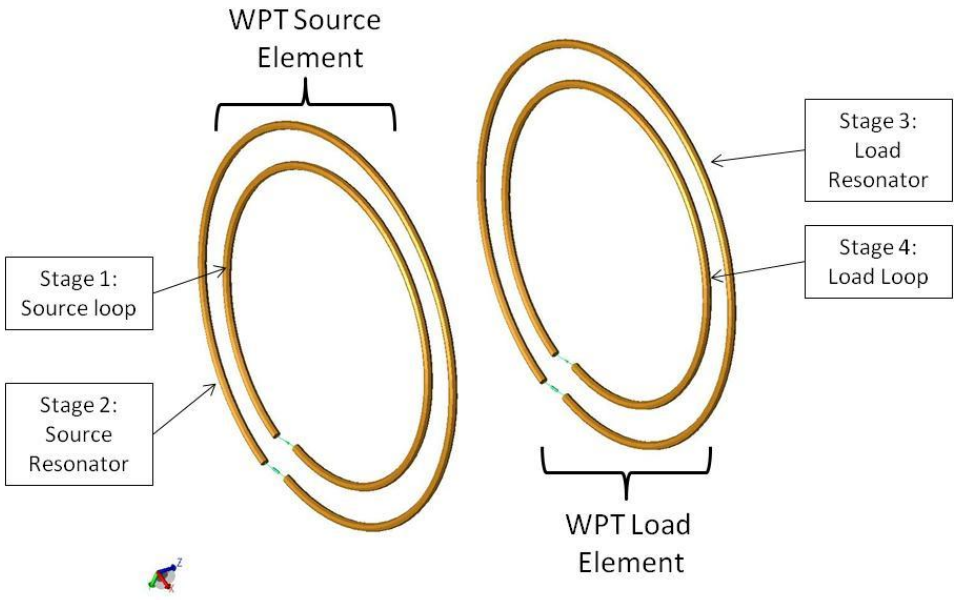

Figure 54: Four stage-four single loops wireless power transfer magnetic element EMPro 3D Model

The four stage-four single loops wireless power transfer magnetic element (WPT 4-4) operates in the principle of magnetic resonance. Figure 55 illustrates the block diagram of the WPT 4-4 system [37].

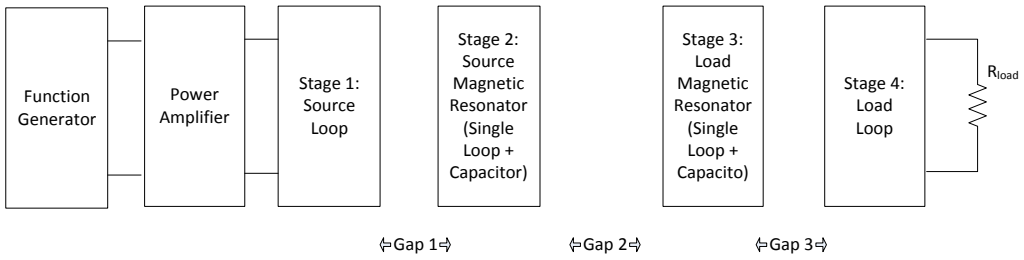

Figure 55: WPT 4-4 Block Diagram

As previously described in earlier chapters, for WPT systems based on magnetic resonance it is required to have a driving power signal at the frequency of operation. For WPT 4-4 magnetic elements, that signal can be provided by a combination of a function generator/power amplifier or by designing a switching power supply (inverter). For the purpose of this study, we are only evaluating the function generator/power amplifier configuration.

The four stages are derived as follow: stages 1 & 4 are the source and load single loops and the stages 2 & 3 are magnetic resonators. The power amplifier signal is connected to the source loop (stage 1) in order to generate a pulsed magnetic field at the frequency of operation. The single loop resonators (stage 2 & 3) are single loops that are carefully paired with coupling capacitors in order to generate a resonance frequency. They will receive the magnetic pulsation from the stage 1 via magnetic induction and the resonators will amplify the magnetic environment. This amplification of the magnetic environment between the resonators will allow

power transfer signals via magnetic resonance between them providing better performance than standard magnetic induction (by orders of magnitude of separation distance) [34] [37] [49]. After the wireless power transfer is been established between stage 2 and stage 3 via magnetic resonance, the stage 4 (loop connected to the load) will pick up the energy of the stage 3 via magnetic induction. This configuration generates three gaps, as illustrated in Figure 55. However, gap #2 is considered to be the separation distance between the source and the load. Table 8 shows the WPT 4-4 element characteristics.

Table 8: WPT 4-4 Element Characteristics

Element Stage	**Element Characteristics and Values**		
	Characteristic	***Value***	***Units***
Loop #1 & #2	Radius	10	cm
	Wire Diameter	0.635	cm
	Treats	1	turns
	Winding thikness (height)	0.635	cm
Single Loop/Capacitor Resonators #1 & #2	Radius	12	cm
	Wire Diameter	0.635	cm
	Treats	1	turns
	Winding thikness (height)	0.635	cm
Additional Model Characteristics	Separation distance between Loop #1 and Resonator #1 (Transmitter)	0	cm
	Separation distance between Loop #1 and Resonator #1 (Receiver)	0	cm
	Separation distance between the transmitter and the receiver	5 to 50 *(25 for SPICE and 3D models)*	cm
	Frequency of Operation	~3	MHz

6.2.1 Step 1: WPT 4-4 Parameters Computation

To determine the parameters required for the WPT 4-4 circuit simulation and 3D characterization, various parameters need to be calculated. Based on the characteristics provided in Table 8 and the parameter methodology showed in previous chapters, Table 9 shows the WPT 4-4 parameters calculated. For additional background on the computation behind Table 9, please refer to Appendix I.

Table 9: WPT 4-4 Calculated Parameters

Parameter	**Symbol**	**Value**	**Unit**
Loop 1 & 4 Inductance	L_1 & L_4	0.455	µH
Loop 2 & 3 Inductance	L_2 & L_3	0.611	µH
Capacitor 2 & 3	C_2 & C_3	4.606	nF
Coupling coefficient (stage 1&2)	k_{12}	0.987	
Coupling coefficient (stage 2&3)	k_{23}	0.079	
Coupling coefficient (stage 3&4)	k_{34}	0.987	
Mutual Inductance 12 (stages 1&2)	L_{M12}	0.366	µH
Mutual Inductance 23 (stages 2&3)	L_{M23}	40.32	nH
Mutual Inductance 34 (stages 3&4)	L_{M34}	0.188	µH
Leakage Inductance 1 (stages 1&2)	$L_{leakage1}$	88.89	nH
Leakage Inductance 2a (stages 1&2)	$L_{leakage2a}$	0.245	µH
Leakage Inductance 2b (stages 2&3)	$L_{leakage2b}$	0.570	µH
Leakage Inductance 3a (stages 2&3)	$L_{leakage3a}$	0.570	µH
Leakage Inductance 3b (stages 3&4)	$L_{leakage3b}$	0.423	µH
Leakage Inductance 4 (stages 3&4)	$L_{leakage4}$	0.267	µH
Series resistance (stage 1&4)	R_1 & R_4	1.938	mΩ
Series resistance (stage 2&3)	R_2 & R_3	2.168	mΩ

6.2.2 Step 2: WPT 4-4 Circuit Simulation

Based on the WPT 4-4 element characteristics in Table 8 and the parameters calculated in Table 9, a series of circuit simulations were performed to determine the WPT 4-4 magnetic element frequency response, transient response and the extraction of the scattering parameters. Appendix J provides further insight in the SPICE simulation possesses of this subsection.

Using the non-ideal transformer equivalent circuit approach explained in Chapter 3, a simulation in the SPICE was executed for the frequency response. Figure 56 shows the resonant characteristic expected. The SPICE model estimates that the circuit is resonating at about 2.1 MHz.

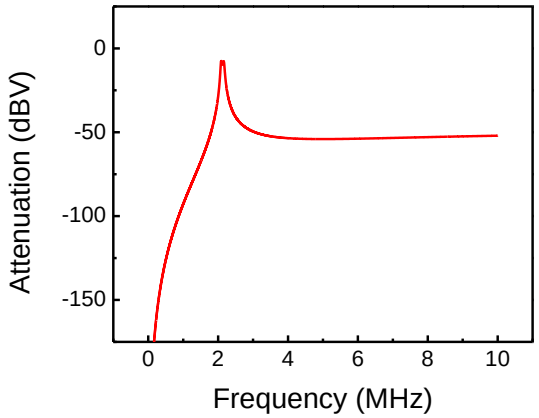

Figure 56: WPT 4-4 frequency response SPICE simulation for a separation distance of 25cm

Using the same SPICE non-ideal transformer WPT electrical model, a transient response simulation is performed. Figure 57 illustrates the transient simulation during the steady state.

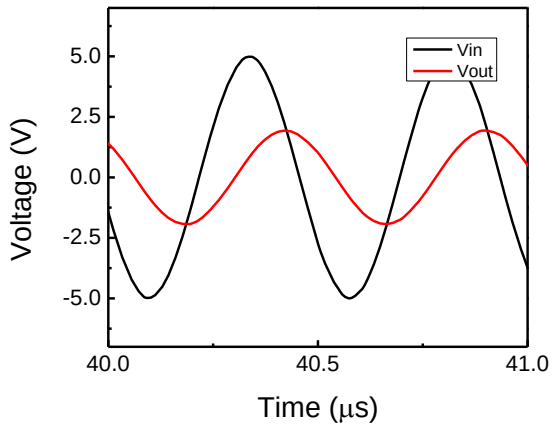

Figure 57: WPT 4-4 transient SPICE simulation (steady state) for a separation distance of 25cm

To determine the scattering parameters of the WPT 4-4 electrical model, the Advanced Design Systems (ADS) software manufactured by Agilent Corporation will be used. The primary reason to extract the scattering parameters of the WPT 4-4 magnetic element is to determine the system attenuation via the S_{21}. This parameter is associated with the system efficiency and the amount of power provided from the source to the load depending on the signal reflections [50]. The simulation shows an S_{21} parameter of -1.61 dB, this is associated with an efficiency of ~70 % for a separation distance of 25 cm.

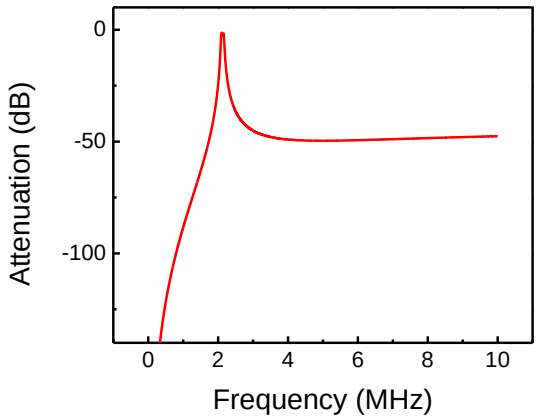

Figure 58: WPT 4-4 S_{21} Parameter (Attenuation) ADS simulation for a separation distance of 25cm

6.2.3 Step 3: WPT 4-4 RF Characterization Using Computational EMC Tools

The prototype WPT 4-4 was evaluated using the Electromagnetic Professional (EMPro) software tool from Agilent Technologies. This software tool performs 3D EM simulations using the computational techniques of Finite Elements Methods (FEM) and Finite-Differential Time-Domain (FDTD). As we previously mention in Chapter Five, the FEM tool will be used to determine the S-Parameters of the WPT element physical characteristics and the FDTD tool will be used to identify the electric and magnetic field intensities.

An EMPro 3D model of the WPT 4-4 (Figure 54) was designed using its characteristics previously described (Table 8). This model was used for the FEM and FDTD simulations. Figure 59 illustrates the mesh generated for the EMPro FEM simulation. It can be seen that the mesh density is adequate for the structure with emphasis on the separation between stages.

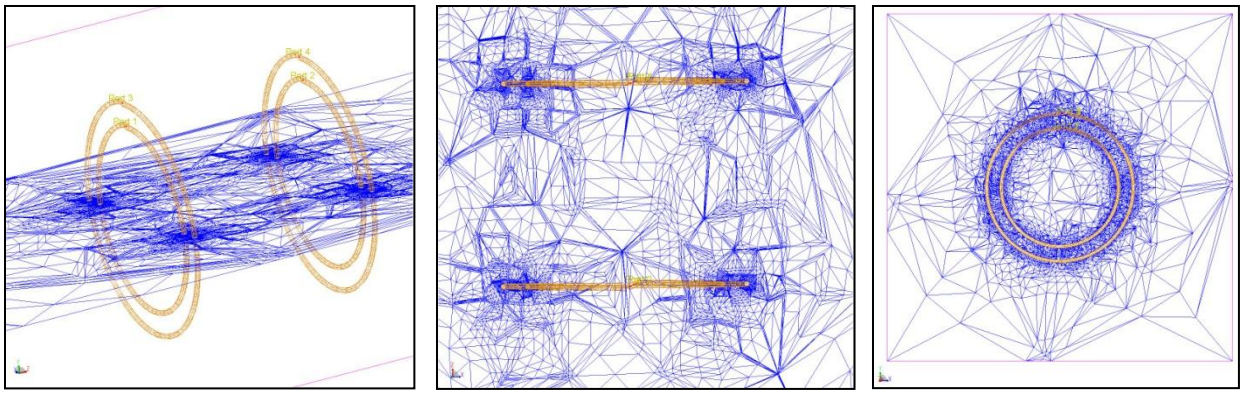

(a) (b) (c)

Figure 59: WPT 4-4 EMPro FEM mesh simulation details views: (a) perspective, (b) top and (c) side

Wireless power transmission can be analytically evaluated by identifying system coupling characteristics. The approach identified to analyze the WPT system with magnetic resonant stages was to demonstrate wireless power transmission based on scattering parameters (S-parameters) FEM simulation . This simulation (specially the S_{21} parameter) will give insight on the frequency of operation and the system coupling characterization of the system [34].

The three conditions that we are trying to identify based on the separation distance between the magnetic resonators (stage 2 and stage 3) are: over-coupled, critically-coupled and under-coupled [34]. Over-coupling occurs if too much capacitive or inductive coupling is inserted in the system, the resonant frequency expands into a band pass response with two peaks [34]. On the other hand, if there is not enough capacitive or inductive coupling, an under-coupled insertion loss can be observed between the source resonant circuit to the load resonant circuit, reducing the power transferred [18]. The desired ideal case will be to operate the system in critically coupled mode, due to the fact that this configuration provides the fewest losses for wireless power transmission. A different power transfer profile will be achieved based on the

WPT system separation. This will also highly depend on the geometry of the stages. Figure 60 illustrates the coupling characteristics of transformer inductive coupled systems.

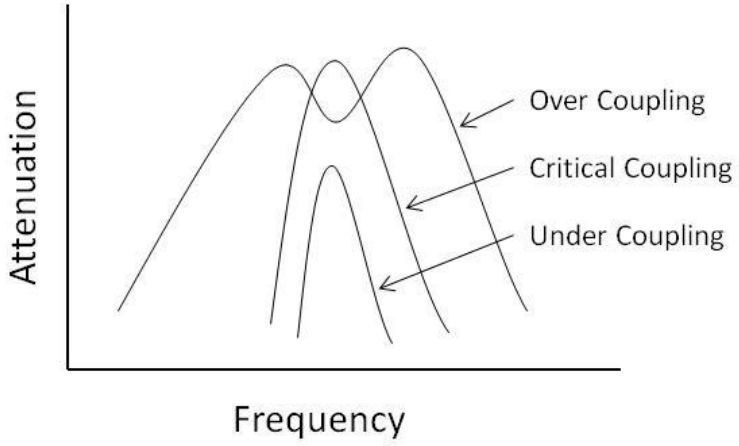

Figure 60: WPT coupling characteristics effects expected for a transformer like resonator system [18] [34]

Following the WPT coupling characteristics effects expected for a transformer like resonator system shown in Figure 60, a series of 3D FEM simulations were performed to identify the over-coupled, critically-coupled and under-coupled cases for the WPT system with magnetic resonant stages shown in Figure 61. To demonstrate the various coupling cases, the 3D WPT 4-4 model was FEM simulated for separation distances from 5 cm to 50 cm. The critically-coupled case was identified at ~25 cm of separation. Therefore, for demonstration purposes, the system was FEM simulated for 5 cm and 50 cm cases to demonstrate the over-coupled and under-coupled cases respectively (as shown in Figure 61).

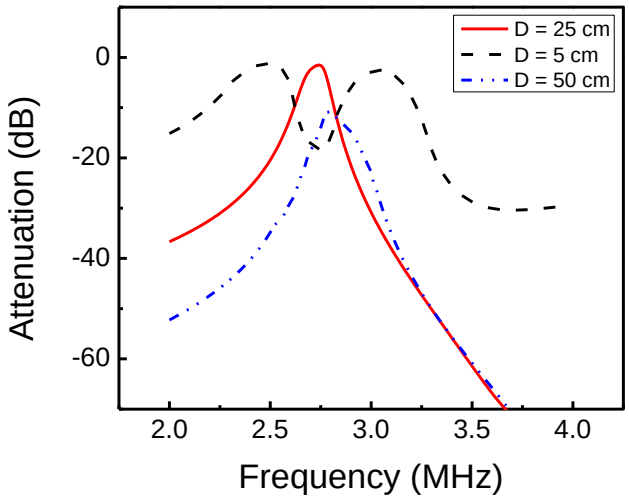

Figure 61: WPT 4-4 S_{21} parameters (attenuation) for various source and load elements separations

The EMPro WPT 4-4 model was also simulated with the FDTD computational tool to determine the electric field intensity at 1 meter of separation and the magnetic field intensity at 7cm of separation as stipulated by the Mil-Std-461E/F in RE-102 [6] [7]. The magnetic field intensity was simulated for illustration purposes; however Mil-Std-461E/F does not require the radiated emissions requirements (RE-101) for systems with a frequency of operation greater than 100 kHz (Figure 36). In this case, the corresponding far field magnetic field intensity for the required electric field intensity of RE-102 will be used for the FDTD field simulation scale. Since we are evaluating the E and F versions of Mil-Std-461, 0.026 A/m and 0.26 A/m are selected as the magnetic field intensities for the corresponding electric fields as maximum limits (20 V/m and 200 V/m) [6] [7]. The FDTD magnetic field intensity results measured at 7 cm is illustrated in Figure 62 (maximum field: 2.72 mA/m). Illustrated in Figure 63 are the FDTD simulation results for the magnetic field intensities around the operational WPT 4-4 magnetic element.

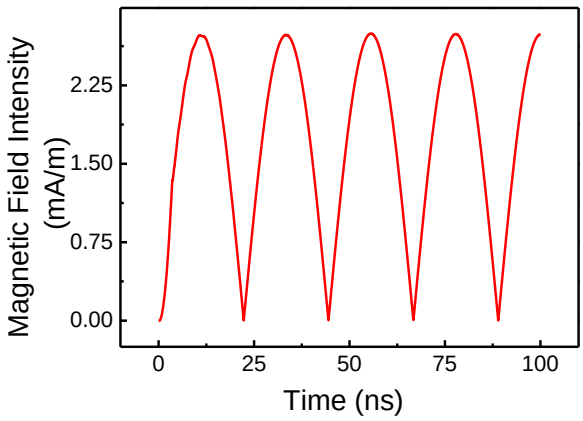

Figure 62: WPT 4-4 magnetic field intensity FDTD simulation according to Mil-Std-461E/F (for illustration purposes only, RE -101 requirement is not applicable for frequencies beyond 100 kHz)

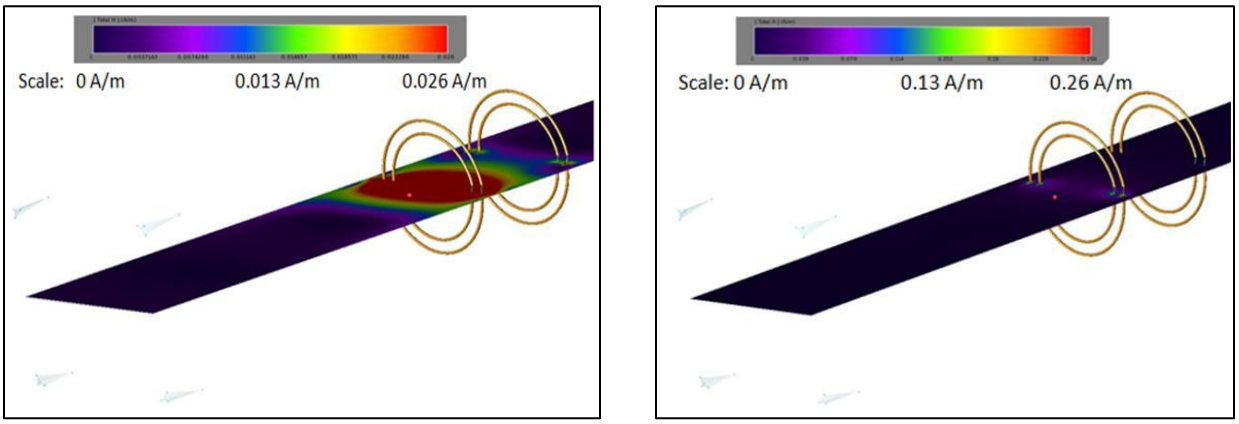

(a) (b)

Figure 63: WPT 4-4 FDTD simulation for the magnetic field intensity (for illustration purposes only, the RE -101 requirement is not applicable for frequencies of operation beyond 100kHz): (a) (scale from 0 to 0.026 A/m, corresponding to far-field approximations of Mil-Std-461E and (b) scale from 0 to 0.26 A/m, corresponding to far-field approximations of Mil-Std-461F

The electric field intensity stipulated by the Mil-Std-461E/F was simulated using the FDTD by placing an electric field intensity prove at 1 meter. Since this system operates at ~2.8 MHz, the RE-102 limit according to Mil-Std-461E/F (Figure 37) is 44 dBµV/m [6] [7]. Since the WPT 4-4 magnetic element produced an electric field intensity of ~93.9 dBµV/m on the FDTD simulation (Figure 64), this is higher than the required limit (44 dBµV/m) and additional assessment (requirement tailoring) will be required. An approach commonly used for launch vehicles is to identify the frequency of operation of the system and evaluate to what levels the surrounding electronic sub-systems were tested for radiated susceptibility (RS) compliance. In addition to RE testing, all the electronics components used in the launch vehicle are also tested for their susceptibility on radiated RF signals. The levels required according to Mil-Std-461E is 20 V/m and for Mil-Std-461F is 200 V/m [6] [7]. The tailoring that has been used in the past is that, if there is no RF receivers at the frequency of operation and the environments generated by the new system are 6dB below the existing systems testing, an exception could be made to the requirements. For the WPT 4-4 magnetic element, 6 dB of 20 V/m (Mil-Std-461E requirement) is 10 V/m and 6 dB of 200 V/m (Mil-Std-461F requirement) is 100 V/m. Therefore, depending of which version of Mil-Std-461 is been used (the heritage "E" version or the current "F" version) the acceptable level changes [6] [7]. Figure 65 illustrates the simulated electric field intensity using as the maximum scale number the 6 dB extrapolation of the electric field intensities used for system RS testing [6] [7].

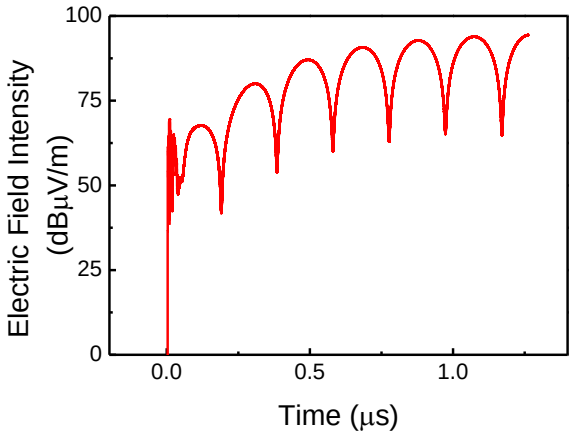

Figure 64: WPT 4-4 electric field intensity FDTD simulation according to Mil-Std-461E/F (1m of separation between the source loop and the electric field intensity meter)

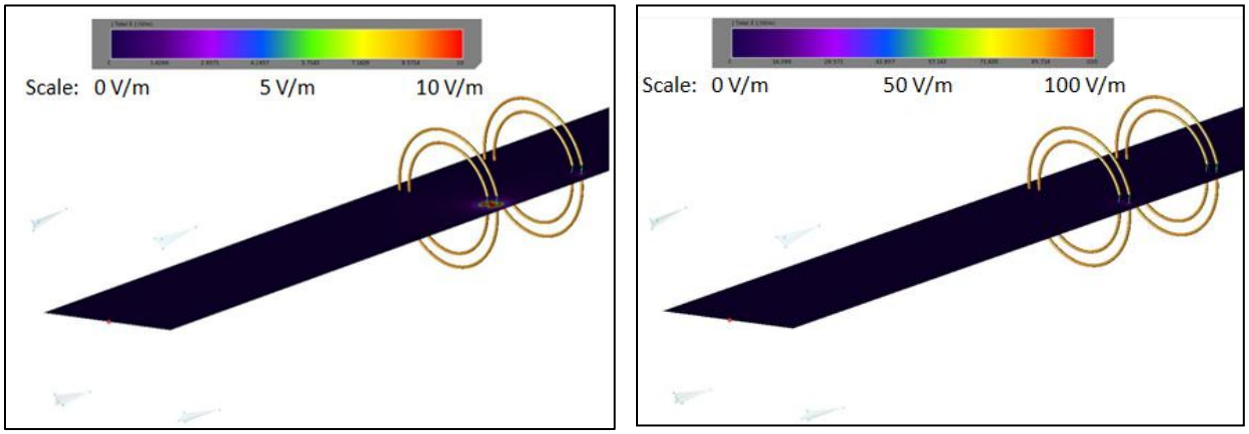

(a) (b)

Figure 65: WPT 4-4 FDTD simulation for the magnetic field intensity: (a) scale from 0 to 10 V/m, corresponding to far-field approximations of Mil-Std-461E and (b) scale from 0 to 100 V/m, corresponding to far-field approximations of Mil-Std-461F

6.2.4 Step 4: WPT 4-4 Prototype Testing

A WPT 4-4 magnetic element prototype was built using the characteristics previously provided in Table 8. The main scope of this section is just demonstrating the concept. Since the magnetic element was built by hand, it is not expected to achieve the efficiencies projected by the simulations. Two prototype tests were performed: induced voltage in the secondary and radiated emissions testing. Using the test configuration described in Figure 33 block diagram, the induced voltage test was performed using the NASA's Flight Analysis RF model validation area (Figure 35). Figure 66 illustrates the WPT 4-4 induced voltage test setup and Figure 67 shows the results.

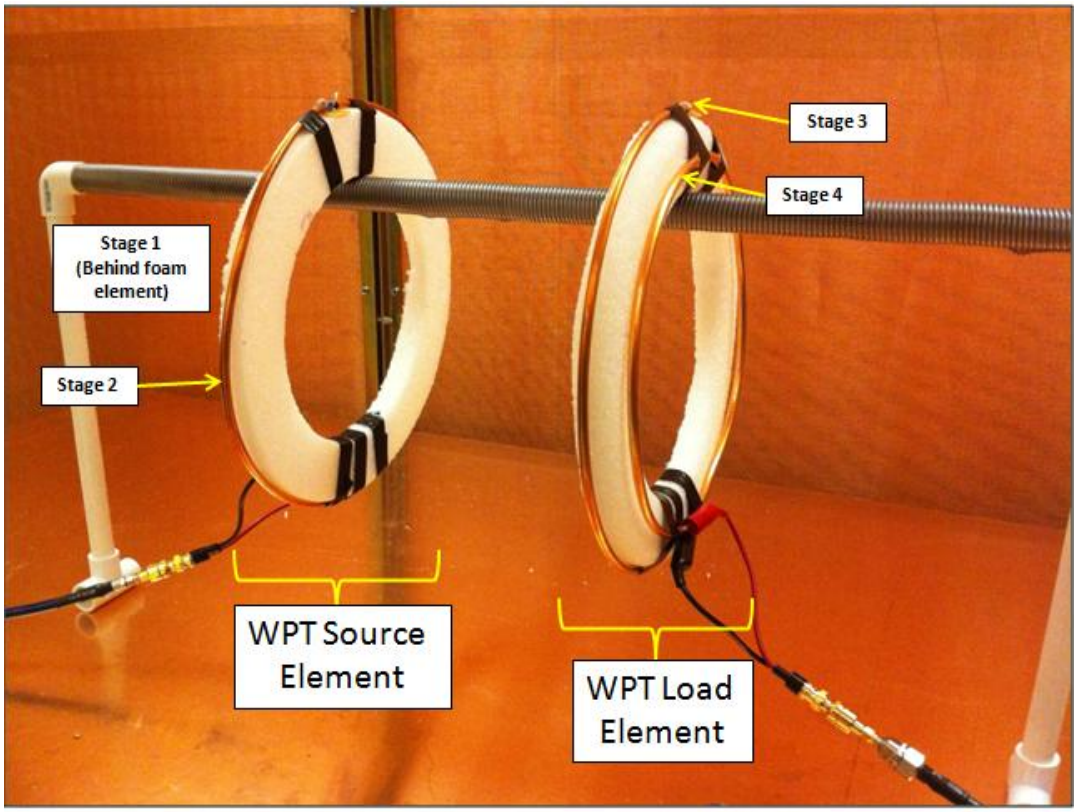

Figure 66: WPT 4-4 induced voltage test magnetic element setup

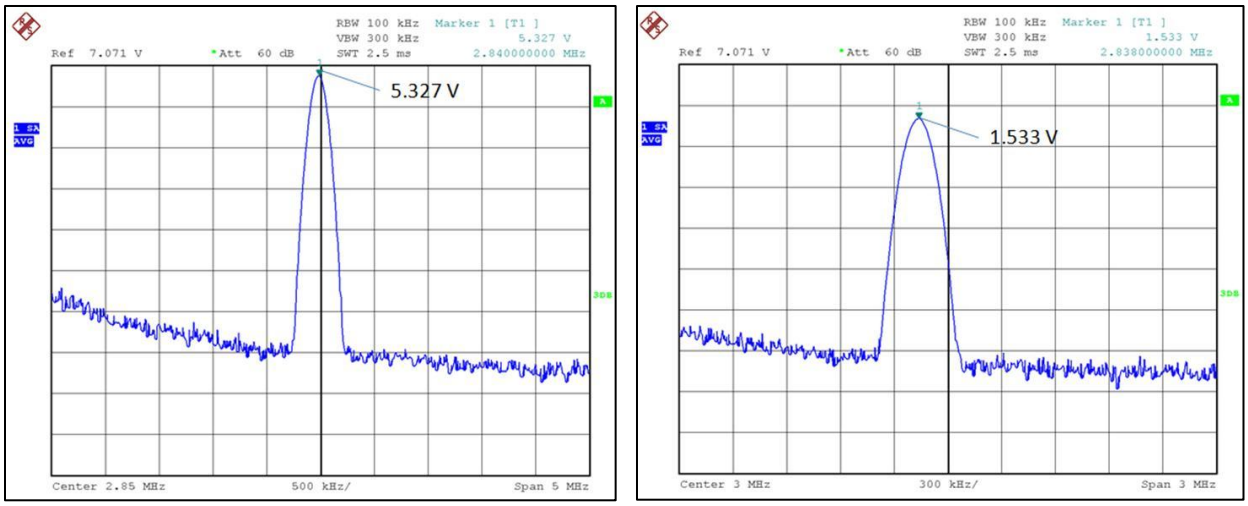

(a) (b)

Figure 67: WPT 4-4 induced voltage test results: (a) voltage supplied without the WPT 4-4 magnetic element and (b) voltage induced in the WPT 4-4 load loop (stage 4)

It can be seen in Figure 67 that voltage of 1.533 V was generated with a supplied 5.327 V. Do to the inaccuracies during the hand-made assembly and the soldering equipment available for the prototype construction, these non-ideal results were expected. However, it was noted that power was transferred wirelessly for a frequency similar to the design one. By transferring power at the design frequency, this experiment met the intended expectations given the known manufacturing limitations.

The next test performed to the WPT 4-4 magnetic element was a radiated emissions test to determine the electric field intensity generated by this prototype. As previously mentioned, and due to the fact that this prototype operates at ~3 MHz, and RE-101 test (magnetic field intensity test) cannot be performed as recommended by Mil-Std-461E/F; the prototype is outside the frequencies of interest (100 kHz is the maximum). Therefore, the only Mil-Std-461 E/F compliance testing that will be performed to the WPT 4-4 magnetic element is the RE-102

(electric field intensity). Using the test setup block diagram illustrated in Figure 34 and the test equipment shown in Figure 35, the WPT 4-4 magnetic element was tested to determine the electric field intensity as shown in Figure 68. Illustrated in Figure 69 are the results of the WPT 4-4 magnetic element RE-102 test performed at the frequency of operation.

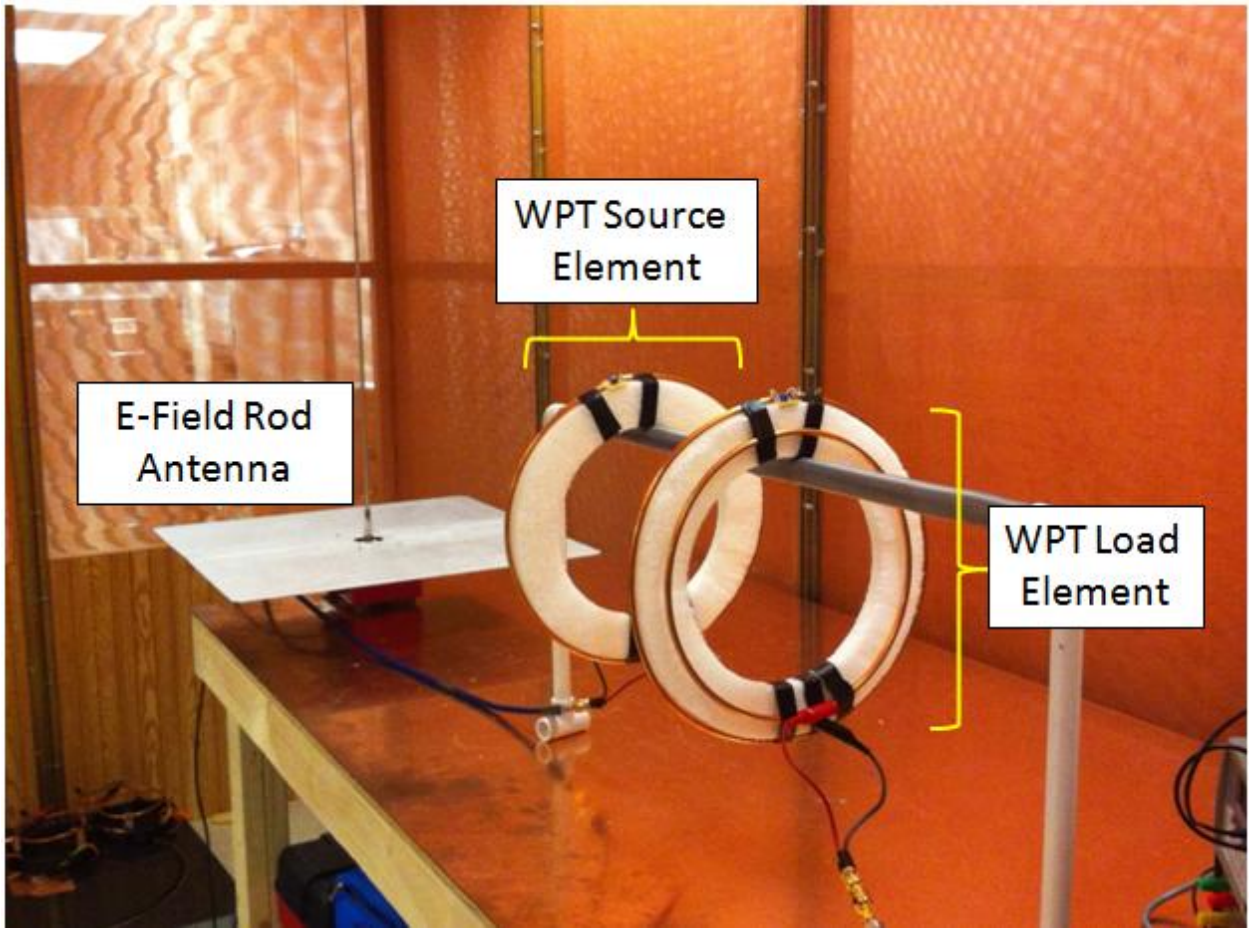

Figure 68: WPT 4-4 magnetic element RE-102 testing setup

The antenna factor was calculated based on the approach delineated in Chapter Two. The antenna factor was applied to the spectrum analyzer reading showed in Figure 69 (49.37 dBµV/m) to reflect the WPT J1 prototype radiated electric field of 28.48 dBµV/m.

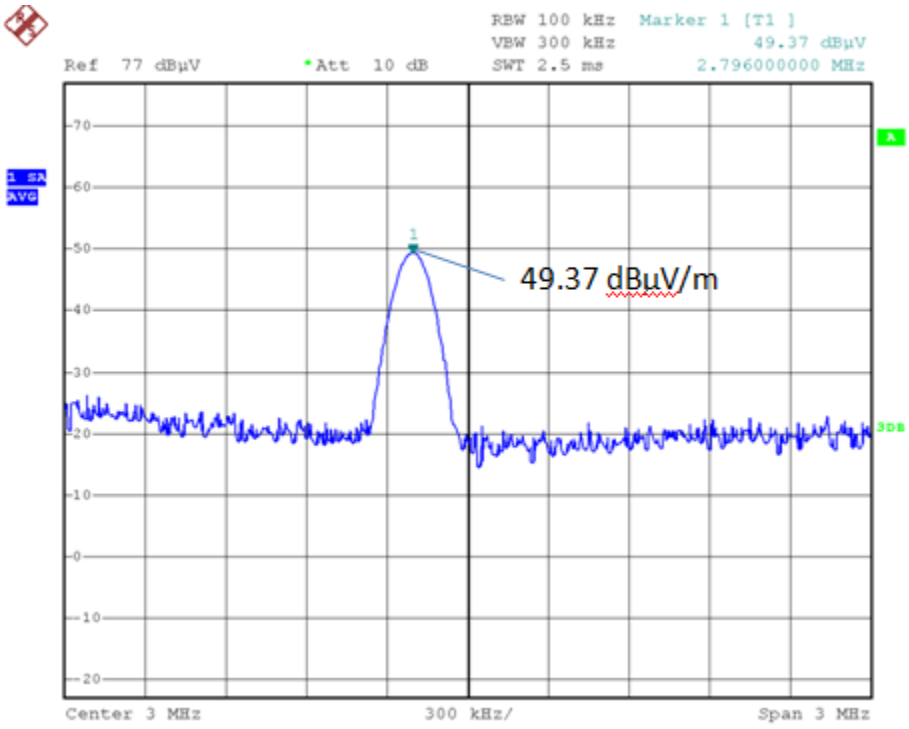

Figure 69: WPT 4-4 magnetic element RE-102 testing results at the frequency of operation

6.2.5 Step 5: WPT 4-4 Compliance with Mil-Std-461E/F for Radiated Emissions

The WPT 4-4 magnetic element compliance with Mil-Std-461E/F will only take into account the electric field intensity requirement (RE-102) due to its frequency of operation. Since WPT 4-4 operates at ~2.78 MHz, the magnetic element prototype is beyond the scope of RE-101; which only covers systems operating at frequencies below 100 kHz. Figure 70 illustrates the comparison between the military standard requirements, the EMPro simulation results and

the test results. It is important to mention that the requirements RE-102 can be tailored for the specific application according to Mil-Std-461E/F [6] [7]. The only aspect considered for military standard compliance is the RE-102 testing (the EMPro simulation is illustrated only for insight). The variation observed between the EMPro result and the test result is attributed to resonator manufacturing limitations. This reduces the efficiency of the magnetic element and the manufacturer imperfections provide a detrimental effect into the overall electric and magnetic field propagation. Assuming that the manufacturing process of these antennas achieved the electric field radiation as the one simulated by the EMPro FDTD tool (93.9 dBμV/m), this will mean that the magnetic element does not comply with the un-tailored RE-102 requirement of the Mil-Std-461E/F. However, a system assessment for possible requirement tailoring could be initiated. By taking the approach that all the surrounding electric/electronic devices in the rocket need to also comply with the radiated susceptibility testing of the Mil-Std-461E/F, these systems are tested for 20 V/m (if version E is applied) or for 200 V/m (if version F is applied) [6] [7]. As explained before, the requirements can be tailored if the WPT radiated emissions is 6dB less than what the rocket electronics are tested too (that is 10 V/m for the E version and 100 V/m for the F version). The simulated electric field of 93.9 dBμV/m corresponds to ~ 0.05 V/m. This means that if the magnetic element is manufactured for the optimal case showed by the simulation, the WPT 4-4 will be radiating orders of magnitudes less electric fields than the electric field intensity margin in which the systems have been tested minus 6 dB.

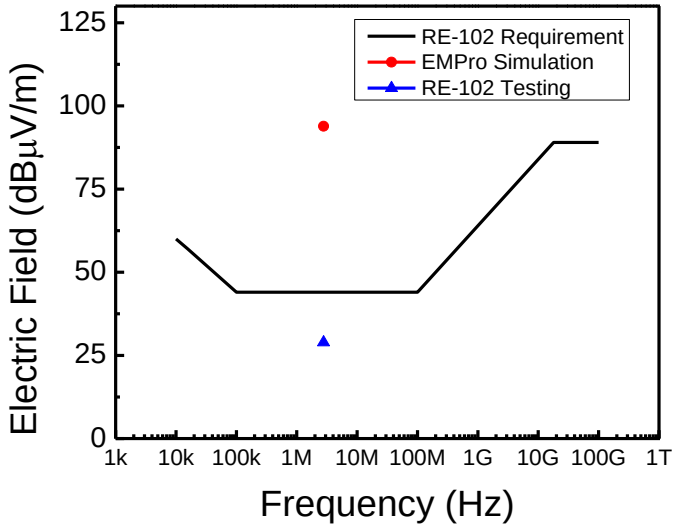

Figure 70: WPT J1 RE-102 (electric field intensity) results comparison between Mil-Std-461E/F requirements, simulations and prototype testing

6.3 Four Stages -Two Single Loops WPT magnetic element (WPT 4-2)

A different approach for WPT magnetic resonant systems is by using resonant structures. One of the most evaluated for wireless power applications is helical resonators [5] [34]. Figure 71 illustrates the block diagram of the WPT System with magnetic resonant structures. The operation of the overall system is similar to the double hollow loop inductor showed previously (Figure 7). However, additional considerations need to be taken for the magnetic element design.

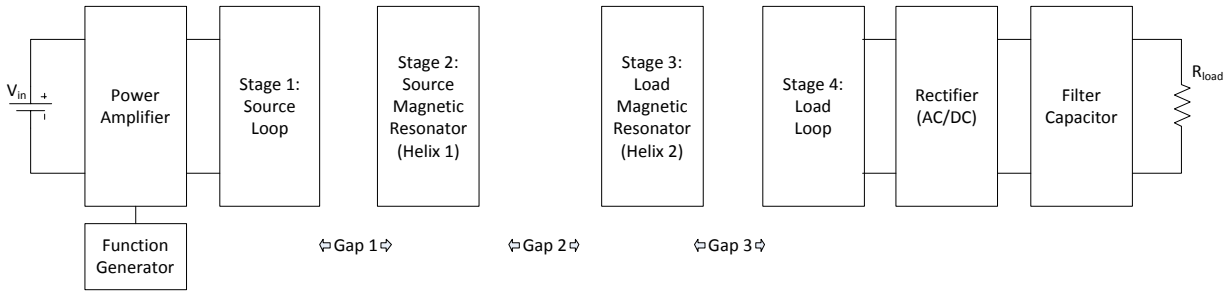

Figure 71: WPT system with magnetic resonator structures block diagram

Wireless power transfer systems with magnetic resonators can either use a power amplifier or an inverter (DC/AC) converter as the AC power source to the source loop at the specific operational frequency. The source loop is considered to be a single loop typically a little smaller than the source magnetic resonator, and needs to be placed near the source magnetic resonator at closed proximity (Gap 1) to provide the excitation energy to the resonator. The source loop and the source magnetic resonator are considered to be the source element of the WPT system. Therefore, the load magnetic resonator and the load loop are considered to be the load element of the WPT system. The source and load magnetic resonators needs to be in a magnetic resonators require additional structural analysis in order to determine its resonant frequency and transfer power wirelessly via magnetic resonance [5] [34]. The method used to determine the prototype's structure resonant frequency is by using Finite Element Simulation (FEM) to acquire the S parameters of the system [34]. The gap between the source and load magnetic resonant structures (Gap 2 in Figure 71) is considered the separation distance between the source and the load elements. The resonant energy irradiated by the load resonator is transfer to the load loop due to a closed proximity [12]. This AC signal is then rectified and filtered to DC for load distribution. Figure 71 illustrates the WPT magnetic resonator FEM 3D Model using Table 10.

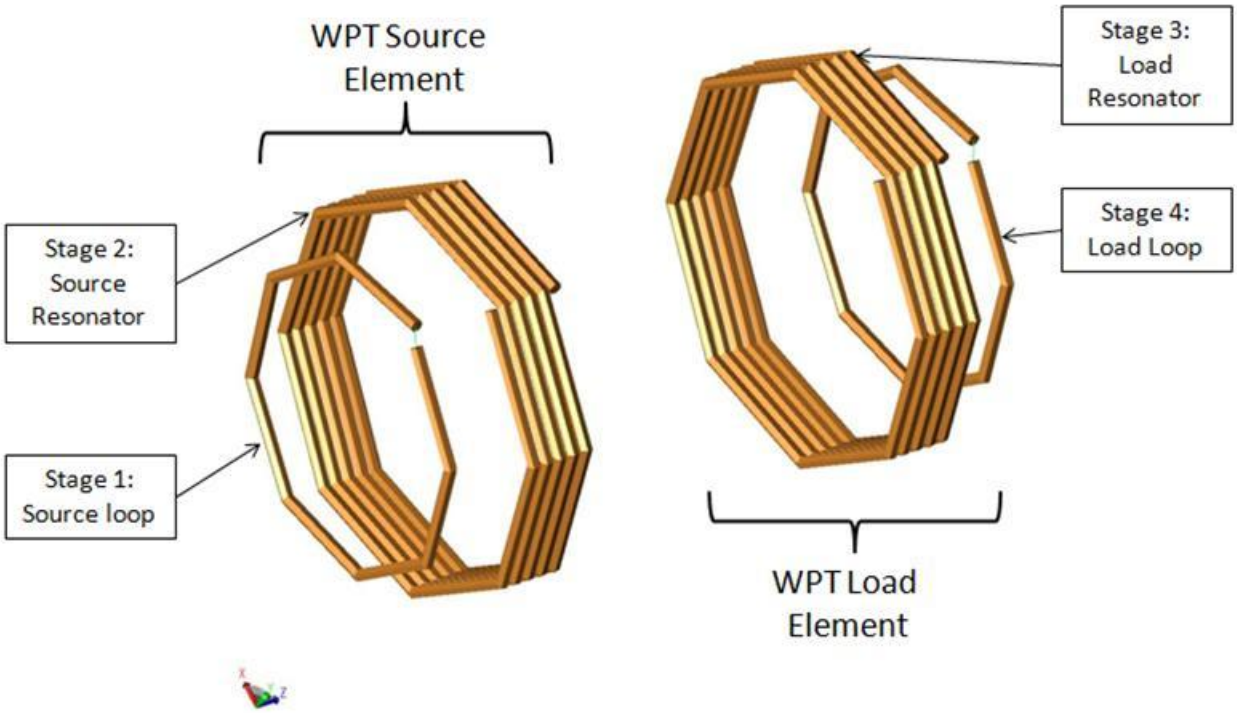

Figure 72: FEM 3D model of the WPT system with magnetic resonant helix structures [34]

Table 10: WPT 4-2 Magnetic Element Characteristics [34]

Element Stage	**Element Characteristics and Values**		
	Characteristic	***Value***	***Units***
Loop #1 & #2	Radius	8	cm
	Wire Diameter	0.635	cm
	Treats	1	turns
	Winding thikness (height)	0.635	cm
	Profilie Segments	6	-
	Path Segments	8	-
	Handedness	right	-
Helical Resonator #1 & #2	Radius	10	cm
	Wire Diameter	0.635	cm
	Treats	5	turns
	Winding thikness (height)	3.81	cm
	Profilie Segments	6	-
	Path Segments	40	-
	Handedness	right	-
Additional Model Characteristics	Separation distance between Loop #1 and Helical Resonator #1 (Transmitter)	5	cm
	Separation distance between Loop #1 and Helical Resonator #1 (Receiver)	5	cm
	Separation distance between the transmitter and the receiver	5 to 50	cm
	Frequency of Operation	~20	MHz

6.3.1 Step 1: WPT 4-4 Parameters Computation

To determine the parameters required for the WPT 4-2 circuit simulation and 3D characterization, various parameters need to be calculated. Based on the characteristics provided in Table 10 and the parameter methodology showed in previous chapters, Table 11 lists the WPT 4-2 parameters calculated for further analysis and simulation. For additional background on the computation behind Table 11, please refer to Appendix K.

Table 11: WPT 4-2 Calculated Parameters

Parameter	Symbol	Value	Unit
Loop 1 & 4 Inductance	L_1 & L_4	0.288	µH
Loop 2 & 3 Inductance	L_2 & L_3	9.695	µH
Capacitances 2 & 3 (induced by the helix resonant structures)	C_2 & C_3	5.115	pF
Coupling coefficient (stage 1&2)	k_{12}	0.546	
Coupling coefficient (stage 2&3)	k_{23}	0.028	
Coupling coefficient (stage 3&4)	k_{34}	0.546	
Mutual Inductance 12 (stages 1&2)	L_{M12}	0.913	µH
Mutual Inductance 23 (stages 2&3)	L_{M23}	0.269	nH
Mutual Inductance 34 (stages 3&4)	L_{M34}	0.913	µH
Leakage Inductance 1 (stages 1&2)	$L_{leakage1}$	0.105	nH
Leakage Inductance 2a (stages 1&2)	$L_{leakage2a}$	5.131	µH
Leakage Inductance 2b (stages 2&3)	$L_{leakage2b}$	9.427	µH
Leakage Inductance 3a (stages 2&3)	$L_{leakage3a}$	9.427	µH
Leakage Inductance 3b (stages 3&4)	$L_{leakage3b}$	5.131	µH
Leakage Inductance 4 (stages 3&4)	$L_{leakage4}$	0.105	µH
Series resistance (stage 1&4)	R_1 & R_4	4.750	mΩ
Series resistance (stage 2&3)	R_2 & R_3	5.849	mΩ

6.3.2 Step 2: WPT 4-2 Circuit Simulation

As in the previous cases studied, the WPT magnetic element underwent three different circuit simulations: SPICE frequency response, SPICE time domain simulation and ADS scattering parameter simulation. Figure 73 illustrates the WPT 4-2 magnetic element SPICE frequency response results. It can be noticed that the system is resonating at approximately 22.5 MHz (significantly closed to the design frequency of operation, f = 20 MHz).

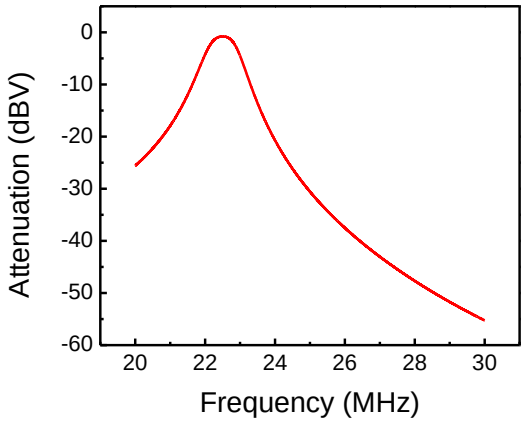

Figure 73: WPT 4-2 magnetic element SPICE frequency response simulation at a 25 cm separation

Illustrated in Figure 74 are the SPICE transient simulation results. It can be noticed that there was a voltage induced of about 2.4 V with an input voltage of 5 V. This demonstrates that WPT can be achieved with the WPT 4-2 configuration.

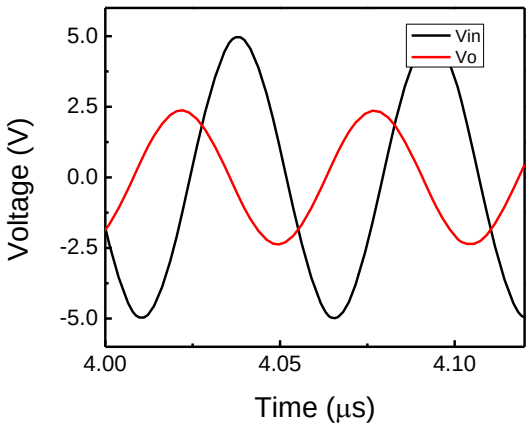

Figure 74: WPT 4-2 transient SPICE simulation (steady state) for a separation distance of 25cm

To determine the scattering parameter, especially S_{21}, we simulated the circuit using Agilent's ADS software package. Figure 75 shows the WPT 4-2 magnetic element ADS S_{21} parameter simulation. This simulation shows an attenuation factor of -0.0494 dB, which corresponds to a maximum possible efficiency of 98% for the WPT 4-2 magnetic element.

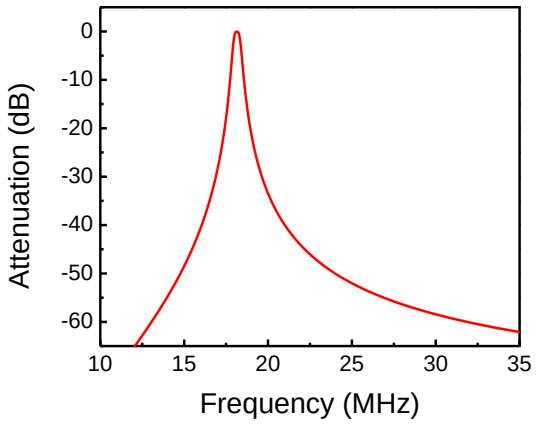

Figure 75: WPT 4-2 magnetic element ADS S_{21} parameter simulation

6.3.3 Step 3: WPT 4-2 RF Characterization Using Computational EMC Tools

The WPT 4-2 magnetic element was simulated using Agilent's EMPro to simulate the electric and magnetic field intensities and the scattering parameters. The scattering parameters were simulated using EMPro's FEM computational tool and the electric/magnetic field intensities were calculated with EMPro's FDTD computational tool. Figure 76 illustrates the WPT 4-2 EMPro FEM mesh simulation details for perspective and top views.

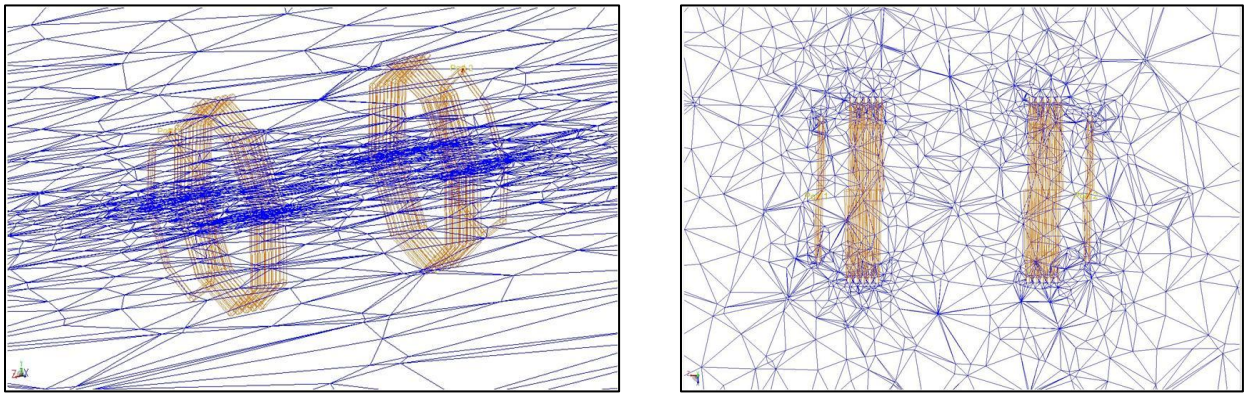

(a) (b)

Figure 76: WPT 4-2 EMPro FEM mesh simulation details views: (a) perspective, and (b) top

Since the WPT 4-2 magnetic element is a four elements with magnetic resonators system, it is expected a compiling characterization variance with separation distance variation similar to the one experienced with the WPT 4-4 magnetic element simulation FEM. For additional insight in the compiling characterization effect (over-coupling, critically-coupled and under-coupling), please refer to section 6.2.3 (Step 2: WPT 4-4 RF Characterization Using Computational EMC Tools). Figure 77 illustrates the three coupling characterization effects expected, based on separation distance variation: over-coupling (D = 5cm), critically coupled (D = 25 cm) and under-coupling (D = 50 cm).

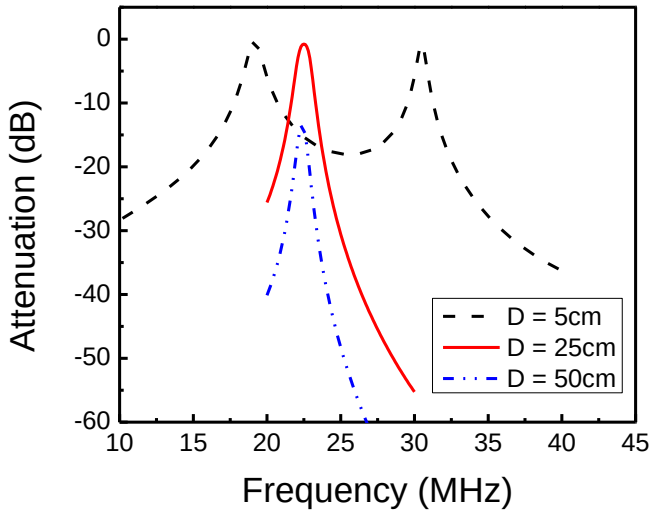

Figure 77: WPT 4-2 magnetic element 3D FEM coupling effects performance based on separation distance operation between source and load. Cases simulated: 5 cm (over-coupled case), 25 cm (critically-coupled case), and 50 cm (under-coupled case)

The WPT 4-2 magnetic element was also simulated using the EMPro FDTD tool to determine the electric and magnetic fields at the separation in which the sensor needs to be placed for the Mil-Std-461E/F RE-101 and RE-102 measurements. It is important to mention that the magnetic field intensity simulation is only provided for illustration purposes. Due to the frequency of operation of WPT 4-2 magnetic element (~ 20 MHz), the RE-101 test is not required for this WPT. Figure 78 illustrates the WPT 4-2 magnetic field intensity FDTD simulation according to Mil-Std-461E/F for the RE-101 test (not applicable for this frequency of operation) and Figure 79 shows the WPT 4-2 FDTD simulation for the magnetic field intensity illustration.

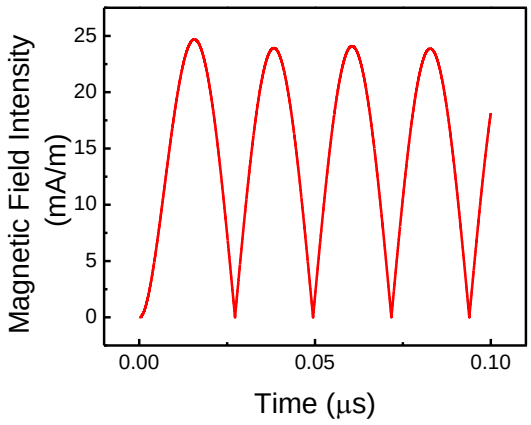

Figure 78: WPT 4-2 magnetic field intensity FDTD simulation (for illustration purposes only, the RE-101 requirement is not applicable for frequencies beyond 100 kHz)

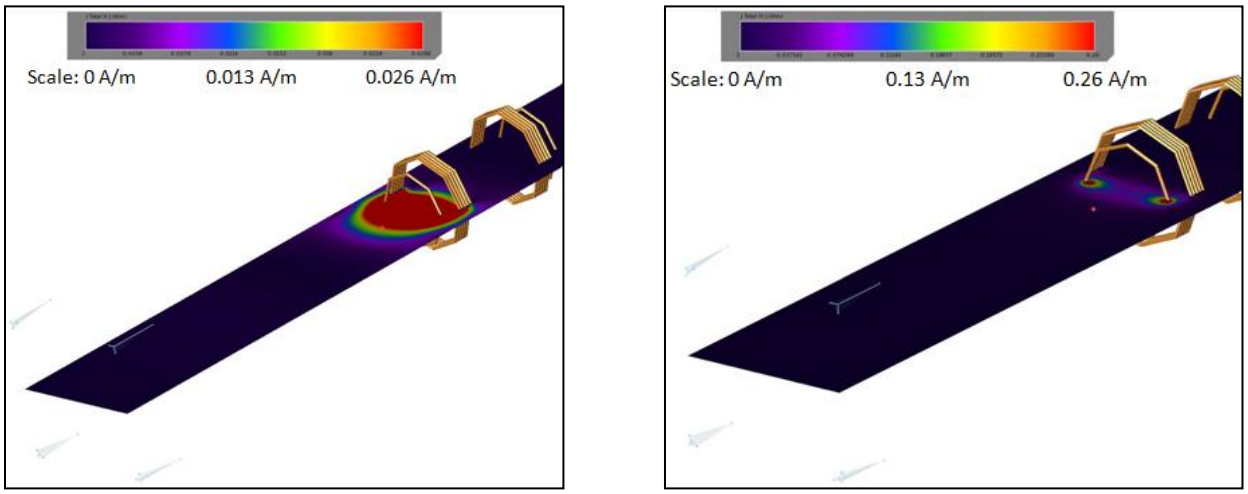

(a) (b)

Figure 79: WPT 4-2 FDTD simulation for the magnetic field intensity (for illustration purposes only, the RE -101 requirement is not applicable for frequencies of operation beyond 100kHz): (a) (scale from 0 to 0.026 A/m, corresponding to far-field approximations of Mil-Std-461E and (b) scale from 0 to 0.26 A/m, corresponding to far-field approximations of Mil-Std-461F

The other implemented FDTD simulation result generated with the EMPro simulation, was the electric field intensity induced at 1 meter of separation (according with the RE-101 testing requirement) [6] [7]. Illustrated in Figure 80 is the electric field intensity at 1 meter of separation between the WPT source device and the virtual EMPro electric field sensor. It can be noticed that the electric field intensity is about 75 dBμV/m. This is considered o to be higher than the Mil-Std-461E/F RE-102, therefore an additional assessment of the surrounding space subsystems needs to be performed in order to evaluate the tailoring possibility of the Mil-Std-461E/F. Figure 81 provides the WPT 4-2 FDTD simulation for the magnetic field intensity for further exploring the Mil-Std-461E/F tailoring possibility. Requirement compliance will be discussed in the following sub-section (Chapter 6.3.5).

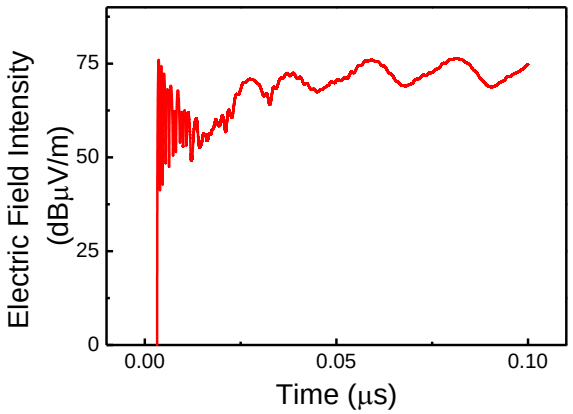

Figure 80: WPT 4-2 electric field intensity FDTD simulation according to Mil-Std-461E/F (1m of separation between the source loop and the electric field intensity meter)

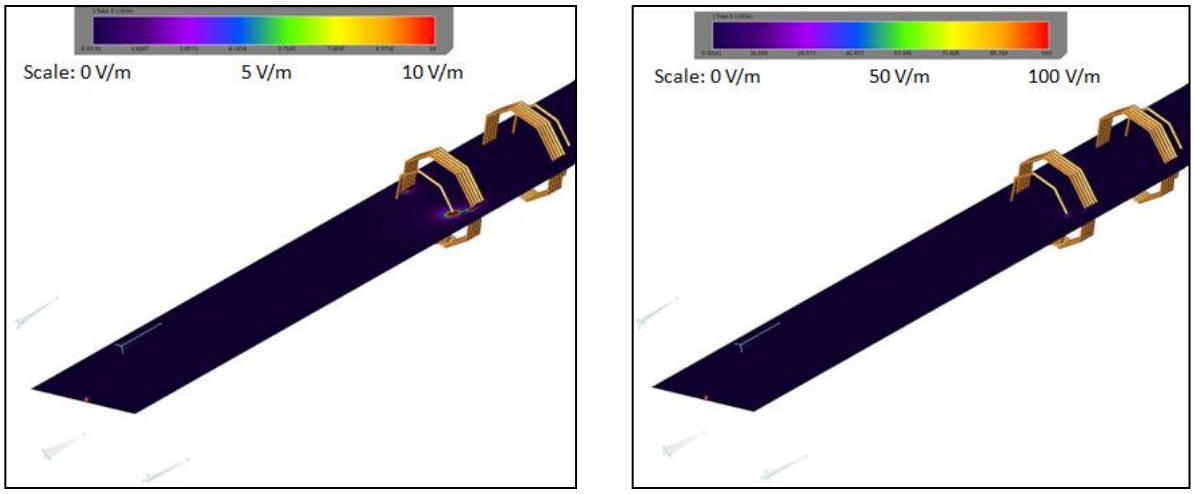

(a) (b)

Figure 81: WPT 4-2 FDTD simulation for the magnetic field intensity: (a) scale from 0 to 10 V/m, corresponding to far-field approximations of Mil-Std-461E and (b) scale from 0 to 100 V/m, corresponding to far-field approximations of Mil-Std-461F

6.3.4 Step 4: WPT 4-2 Prototype Testing

A proof of concept WPT 4-2 magnetic element was developed to acquire insight into the implementation. It is understood that the fabrication by hand of a magnetic resonator will not provide the efficiency reflected during simulation, however is expected to provide additional insight to the design. The WPT 4-2 magnetic element developed was tested for voltage induction and radiated emissions. Figure 82 illustrates the WPT 4-2 magnetic element voltage induction testing setup. Figure 83 shows the voltage induced in the WPT 4-2 load element when voltage is applied to the WPT 4-2 source element.

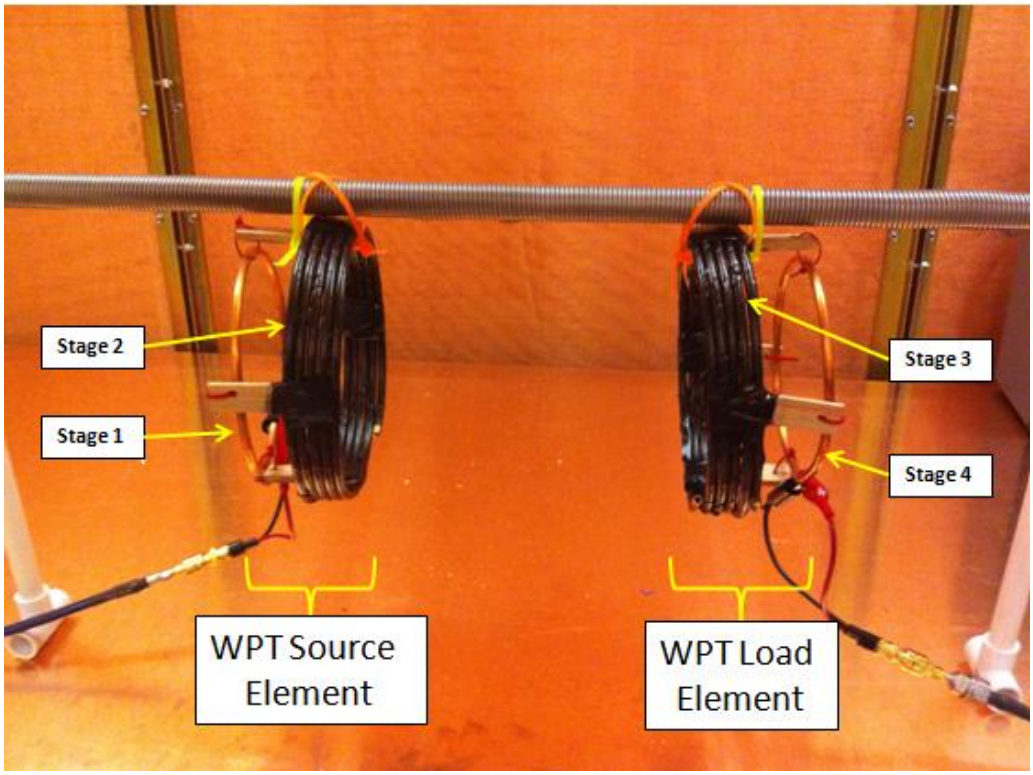

Figure 82: WPT 4-2 magnetic element voltage induction testing setup

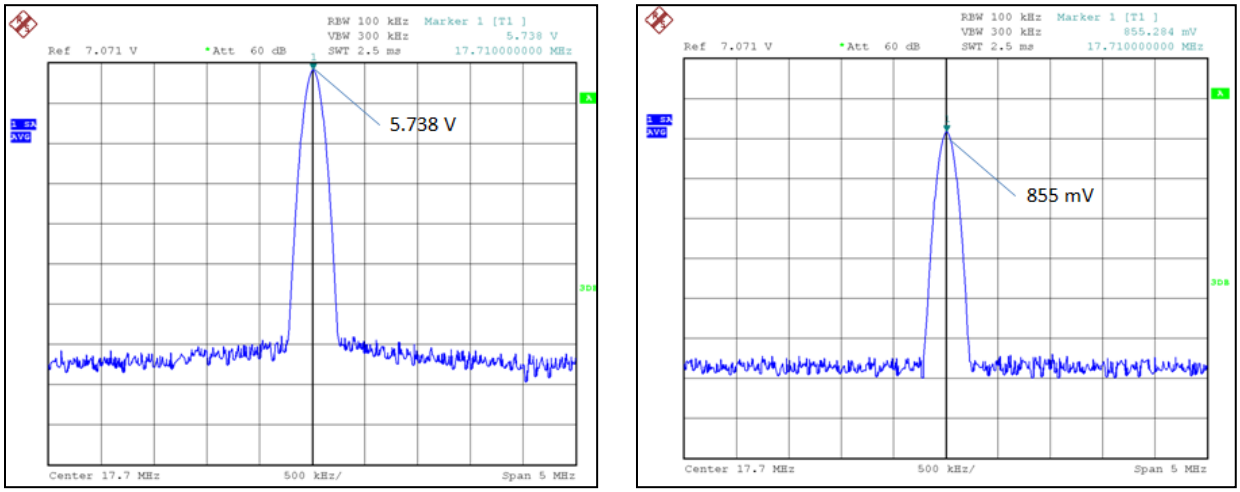

(a) (b)

Figure 83: WPT 4-2 induced voltage test results: (a) voltage supplied without the WPT 4-2 magnetic element and (b) voltage induced in the WPT 4-2 load loop (stage 4)

The WPT 4-2 magnetic element was also tested for electric field intensity radiated emission. This WPT magnetic element will not be tested for the RE-101 (magnetic field intensity) due to the fact that its frequency of operation is outside the scope of the test. Figure 84 illustrates the WPT 4-2 magnetic element RE-102 testing setup. Figure 85 shows the WPT 4-2 magnetic element RE-102 testing results at the frequency of operation. It is important to mention that to get the final measurement of the radiated electric field intensity, we will need to factor in the antenna factor for the frequency of operation. After adding the antenna factor calculated in accordance with the guideline in the Chapter Two, the WPT 4-2 radiated electric field intensity is 82.13 dBµV/m.

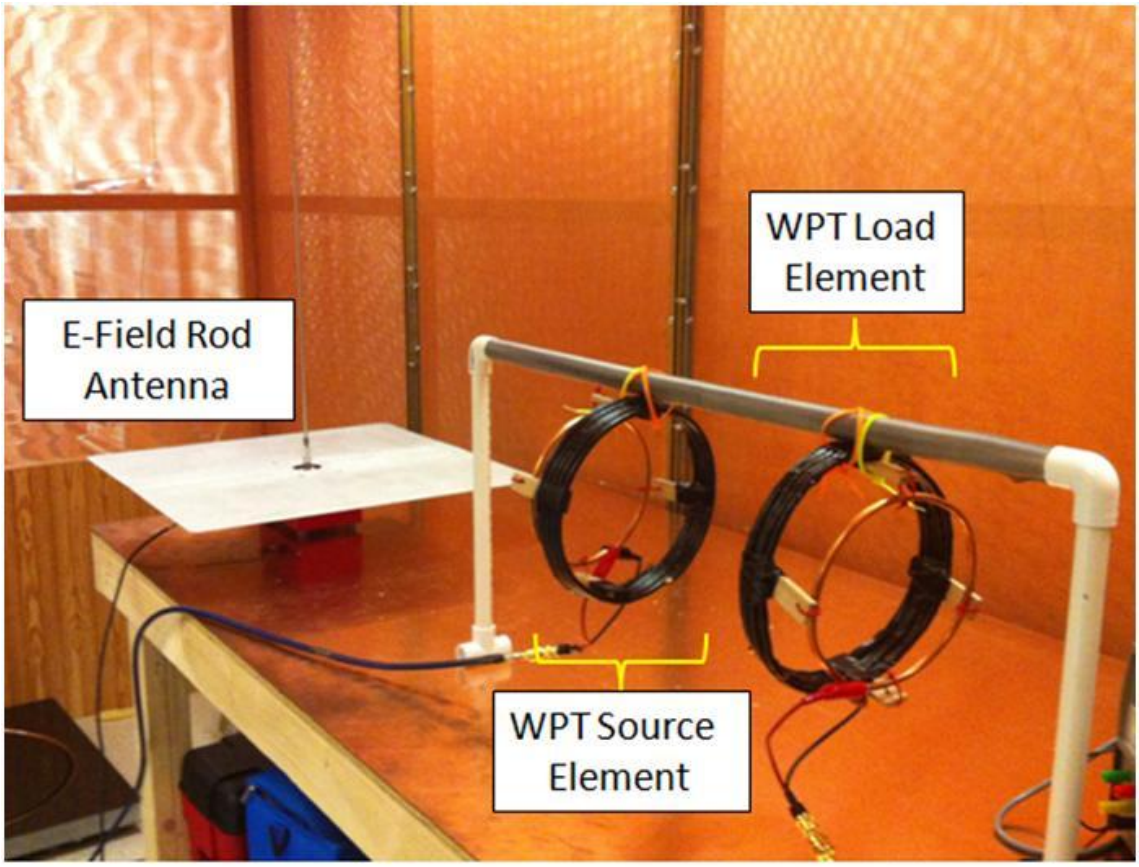

Figure 84: WPT 4-2 magnetic element RE-102 testing setup

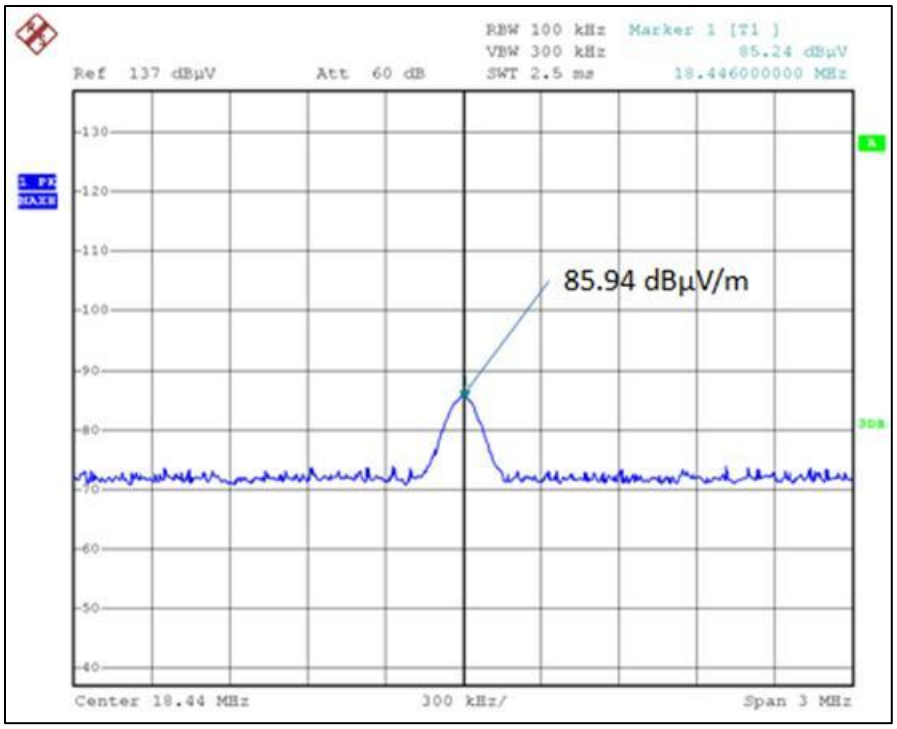

Figure 85: WPT 4-2 magnetic element RE-102 testing results at the frequency of operation

6.3.5 Step 5: WPT 4-2 Compliance with Mil-Std-461E/F for Radiated Emissions

The Mil-Std-461E/F compliance approach for the WPT 4-2 magnetic element is similar to the one already performed for the WPT 4-4 magnetic element. Due to the fact that WPT 4-2 operates at a frequency (~20 MHz) outside the scope of RE-101 (for signals no greater than 100 kHz), the magnetic field intensity will not be assessed. Figure 86 shows the WPT 4-2 RE-102 (electric field intensity) results comparison between Mil-Std-461E/F requirements, simulations and prototype testing. It is important to note that there was a great agreement between the simulated and tested electric field intensity, however none of them met the un-tailored Mil-Std-461E/F requirements. The EMPro simulation showed a 82.13 dBµV/m electric field intensity, while the RE-102 testing showed a 75 dBµV/m electric field intensity. As previously discussed

for WPT 4-4, all the electronics of the launch vehicles are supposed to be tested to 20 V/m (if version "E" of the requirement is used) or 200 V/m (if version "F" of the requirement is used). Due to the fact that the tested electric field intensity according to Mil-Std-461E/F is below 10 V/m (140 dBµV/m), the WPT 4-2 magnetic element could potentially be accepted for the use in space due to the fact that operates at less than 6dB of what the launch vehicle electronics systems are tested.

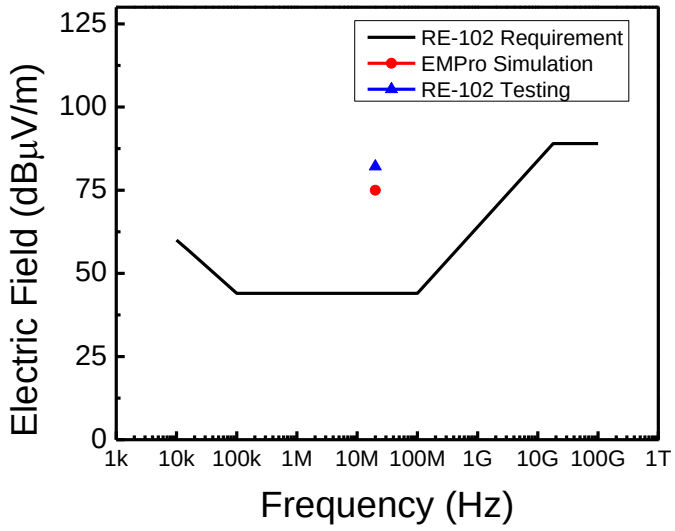

Figure 86: WPT 4-2 RE-102 (electric field intensity) results comparison between Mil-Std-461E/F requirements, simulations and prototype testing

CHAPTER SEVEN: CONCLUSIONS

Wireless Power Transfer systems design and electromagnetic compatibility radiated emissions environments were considered for the use in space systems. The study focused on the possible use of WPT systems in launch vehicles (rockets).

The system design of WPT systems involved an advanced analyses targeted to evaluate the magnetic elements used, the coupling configuration of the source and load resonant circuit and their Q-Factors. Twelve loops pairs where studied with four different loop radius (1.5 cm 3.5 cm, 5 cm and 12 cm) and three different loop materials (Litz wire, solid wire and speaker wire). It was identified by testing and SPICE simulation that the most suitable characteristic for our application was Litz wire with a radius of 12 cm (the best Q-Factor and inductance for the application). There were also four capacitive coupling configurations evaluated: series-series, series-shunt, shunt-series and shunt-shunt. It was also determined by test and simulation that the best capacitive coupling configurations for the application were the series-series and series-shunt configuration.

Taking in consideration the worst environment expected by the WPT systems (radiated emissions), an EMC design approach was developed. This design approach takes into consideration the compliance standard used for space and military systems (Mil-Std-461 E/F). The approach provides a series of recommended simulations to acquire an specific insight of the WPT system and to determine if is going to meet the systems requirements. This approach was successfully validated with three WPT magnetic element prototypes.

APPENDIX A: MATHCAD FILE OF THE WPT SYSTEM PROOF-OF-CONCEPT PROTOTYPE SIMULATIONS VARYING THE CAPACITOR COUPLING CONFIGURATIONS

Prepared by: Gabriel Vázquez Ramos

INPUTS:

$ds := 0.03$ $N1 := 8$ $fs := 23 \cdot 10^{3}$

$d1 := 0.24$ $N2 := 8$ $r\_c := 0.001$

$d2 := 0.24$ $Iin := 0.5$ $u0 := 4 \cdot \pi \cdot 10^{-7}$

CALCULATIONS:

$r1 := \frac{d1}{2}$ $r1 = 0.12$

$r2 := \frac{d2}{2}$ $r2 = 0.12$

$L1 := N1^{2} \cdot r1 \cdot u0 \cdot \left[\ln\left[\frac{(8 \cdot r1)}{r\_c} \right] - 1.75 \right]$ $L1 = 4.938 \times 10^{-5}$

$L2 := N2^{2} \cdot r2 \cdot u0 \cdot \left[\ln\left[\frac{(8 \cdot r2)}{r\_c} \right] - 1.75 \right]$ $L2 = 4.938 \times 10^{-5}$

$C1 := \frac{1}{\left[(2 \cdot \pi \cdot fs)^{2} \cdot L1 \right]}$ $C1 = 9.696 \times 10^{-7}$

$C2 := \frac{1}{\left[(2 \cdot \pi \cdot fs)^{2} \cdot L2 \right]}$ $C2 = 9.696 \times 10^{-7}$

$k := \frac{1}{\left[1 + 2^{\left(\frac{2}{3}\right)} \cdot \left[\frac{ds}{\sqrt{(r1 \cdot r2)}} \right]^{2} \right]^{\left(\frac{3}{2}\right)}}$ $k = 0.868$

$Lm := \sqrt{L1 \cdot L2} \cdot k$ $Lm = 4.285 \times 10^{-5}$

$Llk1 := L1 - Lm$ $Llk1 = 6.533 \times 10^{-6}$

$Llk2 := L2 - Lm$ $Llk2 = 6.533 \times 10^{-6}$

APPENDIX B: SPICE NETLISTS OF THE WPT SYSTEM PROOF-OF-CONCEPT PROTOTYPE SIMULATIONS VARYING THE CAPACITOR COUPLING CONFIGURATIONS

Appendix B.1: Series-Series Coupling Configuration SPICE Simulation Netlist

```
V1 In 0 SINE(0 20 23k) Rser=4
R1 Out+ Out- 4
R2 N001 L1 0.6
R3 L2 N002 0.6
L1 0 L1 49.4µ
L2 0 L2 49.4µ
C1 N002 N003 1µ
C2 In N001 1µ
D1 N003 Out+ D
D2 Out- N003 D
D3 0 Out+ D
D4 Out- 0 D
C3 Out+ Out- 100µ Rser=100m
.model D D
.lib C:\PROGRA~2\LTC\LTSPIC~1\lib\cmp\standard.dio
.tran 3ms
K1 L1 L2 0.868
.backanno
.end
```

Appendix B.2: Series-Shunt Coupling Configuration SPICE Simulation Netlist

```
V1 In 0 SINE(0 20 23k) Rser=4
R1 Out+ Out- 4
R2 N001 L1 0.6
R3 L2 C2 0.6
L1 0 L1 49.4µ
L2 0 L2 49.4µ
C1 C2 0 1µ
C2 In N001 1µ
D1 C2 Out+ D
D2 Out- C2 D
D3 0 Out+ D
D4 Out- 0 D
C3 Out+ Out- 100µ Rser=100m
.model D D
.lib C:\Program Files (x86)\LTC\LTspiceIV\lib\cmp\standard.dio
.tran 3ms
K1 L1 L2 0.868
.backanno
.end
```

Appendix B.3: Shunt-Series Coupling Configuration SPICE Simulation Netlist

```
R1 In N001 0.6
L1 0 N001 49.4µ
C1 In 0 1µ
V1 In 0 PULSE(-5 5 0 1n 1n 21.5u 43u) Rser=4
R2 Out+ Out- 4
R3 N002 N003 0.6
L2 0 N002 49.4µ
C2 N003 N004 1µ
D1 N004 Out+ D
D2 Out- N004 D
D3 0 Out+ D
D4 Out- 0 D
C3 Out+ Out- 100µ Rser=100m
.model D D
.lib C:\Program Files (x86)\LTC\LTspiceIV\lib\cmp\standard.dio
.tran 3ms
K1 L1 L2 0.868
.backanno
.end
```

Appendix B.4: Shunt-Shunt Coupling Configuration SPICE Simulation Netlist

```
R1 Out+ Out- 4
R2 In L1 0.6
R3 L2 C2 0.6
L1 0 L1 49.4µ
L2 0 L2 49.4µ
C1 C2 0 1µ
C2 In 0 1µ
D1 C2 Out+ D
D2 Out- C2 D
D3 0 Out+ D
D4 Out- 0 D
C3 Out+ Out- 100µ Rser=100m
V1 In 0 PULSE(-5 5 0 1n 1n 21.5u 43u) Rser=4
.model D D
.lib C:\Program Files (x86)\LTC\LTspiceIV\lib\cmp\standard.dio
.tran 3ms
K1 L1 L2 0.868
.backanno
.end
```

APPENDIX C: WPT EQUIVALENT IMPEDANCE DERIVATION CODE USING MATLAB SYMBOLIC MATH TOOLBOX

Appendix C.1: WPT Series-Series System Equivalent Impedance Matlab Code

```
clc
close all
clear all
disp('##########################################################################')
disp('##########################################################################')
disp('###                                                                    ###')
disp('###           WPT Equivalent Impedance Calculation                     ###')
disp('###           Series-Series Coupling Configuration                     ###')
disp('###            Prepared by: Gabriel Vázquez Ramos                      ###')
disp('###                                                                    ###')
disp('##########################################################################')
disp('##########################################################################')
fprintf('\n\n');


%        +---------------------------------+
%        | Equivalent Impedance Definition |
%        +---------------------------------+
%
%              +----+           +----+
%          o---| Z1 |-----+-----| Z3 |------+
%              +----+     |     +----+      |
%                         |                 |
%       +-+>           +--+-+            +--+-+
%       |              | Z2 |            | Z4 |
%    +--+--+           +--+-+            +--+-+
%    | Zeq |              |                 |
%    +--+--+              |                 |
%                        -+-               -+-
%                        GND               GND
syms R1 R2 Ro C1 C2 L1 L2 Lm s Lk1 Lk2

% Series-Series Coupling:


display('=================================================================+')
display('Z1=')
Z1=(Lk2*s)+R2+(1/(C2*s))+Ro;
pretty(Z1)

display('=================================================================+')
display('Z2=')
Z2=1/((1/(Lm*s))+(1/Z1));
pretty(Z2)

display('=================================================================+')
display('Zeq=')
Zeq=(1/(C1*s))+(Lk1*s)+R1+Z2
pretty(Zeq)
```

Appendix C.2: WPT Series-Shunt System Equivalent Impedance Matlab Code

```
clc
close all
clear all
disp('#########################################################################')
disp('#########################################################################')
disp('###                                                                   ###')
disp('###           WPT Equivalent Impedance Calculation                    ###')
disp('###            Series-Shunt Coupling Configuration                    ###')
disp('###            Prepared by: Gabriel Vázquez Ramos                     ###')
disp('###                                                                   ###')
disp('#########################################################################')
disp('#########################################################################')
fprintf('\n\n');


%        +---------------------------------+
%        | Equivalent Impedance Definition |
%        +---------------------------------+
%
%              +----+           +----+
%         o----| Z1 |-----+-----| Z3 |------+
%              +----+     |     +----+      |
%                         |                 |
%       +-+>           +--+-+            +--+-+
%       |              | Z2 |            | Z4 |
%    +--+--+           +--+-+            +--+-+
%    | Zeq |              |                 |
%    +--+--+              |                 |
%                        -+-               -+-
%                        GND               GND

syms R1 R2 Ro C1 C2 L1 L2 Lm s Lk1 Lk2

% Series-Shunt Coupling:


display('=============================================================+')
display('Z1=')
Z1=1/((1/Ro)+(s*C2));
pretty(Z1)

display('=============================================================+')
display('Z2=')
Z2=Z1+(Lk2*s)+R2;
pretty(Z2)

display('=============================================================+')
display('Z3=')
Z3=1/((1/(Lm*s))+(1/Z2));
```

```
pretty(Z3)

display('============================================================+')
display('Zeq=')
Zeq=(1/(C1*s))+(Lk1*s)+R1+Z3;
pretty(Zeq)

R = simplify(Zeq);
display('Zeq_simpl=')
pretty(R)
```

APPENDIX D: WPT SYSTEMS SERIES-SERIES AND SERIES-SHUNT COUPLING CONFIGURATION EQUIVALENT IMPEDANCE NUMERICAL SOLUTION PROGRAM

```
clc
close all
clear all
disp('#########################################################################')
disp('#########################################################################')
disp('###                                                                   ###')
disp('###           WPT Equivalent Impedance Calculation                    ###')
disp('###    Series-Series and Series-Shunt Coupling Configuration          ###')
disp('###            Prepared by: Gabriel Vázquez Ramos                     ###')
disp('###                                                                   ###')
disp('#########################################################################')
disp('#########################################################################')
fprintf('\n\n');


%%%%%%%%%%%%%%%%%%%%%%%%%%%%%%%%%%%%%%%%%%%%%%%%%%%%%%%%%%%%%%%%%%%%%%%%%%%%
%%%%%%                          INPUTS                                 %%%%%%
%%%%%%%%%%%%%%%%%%%%%%%%%%%%%%%%%%%%%%%%%%%%%%%%%%%%%%%%%%%%%%%%%%%%%%%%%%%%

% -<( Load )>-
Ro=4;

% -<( WPT Double Loop Parameters given distance and fs )>-

R1=0.4;
R2=0.4;
L1=6.533e-6;
L2=6.533e-6;
Lm=42.85e-6;
C1=1e-6;
C2=1e-6;
fs=23e3;
w=2*pi*fs;



%%%%%%%%%%%%%%%%%%%%%%%%%%%%%%%%%%%%%%%%%%%%%%%%%%%%%%%%%%%%%%%%%%%%%%%%%%%%
%%%%%%                      CALCULATIONS                               %%%%%%
%%%%%%%%%%%%%%%%%%%%%%%%%%%%%%%%%%%%%%%%%%%%%%%%%%%%%%%%%%%%%%%%%%%%%%%%%%%%

% -<( Impedance of the WPT coils and output resistance )>-

Zeq_series_shunt = R1 + L1*(j*w) + 1/(1/(R2 + L2*(j*w) + 1/(C2*(j*w) + 1/Ro))
...
    + 1/(Lm*(j*w))) + 1/(C1*(j*w)); %"ssh" is series-shunt coupling

Zeq_series_series = R1 + L1*(j*w) + 1/(C1*(j*w)) + 1/(1/(R2 + Ro +
L2*(j*w)...
    + 1/(C2*(j*w))) + 1/(Lm*(j*w)));  %"ss" is series-shunt coupling
```

```
% -<( Frequency Response of the WPT coils and output resistance )>-

s = tf('s');  % declaring S-Domain variable

Zeq_ssh = R1 + L1*s + 1/(1/(R2 + L2*s + 1/(C2*s + 1/Ro))...
    + 1/(Lm*s)) + 1/(C1*s);  %"ssh" is series-shunt coupling
Zeq_ss =R1 + L1*s + 1/(C1*s) + 1/(1/(R2 + Ro + L2*s...
    + 1/(C2*s)) + 1/(Lm*s));  %"ss" is series-series coupling


%%%%%%%%%%%%%%%%%%%%%%%%%%%%%%%%%%%%%%%%%%%%%%%%%%%%%%%%%%%%%%%%%%%%%%%%%%%
%%%%%%                              OUTPUT                                %%%%%%
%%%%%%%%%%%%%%%%%%%%%%%%%%%%%%%%%%%%%%%%%%%%%%%%%%%%%%%%%%%%%%%%%%%%%%%%%%%
disp('*********************************************************************')
disp('***                             OUTPUT                              ***')
disp('*********************************************************************')
fprintf('\n\n');

% -<( Display of the Impedance Results )>-

disp('Equivalent WPT Impedance with Series-Series Coupling:')
Zeq_series_series
fprintf('\n');

disp('Equivalent WPT Impedance with Series-Shunt Coupling:')
Zeq_series_shunt
fprintf('\n');

% -<( Frequency Response Plot of the WPT Element and the Load )>-

P = bodeoptions; % Set frequency units to Hz in options
P.FreqUnits = 'Hz'; % Create plot with the options specified by P
bode(Zeq_ssh,Zeq_ss,P) % Bode plot of the System Gvd1 & 2 with P spec's
grid on
```

APPENDIX E: PROTOTYPE WPT TECHNOLOGY PATHFINDER DEMOSNTRATION MATHCAD CALCULATIONS

Prepared by: Gabriel Vázquez Ramos

INPUTS:

$d := 0.15$ $N := 7$ $fs\_84k := 84 \cdot 10^{3}$

$u0 := 4 \cdot \pi \cdot 10^{-7}$ $r\_c := 0.01$ $fs\_839k := 839 \cdot 10^{3}$

$fs\_1757k := 1757 \cdot 10^{3}$

CALCULATIONS

$r := \frac{d}{2}$ $r = 0.075$

$L := N^{2} \cdot r \cdot u0 \cdot \left[\ln\left[\frac{(8 \cdot r)}{r\_c} \right] - 1.75 \right]$ $L = 1.083 \times 10^{-5}$

Coupling Capacitors for fs=84 kHz:

$C\_84k := \frac{1}{\left[(2 \cdot \pi \cdot fs\_84k)^{2} \cdot L \right]}$ $C\_84k = 3.316 \times 10^{-7}$

Coupling Capacitors for fs=839 kHz:

$C\_839k := \frac{1}{\left[(2 \cdot \pi \cdot fs\_839k)^{2} \cdot L \right]}$ $C\_839k = 3.324 \times 10^{-9}$

Coupling Capacitors for fs=1.757 MHz:

$C\_1757k := \frac{1}{\left[(2 \cdot \pi \cdot fs\_1757k)^{2} \cdot L \right]}$ $C\_1757k = 7.579 \times 10^{-10}$

APPENDIX F: SPICE NETLISTS OF THE WPT SYSTEM PROOF-OF-CONCEPT PROTOTYPE SIMULATION

```
V1 In 0 SINE(0 12 15.5k)
R0 Out+ Out- 4
R1 N001 N002 1
R2 N004 C2 1
L_lk1 N002 N003 6.533µ
L_lk2 N003 N004 6.533µ
Lm N003 0 42.85µ
C2 C2 0 2.2µ
C1 In N001 2.2µ
D1 C2 Out+ D
D2 Out- C2 D
D3 0 Out+ D
D4 Out- 0 D
C4 Out+ Out- 100µ Rser=100m
.model D D
.lib C:\PROGRA~2\LTC\LTSPIC~1\lib\cmp\standard.dio
.tran 1ms
K1 L_lk1 L_lk2 0.0
.backanno
.end
```

APPENDIX G: WPT J1 PROTOTYPE PARAMETER COMPUTATION MATHCAD WORKSHEET

WPT J1 PARAMETER CALCULATION

Prepared by: Gabriel Vázquez Ramos

INPUTS:

$ds := 0.03$ $N1 := 8$ $fs := 15.56\,10^{3}$ $ur := 1$

$d1 := 0.24$ $N2 := 8$ $a := 0.001$ $cl := 2.998\times 10^{8}$

$d2 := 0.24$ $Iin := 0.5$ $u0 := 4\cdot\pi\cdot 10^{-7}$ $w := 2\cdot\pi\cdot fs$

$sig := 5.96\,10^{7}$

CALCULATIONS:

$r1 := \frac{d1}{2}$ $r1 = 0.12$

$r2 := \frac{d2}{2}$ $r2 = 0.12$

$L1 := N1^{2}\cdot r1\cdot u0\cdot\left[\ln\left[\frac{(8\cdot r1)}{a}\right] - 1.75\right]$ $L1 = 4.938\times 10^{-5}$ $L2 := L1$

$C1 := \frac{1}{\left[(2\cdot\pi\cdot fs)^{2}\cdot L1\right]}$ $C1 = 2.119\times 10^{-6}$ $C2 := C1$

$$k := \frac{1}{\left[1 + 2^{\left(\frac{2}{3}\right)}\cdot\left[\frac{ds}{\sqrt{(r1\cdot r2)}}\right]^{2}\right]^{\left(\frac{3}{2}\right)}} \qquad k = 0.868$$

$Lm := \sqrt{L1\cdot L2}\cdot k$ $Lm = 4.285\times 10^{-5}$

$Llk1 := L1 - Lm$ $Llk1 = 6.533\times 10^{-6}$

$Llk2 := L2 - Lm$ $Llk2 = 6.533\times 10^{-6}$

Series Resisntance:

Ohmic Resistances (Ro):

$$Ro1 := \sqrt{\frac{(w\cdot u0\cdot ur\cdot r1)}{2\cdot sig\cdot a}}$$

Radiation Resistances (Rr):

$$Rr1 := 20\cdot\left[\left[\frac{(2\cdot\pi\cdot fs)}{cl}\right]^{2}\cdot\pi\cdot r1^{2}\right]^{2}$$

Total Resistance (R):

$R1 := Ro1 + Rr1$ $R1 = 3.517\times 10^{-4}$

$R2 := R1$ $R2 = 3.517\times 10^{-4}$

APPENDIX H: WPT J1 MAGNETIC ELEMENT CIRCUIT SIMULATION

Appendix H.1 WPT J1 Frequency Response SPICE Simulation Netlist

```
V1 In 0 SINE() AC 1 0
R0 Out 0 4
R1 N001 N002 0.2
R2 N004 Out 0.2
L_lk1 N002 N003 6.533µ
L_lk2 N003 N004 6.533µ
Lm N003 0 42.85µ
C2 Out 0 2.2µ
C1 In- N001 2.2µ
R3 In In- 4
.ac dec 100000 1k 50k
.backanno
.end
```

Appendix H.2 WPT J1 Transient Response SPICE Simulation Netlist

```
V1 In 0 SINE(0 12 15.5k)
R0 Out 0 4
R1 N001 N002 0.2
R2 N004 Out 0.2
L_lk1 N002 N003 6.533µ
L_lk2 N003 N004 6.533µ
Lm N003 0 42.85µ
C2 Out 0 2.2µ
C1 In+ N001 2.2µ
R3 In In+ 4
.tran 1ms
.backanno
.end
```

Appendix H.3 WPT J1 Scattering Parameters Simulation in ADS

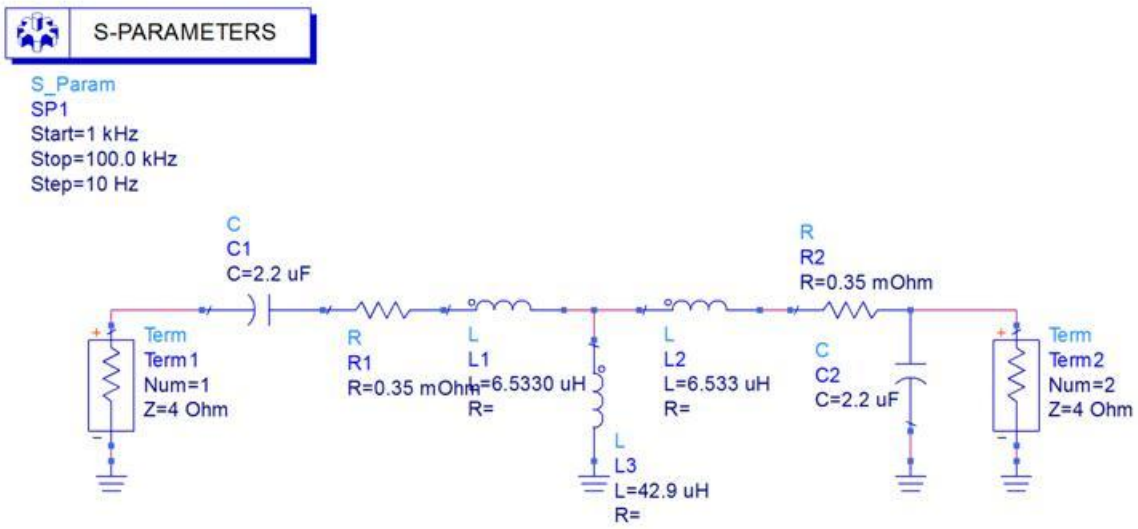

Figure 87: WPT J1 scattering parameters circuit simulation in ADS

APPENDIX I: WPT 4-4 MAGNETIC ELEMENT PARAMETER COMPUTATION MATHCAD WORKSHEET

WPT 4-4 PARAMETER COMPUTATION

Prepared by: Gabriel Vázquez Ramos

INPUTS:

$d1 := 0.24$ $d3 := 0.30$ $N1 := 1$ $N3 := 1$ $D12 := 0.01$ $fs := 3 \cdot 10^{6}$

$d2 := 0.30$ $d4 := 0.24$ $N2 := 1$ $N4 := 1$ $D23 := 0.25$ $a := 0.00635$

$n12 := \frac{N2}{N1}$ $n23 := \frac{N3}{N2}$ $n34 := \frac{N4}{N3}$ $D34 := 0.01$ $u0 := 4 \cdot \pi \cdot 10^{-7}$

$w := 2 \cdot \pi \cdot fs$ $ur := 1$

$sig := 5.96 10^{7}$ $cl := 2.998 \times 10^{8}$

CALCULATIONS:

FOR Lm12

$r1 := \frac{d1}{2}$ $r1 = 0.12$

$r2 := \frac{d2}{2}$ $r2 = 0.15$

$L1 := N1^{2} \cdot r1 \cdot u0 \cdot \left[\ln\left[\frac{(8 \cdot r1)}{a} \right] - 2 \right]$ $L1 = 4.552 \times 10^{-7}$

$L2 := N2^{2} \cdot r2 \cdot u0 \cdot \left[\ln\left[\frac{(8 \cdot r2)}{a} \right] - 2 \right]$ $L2 = 6.11 \times 10^{-7}$

$C2 := \frac{1}{\left[(2 \cdot \pi \cdot fs)^{2} \cdot L2 \right]}$ $C2 = 4.606 \times 10^{-9}$

$k12 := \frac{1}{\left[1 + 2^{\left(\frac{2}{3}\right)} \cdot \left[\frac{D12}{\sqrt{(r1 \cdot r2)}} \right]^{2} \right]^{\left(\frac{3}{2}\right)}}$ $k12 = 0.987$

$Lm12 := \frac{\pi \cdot u0 \cdot (r1 \cdot r2)^{2}}{2 \cdot \left(D12^{2} + r1^{2} \right)^{\frac{3}{2}}}$ $Lm12 = 3.663 \times 10^{-7}$

$Llk1 := L1 - \frac{Lm12}{n12}$ $Llk1 = 8.889 \times 10^{-8}$

$Llk2a := L2 - (Lm12 n12)$ $Llk2a = 2.447 \times 10^{-7}$

FOR Lm23:

$$r3 := \frac{d3}{2} \qquad r3 = 0.15$$

$$L3 := N3^2 \cdot r3 \cdot u0 \cdot \left[\ln\left[\frac{(8 \cdot r3)}{a} \right] - 2 \right] \qquad L3 = 6.11 \times 10^{-7}$$

$$C3 := \frac{1}{\left[(2 \cdot \pi \cdot fs)^2 \cdot L3 \right]} \qquad C3 = 4.606 \times 10^{-9}$$

$$k23 := \frac{1}{\left[1 + 2^{\left(\frac{2}{3}\right)} \cdot \left[\frac{D23}{\sqrt{(r2 \cdot r3)}} \right]^2 \right]^{\left(\frac{3}{2}\right)}} \qquad k23 = 0.079$$

$$Lm23 := \frac{\pi \cdot u0 \cdot (r2 \cdot r3)^2}{2 \cdot \left(D23^2 + r2^2 \right)^{\frac{3}{2}}} \qquad Lm23 = 4.032 \times 10^{-8}$$

$$Llk2b := L2 - \frac{Lm23}{n23} \qquad Llk2b = 5.707 \times 10^{-7}$$

$$Llk3a := L3 - (Lm23 n23) \qquad Llk3a = 5.707 \times 10^{-7}$$

FOR Lm34:

$$r4 := \frac{d4}{2} \qquad r4 = 0.12$$

$$L4 := N4^2 \cdot r4 \cdot u0 \cdot \left[\ln\left[\frac{(8 \cdot r4)}{a} \right] - 2 \right] \qquad L4 = 4.552 \times 10^{-7}$$

$$k34 := \frac{1}{\left[1 + 2^{\left(\frac{2}{3}\right)} \cdot \left[\frac{D34}{\sqrt{(r3 \cdot r4)}} \right]^2 \right]^{\left(\frac{3}{2}\right)}} \qquad k34 = 0.987$$

$$Lm34 := \frac{\pi \cdot u0 \cdot (r3 \cdot r4)^2}{2 \cdot \left(D34^2 + r3^2\right)^{\frac{3}{2}}} \qquad Lm34 = 1.882 \times 10^{-7}$$

$$Llk3b := L3 - \frac{Lm34}{n34} \qquad Llk3b = 4.228 \times 10^{-7}$$

$$Llk4 := L4 - (Lm34 n34) \qquad Llk4 = 2.669 \times 10^{-7}$$

Series Resistance:

Ohmic Resistances (Ro):

$$Ro1 := \sqrt{\frac{(w \cdot u0 \cdot ur \cdot r1)}{2 \cdot sig \cdot a}}$$

$$Ro2 := \sqrt{\frac{(w \cdot u0 \cdot ur \cdot r2)}{2 \cdot sig \cdot a}}$$

$$Ro4 := Ro1 \qquad Ro3 := Ro2$$

Radiation Resistances (Rr):

$$Rr1 := 20 \cdot \left[\left[\frac{(2 \cdot \pi \cdot fs)}{cl}\right]^2 \cdot \pi \cdot r1^2\right]^2$$

$$Rr2 := 20 \cdot \left[\left[\frac{(2 \cdot \pi \cdot fs)}{cl}\right]^2 \cdot \pi \cdot r2^2\right]^2$$

$$Rr4 := Rr1 \qquad Rr3 := Rr2$$

Total Resistance (R):

$$R1 := Ro1 + Rr1 \qquad R1 = 1.938 \times 10^{-3}$$

$$R4 := R1 \qquad R4 = 1.938 \times 10^{-3}$$

$$R2 := Ro2 + Rr2 \qquad R2 = 2.168 \times 10^{-3}$$

$$R3 := R2 \qquad R3 = 2.168 \times 10^{-3}$$

APPENDIX J: WPT 4-4 MAGNETIC ELEMENT CIRCUIT SIMULATION

Appendix J.1 WPT 4-4 Frequency Response SPICE Simulation Netlist

```
V1 N001 0 SINE() AC 1
R1 N002 N001 50
R2 N003 N002 1.938m
R3 N006 N005 2.168m
C1 N006 N007 4.606n
C2 N008 N009 4.606n
R4 N009 N010 2.168m
R5 N012 N013 1.938m
R6 N013 N014 50
L1 N003 N004 0.08889µ
L2 N004 N005 0.2447µ
L3 N010 N011 0.4228µ
L4 N011 N012 0.2669µ
L5 N004 0 0.3663µ
L6 N014 N008 0.611µ Rser=0
L7 0 N007 0.611µ Rser=0
L8 N011 N014 0.1882µ
K1 L7 L6 0.784
.ac dec 100000 0.001e6 10e6
.backanno
.end
```

Appendix J.2 WPT 4-4 Transient Response SPICE Simulation Netlist

```
V1 in 0 SINE(0 5 2.0887e6) AC 1
R1 in_s_s in 50
R2 N001 in_s_s 1.938m
R3 N004 N003 2.168m
C1 N004 N005 4.606n
C2 N006 N007 4.606n
R4 N007 N008 2.168m
R5 N010 +out 1.938m
R6 +out -out 50
L1 N001 N002 0.08889µ
L2 N002 N003 0.2447µ
L3 N008 N009 0.4228µ
L4 N009 N010 0.2669µ
L5 N002 0 0.3663µ
L6 -out N006 0.611µ
L7 0 N005 0.611µ
L8 N009 -out 0.1882µ
K1 L7 L6 0.079
.tran 50u
.backanno
.end
```

Appendix J.3 WPT 4-4 Scattering Parameters Simulation in ADS

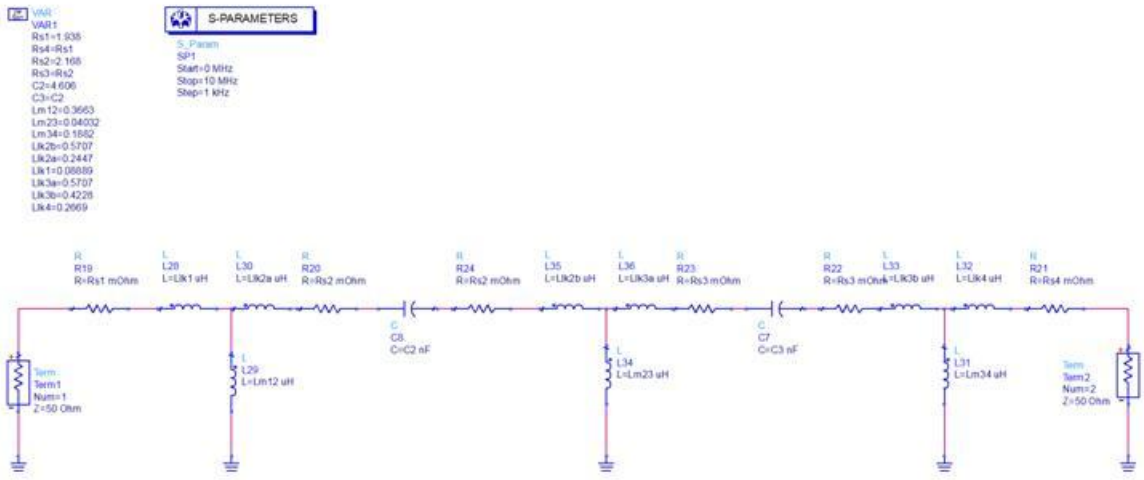

Figure 88: WPT 4-4 scattering parameters circuit simulation in ADS

APPENDIX K: WPT 4-2 MAGNETIC ELEMENT PARAMETER COMPUTATION MATHCAD WORKSHEET

WPT 4-2 Parameter Calculation

Prepared by: Gabriel Vázquez Ramos

INPUTS:

$d1 := 0.16$ $d3 := 0.20$ $N1 := 1$ $N3 := 5$ $ds12 := 0.05$ $fs := 22.6\,10^{6}$

$d2 := 0.20$ $d4 := 0.16$ $N2 := 5$ $N4 := 1$ $ds23 := 0.25$ $r\_c := 0.00635$

$n12 := \frac{N2}{N1}$ $n23 := \frac{N3}{N2}$ $n34 := \frac{N4}{N3}$ $ds34 := 0.05$ $u0 := 4\cdot\pi\cdot 10^{-7}$

$w := 2\cdot\pi\cdot fs$ $ur := 1$

$sig := 5.96\,10^{7}$ $cl := 2.998\times 10^{8}$

CALCULATIONS:

FOR Lm12

$r1 := \frac{d1}{2}$ $r1 = 0.08$

$r2 := \frac{d2}{2}$ $r2 = 0.1$

$L1 := N1^{2}\cdot r1\cdot u0\cdot\left[\ln\left[\frac{(8\cdot r1)}{r\_c}\right] - 1.75\right]$ $L1 = 2.878\times 10^{-7}$

$L2 := N2^{2}\cdot r2\cdot u0\cdot\left[\ln\left[\frac{(8\cdot r2)}{r\_c}\right] - 1.75\right]$ $L2 = 9.695\times 10^{-6}$

$C1 := \frac{1}{\left[(2\cdot\pi\cdot fs)^{2}\cdot L1\right]}$ $C1 = 1.723\times 10^{-10}$

$C2 := \frac{1}{\left[(2\cdot\pi\cdot fs)^{2}\cdot L2\right]}$ $C2 = 5.115\times 10^{-12}$

$$k12 := \frac{1}{\left[1 + 2^{\left(\frac{2}{3}\right)}\cdot\left[\frac{ds12}{\sqrt{(r1\cdot r2)}}\right]^{2}\right]^{\left(\frac{3}{2}\right)}} \qquad k12 = 0.546$$

$Lm12 := \sqrt{L1\cdot L2}\cdot k12$ $Lm12 = 9.129\times 10^{-7}$

$Llk1 := L1 - \frac{Lm12}{n12}$ $Llk1 = 1.052\times 10^{-7}$

$Llk2a := L2 - (Lm12\,n12)$ $Llk2a = 5.131\times 10^{-6}$

FOR Lm23:

$r3 := \frac{d3}{2}$ $\quad r3 = 0.1$

$L3 := N3^2 \cdot r3 \cdot u0 \cdot \left[\ln\left[\frac{(8 \cdot r3)}{r\_c} \right] - 1.75 \right]$ $\quad L3 = 9.695 \times 10^{-6}$

$C3 := \frac{1}{\left[(2 \cdot \pi \cdot fs)^2 \cdot L3 \right]}$ $\quad C3 = 5.115 \times 10^{-12}$

$k23 := \frac{1}{\left[1 + 2^{\left(\frac{2}{3}\right)} \cdot \left[\frac{ds23}{\sqrt{(r2 \cdot r3)}} \right]^2 \right]^{\left(\frac{3}{2}\right)}}$ $\quad k23 = 0.028$

$Lm23 := \sqrt{L2 \cdot L3} \cdot k23$ $\quad Lm23 = 2.686 \times 10^{-7}$

$Llk2b := L2 - \frac{Lm23}{n23}$ $\quad Llk2b = 9.427 \times 10^{-6}$

$Llk3a := L3 - (Lm23 n23)$ $\quad Llk3a = 9.427 \times 10^{-6}$

FOR Lm34:

$r4 := \frac{d4}{2}$ $\quad r4 = 0.08$

$L4 := N4^2 \cdot r4 \cdot u0 \cdot \left[\ln\left[\frac{(8 \cdot r4)}{r\_c} \right] - 1.75 \right]$ $\quad L4 = 2.878 \times 10^{-7}$

$C4 := \frac{1}{\left[(2 \cdot \pi \cdot fs)^2 \cdot L4 \right]}$ $\quad C4 = 1.723 \times 10^{-10}$

$k34 := \frac{1}{\left[1 + 2^{\left(\frac{2}{3}\right)} \cdot \left[\frac{ds34}{\sqrt{(r3 \cdot r4)}} \right]^2 \right]^{\left(\frac{3}{2}\right)}}$ $\quad k34 = 0.546$

$Lm34 := \sqrt{L3 \cdot L4} \cdot k34$ $\quad Lm34 = 9.129 \times 10^{-7}$

$Llk3b := L3 - \frac{Lm34}{n34}$ $\quad Llk3b = 5.131 \times 10^{-6}$

$Llk4 := L4 - (Lm34 n34)$ $\quad Llk4 = 1.052 \times 10^{-7}$

Series Resistance:

Ohmic Resistances (Ro):

$$Ro1 := \sqrt{\frac{(w \cdot u0 \cdot ur \cdot r1)}{2 \cdot sig \cdot r\_c}}$$

$$Ro2 := \sqrt{\frac{(w \cdot u0 \cdot ur \cdot r2)}{2 \cdot sig \cdot r\_c}}$$

$Ro4 := Ro1$ $Ro3 := Ro2$

Radiation Resistances (Rr):

$$Rr1 := 20 \cdot \left[\left[\frac{(2 \cdot \pi \cdot fs)}{cl} \right]^2 \cdot \pi \cdot r1^2 \right]^2$$

$$Rr2 := 20 \cdot \left[\left[\frac{(2 \cdot \pi \cdot fs)}{cl} \right]^2 \cdot \pi \cdot r2^2 \right]^2$$

$Rr4 := Rr1$ $Rr3 := Rr2$

Total Resistance (R):

$R1 := Ro1 + Rr1$ $R1 = 4.75 \times 10^{-3}$

$R4 := R1$ $R4 = 4.75 \times 10^{-3}$

$R2 := Ro2 + Rr2$ $R2 = 5.849 \times 10^{-3}$

$R3 := R2$ $R3 = 5.849 \times 10^{-3}$

APPENDIX L: WPT 4-2 MAGNETIC ELEMENT CIRCUIT SIMULATION

Appendix L.1 WPT 4-2 Frequency Response SPICE Simulation Netlist

```
V1 N001 0 SINE() AC 1
R1 N002 N001 50
R2 N003 N002 4.75m
R3 N006 N005 5.849m
C1 N006 N007 5.115p
C2 N008 N009 5.115p
R4 N009 N010 5.849m
R5 N012 N013 4.75m
R6 N013 N014 50
L1 N003 N004 0.1052µ
L2 N004 N005 5.131µ
L3 N010 N011 5.131µ
L4 N011 N012 0.1052µ
L5 N004 0 0.9129µ
L6 N014 N008 9.695µ Rser=0
L7 0 N007 9.695µ Rser=0
L8 N011 N014 0.9129µ
K1 L7 L6 0.028
.ac dec 1000001 1e6 500e6
.backanno
.end
```

Appendix L.2 WPT 4-2 Transient Response SPICE Simulation Netlist

```
V1 In 0 SINE(0 5 18.14Meg)
R1 in_sys In 50
R2 N001 in_sys 4.75m
R3 N004 N003 5.849m
C1 N004 N005 5.115p
C2 N006 N007 5.115p
R4 N007 N008 5.849m
R5 N010 Out+ 4.75m
R6 Out+ Out- 50
L1 N001 N002 0.1052µ
L2 N002 N003 5.131µ
L3 N008 N009 5.131µ
L4 N009 N010 0.1052µ
L5 N002 0 0.9129µ
L6 Out- N006 9.695µ Rser=0
L7 0 N005 9.695µ Rser=0
L8 N009 Out- 0.9129µ
K1 L7 L6 0.028
.tran 5u
.backanno
.end
```

Appendix L.3 WPT 4-2 Scattering Parameters Simulation in ADS

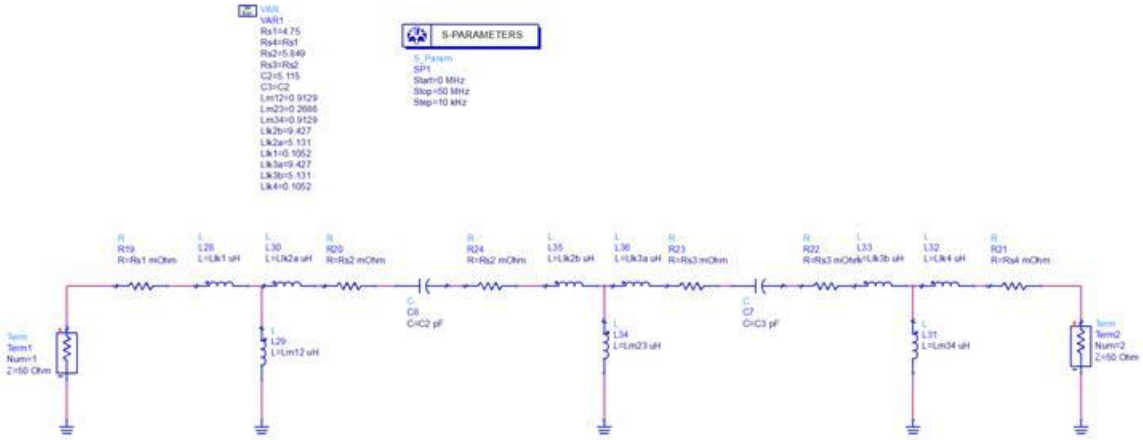

Figure 89: WPT 4-2 scattering parameters circuit simulation in ADS

LIST OF REFERENCES

[1] National Geographic, National Geographic Society, [Online]. Available: science.nationalgeographic.com/science/space/space-exploration/ . [Accessed 2 June 2012].

[2] M. D. a. J. R. F. Griffin, Space Vehicle Design, Second Edition, AIAA, 2004.

[3] G. Vazquez Ramos and J. Yuan, "Development of a Novel Wireless Electric Power Transfer Systems for Space Applications," in *The 15th World Multi-Conference on Systemics, Cybernetics and Informatics*, Orlando, FL, 2011.

[4] G. Vazquez Ramos and J. Yuan, "Wireless Power Transfer for Space Applications," *US Department of Commerce (National Information Systems),* no. KSC-2011-224, 2011.

[5] A. Karalis, J. Joannopoulos and M. Soljacic, "MIT's Efficient wireless non-radiative mid-range energy transfer," *Annals of Physics,* vol. 323, no. Annals of Physics 323 (2008), pp. 34-48, April 2007.

[6] US Department of Defense, "Requirements for the Control of Electromagnetic Interference Characteristics of Sub-Systems and Equipment," 1999.

[7] US Department of Defense, "Requirements for the Control of Electromagnetic Interference Characteristics of Subsystems and Equipment," 2007.

[8] US Department of Defense, "Electromagnetic Compatibility Requirements for Space Systems," 1987.

[9] US Department of Defense, "Product Verification Requirements for Launch, Upper Stage, and Space Vehicles," 1999.

[10] W. Kuen-Cheng, H. Che-Wei, C. Tung- Jung, C. Tsung-Shih and C. Tsair-Rong, "Study of Applying Contactless Power Transmission System to Battery Charge," in *International Conference on Power Electronics and Drive Systems, 2009*, 2009.

[11] Y. L. X. S. Wu Ying, "Modeling and performance analysis of the new contactless power supply system," in *Proceedings of the Eighth International Conference on Electrical Machines and Systems, 2005.*, 2005.

[12] H. Ayano, K. Yamamoto, N. Hino and I. Yamato, "Highly efficient contactless electrical energy transmission system," in *IEEE 2002 28th Annual Conference of the Industrial Electronics Society*, 2002.

[13] A. P. H. a. N.-K. C. N. Chao Liu, "Coupling study of a rotary capacitive power transfer system," in *IEEE International Conference on Industrial Technology, 2009*, 2009.

[14] H. Fnato, Y. Chiku and K. Harakawa, "Wireless power distribution with capacitive coupling excited by switched mode active negative capacitor," in *Conference on Electrical Machines and Systems (ICEMS), 2010 International* , 2010.

[15] M. Kline, I. Izyumin, B. Boser and S. Sanders, "Capacitive power transfer for contactless charging," in *Applied Power Electronics Conference and Exposition (APEC), 2011 Twenty-Sixth Annual IEEE*, 2011.

[16] Duracell Corporation, "myGrid Specifications," 2010. [Online]. Available: http://www.duracell.com/en-US/product/mygrid-kits.jspx.

[17] C. R. Paul, Introduction to Electromagnetic Compatibility, 2nd Edition, 2006.

[18] C. Bowick, RF Circuit Design, 2nd Edition ed., Burlington: Elsevier, 2008.

[19] A. H. Systems Inc., "Typical Conversion Formulas," Chatsworth, CA..

[20] Solar Electronics Company, "TYPE 7334-1 Loop Antenna for RE 01 and RE101 Magnetic Emission Test".

[21] ETS - Lindgren, "Active Rod & Field Antenna User Manual," 2010.

[22] T. Williams, "EMC for Product Designers, Fourth Edition," in *Newnes*, 2007.

[23] H. Trzaska, "Electromagnetic Field Measurements in the Near Field," in *SciTech*, 2001.

[24] M. N. Sadiku, Numerical Techniques in Electromagnetics with Matlab, CRC Press, 2009.

[25] B. Archambeault, EMI/EMC Computational Modeling Handbook, 2nd Edition, Kluwer Academic Publishers, 2001.

[26] L. Tarricone, Grid Computing for Electromagnetics, Artech House, 2004.

[27] Agilent Technologies , "FEM Simulation," Agilent Technologies , Santa Clara, CA, 2011.

[28] G. Pelosi, R. Coccioli and S. Selleri, Quick Finite Elements for Electromagnetic Waves, Second Edition., Artech House, 2009.

[29] K. Coburn, "Computational Electromagnetics," Applied Technology Institute, Riva, Maryland.

[30] N. Tesla, "System of transmission of electrical energy". United States of America Patent 645,576, September 1897.

[31] N. Tesla, "Apparatus for transmission of electrical energy". United States of America Patent 649,621, September 1897.

[32] N. Tesla, "Art of transmitting electrical energy through the natural medium". United States of America Patent 787,412, May 1900.

[33] N. Tesla, "Apparatus for transmitting electrical energy". United States of America Patent 1,119,732, January 1902.

[34] G. Vazquez Ramos and J. Yuan, "FEM Simulation to Characterize Wireless Electric Power Transfer Elements," in *IEEE SouthEastCon 2012*, Orlando, FL, 2012.

[35] G. Vazquez Ramos and J. Yuan, "Radiated Emissions Testing of Space Wireless Electric

Power Transfer Systems," in *IEEE SouthEastCon 2012*, Orlando, FL, 2012.

[36] O. Stielau and G. Covic, "Design of loosely coupled inductive power transfer system," in *Int. Conf. Power System Technology 2000*, 2000.

[37] H.-C. Son, J.-W. Kim, Y.-J. Park and K.-H. Kim, "Efficiency analysis and optimal design of a circular loop resonant coil for wireless power transfer," in *Microwave Conference Proceedings (APMC), 2010 Asia-Pacific* , 2010.

[38] J. Mur-Miranda, G. Fanti, Y. Feng, K. Omanakuttan, R. Ongie, A. Setjoadi and N. Sharpe, "Wireless Power transfer using weakly coupled magnetostatic resonators," in *2010 IEEE Energy Conversion Congress and Exposition (ECCE)*, 2010.

[39] S. Judek and K. Karwowski, "Supply of electric vehicles via magnetically coupled air coils," in *Power Electronics and Motion Control Conference, 2008*, 2008.

[40] H. Kim, D. Won and B. Jang, "Simple design method of wireless power transfer system using 13.56MHz loop antennas," in *2010 IEEE International Symposium on Industrial Electronics (ISIE)*, 2010.

[41] G. Vazquez Ramos and J. Yuan, "Wireless Power Transfer for Space Applications," *US Department of Commerce (National Information Systems)*, pp. KSC-2011-224, 2011.

[42] Lexmark Corporation, "Z13, Z23 and Z33 Color Jet-printer, From Setup to Printing," 2001.

[43] Fairchild Semiconductor, "LM78XX/LM78XXA 3-Terminal 1A Positive Voltage Regulator," 2011.

[44] EXAR Corporation, "XR 2206 Function Generator IC," 2007.

[45] Matlab 2008, "Wavewrite Matlab Function "wavwrite()" (software help documentation)," 2008.

[46] Velleman Components , "7W Mono Amplifier Kit," Belgium, 2004.

[47] Fairchild Semiconductor , "1N5817 Schottky Barrier Rectifier," 2010.

[48] ST Microelectronics, "10W CAR RADIO AUDIO AMPLIFIER," 1998.

[49] O. Jonah and S. Georgakopoulos, "Wireless power transmission to sensors embedded in concrete via Magnetic Resonance," in *Wireless and Microwave Technology Conference (WAMICON), 2011 IEEE 12th Annual* , 2011.

[50] K. E. Lonngren, S. Savov and R. J. Jost, Fundamentals of Electromagnetics with Matlab, 2nd ed., Scitech Publishing Inc, 2007.